Republic of Iraq
Ministry of Higher Education and Scientific Research
University of Babylon
College of Engineering
Civil Engineering Department

Geospatial-Based Investigation of Meteorological Drought Impact on Vegetation Cover and Land Surface Temperature in the Greater Zab River Basin

A Thesis

Submitted to the Department of Civil Engineering, College of Engineering, University of Babylon in Partial Fulfilment of the Requirements for the Master Degree in Engineering /Civil Engineering /Water Resources Engineering

By:

Doaa Riyadh Mohammed Ali Mohammed Hussain

Supervised by:

Prof. Dr. Ruqayah Kadhim Mohammed

2023 A.D **1445 A.H**

بِسْمِ اللَّهِ الرَّحْمَنِ الرَّحِيمِ

الَّذِي جَعَلَ لَكُمُ الْأَرْضَ فِرَاشًا وَالسَّمَاءَ بِنَاءً وَأَنزَلَ مِنَ

السَّمَاءِ مَاءً فَأَخْرَجَ بِهِ مِنَ الثَّمَرَاتِ رِزْقًا لَّكُمْ ۖ فَلَا تَجْعَلُوا لِلَّهِ

أَندَادًا وَأَنتُمْ تَعْلَمُونَ

صدق اللَّهُ العلي العظيم

سورة البقرة {الأية:22}

Supervisor's Certificae

I certify that this thesis which is entitled **(*Geospatial-Based Investigation of Meteorological Drought Impact on Vegetation Cover and Land Surface Temperature in the Greater Zab River Basin*)** was prepared by **(*Doaa Riyadh Mohammed Ali*)** under my supervision at College of Engineering, Babylon University, in partial fulfillment of the requirements for the degree of Master in Civil Engineering / Water Resources Engineering.

Signature:

Name: ***Prof. Dr. Ruqayah Kadhim Mohammed***

Date: / / 2023

Examination Committee's Certificate

We certify that we have read this thesis entitled ***(Geospatial-Based Investigation of Meteorological Drought Impact on Vegetation Cover and Land Surface Temperature in the Greater Zab River Basin)*** *presented by* ***(Doaa Riyadh Mohammed Ali) and*** as an examining committee, we examined the student in its content and in what is connected with it, and that in our opinion it meets standard of a thesis for the degree of Master in Civil Engineering / Water Resources Engineering.

Signature:

Name: ***Prof. Dr. Ruqayah K. Mohammed***

(Supervisor and Member)

Date: / / 2023

Signature:

Name**: *Asst. Prof. Dr.Mahmoud S. Mahdi***

(Member)

Date: / / 2023

Signature:

Name: ***Asst. Prof. Dr.Mohammed A.M. Abdl Abbas***

(Member)

Date: / / 2023

Signature:

Name: ***Prof. Dr. Najm Obaid Salim Alghazali***

(Chairman)

Date: / / 2023

Approved by the Head of the Civil Engineering Department

Signature:

Name: ***Asst.Prof. Dr. Zaid H. Al-Hasson***

Date: / / 2023

Approved by the Dean of the College of Engineering

Signature:

Name: ***Prof. Dr. Laith A. Abdul Rahaim***

Date: / /2023

الإهـــــــداء

الى من لا يضاهيهما أحد في الكون، إلى من أمرنا الله ببرّهما، إلى من بذلا الكثير، وقدّما ما لا يمكن أن يردّ، إليكما تلك الكلمات أمي وأبي الغاليان، أهدي لكما هذا البحث؛ فقد كنتما خير داعم لي طوال مسيرتي الدراسية.

إلى زوجي الغالي: أهدي هذا البحث؛ فقد كان الداعم الأكبر في كلّ شيء، فشكرًا كثيرًا على ثقتك بنجاحي ودفعي نحو الأفضل.

إلى أخوتي والأقارب الذين وقفوا إلى جانبي، كما وقف أهلي أهدى هذا البحث، فأمنياتهم اللطيفة لي بالنجاح ودعمهم وتشجيعهم، مكّنتني اجتياز مرحلة من مراحل حياتي، فلكم جزيل الشكر، ووافر الاحترام .

Acknowledgments

In the name of Allah, the Most Gracious, the Most Merciful. Praise be to Allah for the blessing he has bestowed upon me, and prayers and peace be upon the one who was sent with mercy.

*"Who does not thank people does not thank God". When I am putting the final touches on my humble effort, which would not have seen the light without the strenuous efforts and meticulous follow-up of those loyal and in the forefront of "**Prof. Dr. Ruqayah Kadhim Mohammed**" my supervisor and my support, thanks to her, after God, I completed my thesis, those who spared no effort in helping me, may Allah reward them with the best reward and I have all the appreciation and respect. Also, I cannot forget the efforts made by "**Prof. Dr. Thair Jabbar Mizhir Alfatlawi**", and all of my teachers since I took my first steps in my primary school until today, especially my teachers.*

*To, **Prof Dr. Mahmoud Al-Khafaji**, who did not skimp on any information or advice that I asked him to complete my work*

*To all **my family members, and close friends** who supported me with prayers and information*

Finally, many thanks to everyone who helped me in the departments and everyone who contributed to show this effort for existence.

Doaa Riyadh Tahhan

Abstract

Iraq has had severe drought spells during the past twenty years, which are a typical occurrence in the country climate. The Greater Zab Basin (GZB) is located in the semi-arid region of Iraq, whose water resources have been scarce for decades and are primarily shared with other surrounding countries. Remote sensing (RS) and Geographical Information Systems (GIS) have been used in this work to assess how drought has affected the vegetation cover and land surface temperature in the GZB over the course of 32 years, from 1990 to 2022. For this thesis, 64 Landsat satellite images were downloaded and used. For each year of the study period, four images covering the whole study area were used. Multi-temporal categorized drought maps were created using the Land Surface Temperature Index (LST), Normalized Difference Vegetation Index (NDVI), Vegetation Condition Index (VCI), and Modified Soil-Adjusted Vegetation Index (MSVI). The findings showed an increase in the frequency and severity of drought across the study period, especially in the years 2000 and 2008, which were marked by an increase in land surface temperatures, a loss in vegetation cover, and a lack of average precipitation. The mean LST varied from 37.28 °C in 2008 to 37.56 °C in 2014. As shown by the basin's NDVI, one effect of rising LST is a decrease in vegetation cover in the southeast and southwest parts of the GZRB. The years with the lowest NDVI readings were 2000, 2002, and 2008, respectively, with values of (0.196, 0.131, and 0.202) km^2. The four years in this analysis had the highest risk of experiencing a drought, according to the VCI, were 1992, 2000, 2002, and 2008. In a vast area of the region, severe drought conditions prevailed between 2000 and 2008.The data also revealed that 13667.5 km^2, or 66.5% of the total area, was covered by the severe drought zone in the basin with MSAVI values less than 0.2. The province study area northern portions show a decline in vegetation. Another explanation for this decline is a mismatch between normal rainfall and plant

needs during the crucial growing season. Also, In the current thesis, daily climatic data from the past and projected future were simulated using LARS-WG 6.0. The model was also utilized to estimate daily rainfall and a day temperature. Using the RCP4.5 and RCP8.5 main emission scenarios to estimate the future climate throughout the course of the current century utilizing the MIROC5, CanESM2, HadGEM2-ES, ESM1-M, and CSIRO-Mk3.6.0 general circulation models (GCMs). This was done in light of the significant uncertainty related to estimate the future climate. The model, which was constructed using thirty years' worth of historical data, was validated using climate data from the Greater Zab Basin in northern Iraq (1990–2021). According to the data, the monthly maximum temperature declines by 6.20–5.78 °C under RCP4.5 and 6.10–5.58 °C under RCP8.5, by the end of the twenty-first era, for the Northern and Southern parts for basin. Precipitation projections from all GCMs show varying patterns. Given that some models, like CanESM2, expect a rise in precipitation while others, like MIROC5, forecast a future with no change in precipitation or a falling trend. Furthermore, the southern part of the basin suffered the most during the droughts of 1999–2000 and 2007–2008, with average RDIst values of -1.97 and -1.64, respectively. However, the northern part of the basin had moderate to severe droughts in 1999–2000 and 2007–2008, with average RDIst values of -0.81 and -1.84, respectively This illustrates the significant level of uncertainty in precipitation forecast when only one model is utilized. The amount of water available in the study area location will be significantly impacted by variations in rainfall and temperature.

TABLE OF CONTENTS

LIST OF FIGURES

LIST OF TABLES

LIST OF ABBREVIATIONS

ABBREVIATION	DESCRIPTION
AVHRR	Advanced Very High-Resolution Radiometer
CanESM2	Canadian Centre for Climate Modeling and Analysis
CFSR	Climate Forecast System Reanalysis
CHIRPS	Climate Hazards Group InfraRed Precipitation with Station data
CMIP5	Coupled Model Intercomparison Project Phase 5
CSIRO-Mk3.6.0	Commonwealth Scientific and Industrial Research Organization, Australia
DEM	Digital Elevation Model
DJF	December, January, and February
DrinC	Drought Index Calculator
GCMs	General Circulation Models
GIS	Geographic Information System
GZRB	The Greater Zab Riv0er Basin
GZRC	The Greater Zab River Catchment
IPCC	Intergovernmental Panel on Climate Change
JJA	June, July, and August
K-S	Kolmogorov-Smirnov
LARS-WG	Long Ashton Research Station Weather Generator
LST	Land Surface Temperature
LULC	Land Cover/Land Use
MAM	March, April, and May
masl	Meters Above Sea Level

MIROC5	Atmosphere and Ocean Research Institute (The University of Tokyo), National Institute for Environmental Studies, and Japan Agency for Marine-Earth Science and Technology, Japan
MSAVI	Modified Soil-Adjusted Vegetation Index
NASA	National Aeronautics and Space Administration
NDVI	Normalized Difference Vegetation Index
NDVImax	Maximum Normalized Difference Vegetation Index
NDVImin	Minimum Normalized Difference Vegetation Index
NIR	Near Infra-Red
NOAA	The National Oceanic and Atmospheric Administration
OLI	Operational Land Image
PD	Precipitation Deciles
PET	Potential Evapotranspiration
RainD	Daily Rainfall Distributions
RCP	Representative Concentration Pathway
RCP4.5	RCP with the scenario of 4.5
RCP8.5	RCP with the scenario of 8.5
RDI	Reconnaissance Drought Index
RDIn	Normalized Reconnaissance Drought Index
RDIst	Standard Reconnaissance Drought Index
RDIαk	Initial Reconnaissance Drought Index
SDI	Streamflow Drought Index
SON	September, October, and November
SPI	Standardized Precipitation Index

SPSS	Statistical Package for Social Science
SRTM	Shuttle Radar Topography Mission
TIRS	Thermal Infrared Sensor
TM	Thematic Mapper
TmaxD	Maximum Temperature Distributions
TminD	Minimum Temperature Distributions
TOA	Top of Atmosphere
TRB	Tigris River Basin
USGS	United States Geological Survey
UTM	Universal Transverse Mercator
VC	Vegetation Cover
VCI	Vegetation Condition Index
VD	Vegetation Density
WCRP	World Climate Research Program
WDSeries	Wet/Dry Series Periodic Distributions
WGS	World Geodetic System
WGS84	World Geodetic System Reference 1984

LIST OF SYMBOLS

SYMBOL	DESCRIPTION
TB	Brightness Temperature
K_1	Thermal Conversion Constant For A Certain Band (In Watts/M^2 × Srad × μm)
K_2	Thermal Conversion Constant That Is Band-Specific (In Kelvin)
L_λ	Spectral Radiance At The Sensor's Aperture
T	The Temperature At The Land's Surface In Kelvin
λ	The Radiance's Wavelength
ε	Emissivity
σ	Boltzmann's Constant
h	Plank's constant
c	Light Velocity
Tc	Temperature At the Same Location In Celsius
$\bar{y}$	Arithmetic Mean
$\hat{\sigma y}$	The Corresponding Standard Deviation

CHAPTER ONE

INTRODUCTION

1.1 Overview

Climate change and population growth is the major challenges facing the water security and food security. Every year, drought hits various regions worldwide causing severe damage on the economy, social and ecological systems on the regional and international levels. In recent decades, climate change increases the frequency and intensity of drought because the spatiotemporal alteration in weather elements that mean a real threat on humanity life is expected in future. The meteorological drought is widely utilized to measure the degree of dryness and duration of the dry period. The meteorological drought explains the atmosphere conditions as a function of deficiencies in precipitation on specific region. This type of drought is important in the detection of dryness because the other types of droughts (agricultural and hydrological droughts) are related to it.

Drought monitoring is an important component to reduce or prevent the damages excreted by drought. The drought can be evaluated seasonally or annually by comparing incremental meteorological data with long-term period of records in specific location or region. However, the difficulty in drought monitoring is involved by developing an operational model that can serve timely decision in response of drought. Therefore, many indices were developed to mark the drought based on observed precipitation, vegetation cover and streamflow. The current development on satellite technology that focusing on earth observation are facilitated drought monitoring as the presented data can be processed, analyzed and displayed to perform an understanding on current and past drought as well as the expected future drought based on data provided by climate change models.

Northern region of Iraq (Kurdistan Region of Iraq) is considering the

main water resources suppler of Tigris River by the Greeter Zab and Lesser Zab tributaries. During the last decades, Greeter Zab Basin (GZB) subsequently Tigris River Basin (TRB) suffer from frequent drought due to decreasing precipitation. Therefore, it is important to investigate and analyze these phenomena and explore its extent in the future.

1.2 Thesis Problem

Most of water resources management plans fail due to lack of drought assessment. In the GZB and TRB, in general, these plans take a little consideration of the impact of drought on water resources distribution as the upstream regions may produce less than the expected and water demand increase as a result of drought. In addition, the future drought frequency and intensity addressed by climate change will alter the plans such as operation current irrigation projects, development new irrigation projects, domestic water supply and planed hydraulic structures. The evaluation of drought in spatiotemporal manner is an efficient method to improve the accuracy of water resources management. Moreover, it is highly motivated to investigate the impact of meteorological drought on natural land cover.

1.3 Aim of the Thesis

This thesis aims to evaluate the spatiotemporal variability of meteorological drought and its impact on the vegetation cover and land surface temperature events within the GZRB during the growing seasons from 1990 to 2022.

1.4 Objectives of the Thesis

The main objectives of this thesis are:

1. Evaluating the variability of droughts by analyzing the Normalized Difference Vegetation Index (NDVI), Vegetation Condition Index (VCI), and Modified Soil-Adjusted Vegetation Index (MSAVI). In addition, to examine the relationship between these indices and Land Surface

Temperature (LST).

2. Investigating the correlation between the Digital Elevation Model (DEM) and precipitation (P) as well as LST and spectral drought indices.

3. Assessing the impact of climate change under two Reprehensive Concentration Pathways (RCP4.5 and RCP8.5) scenarios on meteorological drought (RDI) during the period 2020-2040.

1.5 Contribution to the Knowledge

This thesis contributes valuable insights into understanding drought variability and its implications for the GZRB with focusing on the interactions between climate, vegetation, and land surface temperature. The findings can provide more understanding the effects of climate change on drought patterns and contribute to improve water resource management and agricultural practices in the region.

1.6 Justifications of the Study

The GZRB is considered an important region because its significant contribution on crops yields and water resources supplying, therefore:

1. The study area needs more studies to pave the way for various development processes and to benefit from all the resources and capabilities available in the study area, in establishing agricultural expansion projects and establishing new urban, agricultural, and industrial communities.

2. The study area requires more understanding on the effects of meteorological drought on land surface temperature and vegetation cover in the GZB. The remote sensing techniques and Geographic Information Systems (GIS) is the best tools to achieve these objectives.

1.7 Thesis Structure

The scientific rigor of this study necessitated the organization into five distinct chapters. The structure of each chapter is outlined below:

Chapter one, includes an introduction, provides an essential information concerning vegetation cover, surface temperatures, and their implications on drought monitoring. This chapter also outlines the objectives, aims and contribution to the knowledge of this thesis.

Chapter two, delves into an extensive literature review, focusing on the most pertinent subjects related to this research, including the influential climatic factors, vegetation indices, modified vegetation status index, and surface temperature within the study area.

Chapter three, presents a comprehensive description of the research methods, including data collection techniques and the software implemented to analyze and visualize the drought indicators mapped in this study. Additionally, this chapter elaborates on the study area's geographical location and boundaries.

Chapter four, entails the presentation and thorough discussion of the results attained, based on the methodologies and data inputs elucidated in the chapter three. This section offers comprehensive insights into the study findings.

Chapter five, encompasses the conclusions drawn from the study outcomes and provides several recommendations aim at mitigating drought-related challenges and reducing their impact.

CHAPTER TWO

PREVIOUS WORK

2.1 Introduction

Drought is the moisture deficit relative to the average water availability at a given location and season (IPCC, 2022). The deficiency of precipitation leds to reduce soil moisture and dimension plant growth. Early warning of drought is difficult because the forecasting of extreme meteorological events is subjected to uncertainty and need short time to specify. Furthermore, various indicators involved drought as continuous function of meteorological elements such as precipitation, vegetation cover and soil surface temperature. The mitigation from negative impact of drought depends on temporally information and spatial extent. The production of satellite can serve in monitoring precipitation, vegetation cover, soil moisture, evapotranspiration and groundwater, which can be used in monitoring the drought by providing high resolution of spatial and temporal data.

Iraq is located in arid and semi-arid region of the Middle East and the drought frequency was increased in last few years. Therefore, drought monitoring become an essential role to control of negative effect of drought. Many reports indicated that the drought events that hit Iraq tend to increase in its intensity, duration and frequency. Moreover, the lack of precipitation in Iraq generates a new condition represented by desertification, land degradation, lack vegetation and reduced water bodies of that means a real threat on water security and food security can be expected due exceptional drought and effect of climate change.

Many studies and researchers used remote sensing and GIS techniques to monitor vegetation cover, soil moisture and soil temperature based on reflected energy from land surface. Usually, the received data is collected by

satellite or aerial sensors transformed to ground station to be corrected and validated due to atmosphere scattering, ground surface scattering and cloud effects. Generally, these data are provided by many agencies as open excess data of free charge. Moreover, these data can be projected, processed and displayed by using GIS to drive drought monitoring indices of different base of theoretical processing. The continuous time series of remote sensing data encourage the researchers to use these data in terms of drought monitoring.

2.2 Vegetation and LST Spectral Indices

2.2.1 The Normalized Difference Vegetation Index (NDVI)

Currently, the Normalized Difference Vegetation Index (NDVI) that extracted from satellite observed data is considered as an important tool in large scale vegetation drought monitoring (Gu et al., 2007); (Brown et al., 2008). Based on spectral reflectance of green color of plants, the NDVI indicated of greenness value of extended land. The NDVI measures the photosynthetic process related to biomass of plant, which absorbs the part of radiance coming from sunlight (Zhou et al., 2009). However, the reflected energy from vegetation cover is subjected to satellite sensor calibration and atmosphere correction to increase the accuracy of vegetation monitoring (Beck et al., 2006). The National Oceanic and Atmospheric Administration (NOAA) and Advanced Very High-Resolution Radiometer (AVHRR) satellite data were early utilized in prediction of NDVI. Later, the Landsat, IKONOS, SPOT, MODIS data, etc were, increasingly, used worldwide in monitoring vegetation cover as the spatial resolution improved by 8 km for AVHRR, 1 km for SPOT, 250 m for MODIS, 30 m for Landsat and 10 m for Sentinal-2 and time series becomes longer to around half century (Xu et al., 2022) .

The NDVI was applied in many regions as an indicator of vegetation cover, consequently, as drought evaluation tool. (Foody, 2003), investigated

the relationship between rainfall and NDVI based on data extracted from NASA Goddard Distributed Active Archive Center from the year 1987. The study indicated that vegetation cover of Middle East is highly related to rainfall amount and the region mostly covered by bare land, pasture and small shrubs. (Julien et al., 2006), successfully used AVHRR dataset to evaluate the NDVI over Europe, North Africa and Middle East regions for the period from 1982 to 1999. The results showed that the average NDVI in arid and semi-arid regions of studied areas is stable with small deceasing was observed during this period. (Alphan & Derse, 2013), analyzed the thematic map of Landsat images considering latitudes extracted from Quick bird and ASTER data over the area extended over southern Turkey for the period from 1984 to 2006. The study showed that lower latitudes regions can be covered by agricultural, forested and shrub lands because high soil moisture availably in these regions.(Gholamnia et al., 2019), examined the spatiotemporal of NDVI extracted from MODIS data for the semi-arid region western north of Iran between the years 2000 and 2016. The main findings of this study were indicated that the maximum NDVI value was observed after one month of precipitation peak and the study area is subjected to more drought condition. Furthermore, high variation in NDVI was found in 2008 and 2010.

Many researchers deal with NDVI as vegetation cover index considering the geographical extent of Iraq. Based on data extracted from AVHRR (Nielsen & Adriansen, 2005), observed that almost 3% of deceasing in vegetation cover over Middle East region during the period from 1982 to 2005 and Iraqi areas tend to desertification with three times of other region of Middle East. (Fadhil, 2011), concluded that the vegetation cover significantly decreased by 56.7% in Kurdistan region northern of Iraq based on Landsat-7 images extracted in 2007 and 2008. (Al-Timimi et al., 2012), investigated the drought level in Iraq using the 8 km NOAA–AVHRR images during winter and spring seasons from 1980 to 2010 considering

NDVI as indication of drought. The results showed that the 14, 62, 23 and 1% of Iraqi area under lower, moderate, severe and very severe risk of drought, respectively. Furthermore, northern region of Iraq tends to receive more drought.(Eklund & Thompson, 2017), used MODIS data extracted in 2001-2015 with 250 m of spatial resolution in the analysis of drought for the region reach Iraqi-Syria borders by using NDVI. The results indicated that lack of rainfall generate a worst drought can be recorded. Therefore, the contribution of agricultural in Iraqi economy was decreased due to this drought.(Allawai & Ahmed, 2020) evaluated the land cover change in the region around Mosul City in northern Iraq utilizing GIS and remote sensing methods between the years 2014 and 2018. The findings showed that the vegetative distribution ratio was 4.98, 4.77, 4.54, 3.59 and 4.39% in the 2014, 2015, 2016, 2017, and 2018, respectively. (Al-Quraishi et al., 2020) analyzed the drought in Erbil, northern of Iraq from fourteen images produced by Landsat-8 OLI, Landsat-7 ETM+ and Landsat-5 TM data in April of years 1998 to 2017. The results showed that the years 1999, 2000, 2008, 2009, and 2012 endured a severe drought as a lack of precipitation and the vegetative cover decreased by 33.3% in 2000 as lowest percentage in the time of analysis. The study pointed out that the region exposed by exceptional drought during the 20 years of study.

(Gaznayee et al., 2022)examined the variability of drought indices using 144 images produced by Landsat that obtained for the end of vegetation growing season (April and May) for the period from 1998 to 2021, the study focused on Kurdistan region of Iraq. The findings indicated an increase in the frequency and severity of drought over the course of the research period particularly years 2000, 2008 and 2012 with deceasing in vegetation cover of 36, 40 and 46%, respectively, due to rainfall deficit.

2.2.2 Vegetation Condition Index (VCI)

Traditionally, the Vegetation Condition Index (VCI) obtained to perform the desired data about drought such as; starting, severity, duration of drought considering the drought on vegetation. Compared with NDVI, the VCI used the highest and lowest values of NDVI along the analysis period. The VCI is presented as percentage from 0-100%. The lower value of VCI refers to bad condition of vegetation while the high value refers to good condition of vegetation. The VCI is derived, in the same way, of NDVI, on the other word, the VCI can be obtained by the reflectance from vegetation cover that usually collected by satellite (Dikici & Aksel, 2021). However, the VCI depends on the value of NDVI. Therefore, the spatiotemporal accuracy of VCI depends on spatiotemporal accuracy of NDVI (Baniya et al., 2019). The VCI, usually, is utilized in eliminating the fluctuation in NDVI generated from short-term weather conditions and long-term fluctuation coming from ecosystem (Kogan, 1995).

The VCI is widely used in assessment of drought severity around the world. (Liu & Kogan, 2002), studied the soybean yield in Brazil utilizing the NOAA-AVHRR images of 16 km spatial resolution in driving VCI during the period from 1996 to 1998. The finding refers that VCI is helpful in plant yield monitoring with absolute error lower than 10%. (Ghaleb et al., 2015), examined the accuracy of drought monitoring using Landsat images of 30 m of spatial resolution in Bekaa valley, Lebanon during the period from 1982 to 2014. The study concluded that the accuracy of drought monitoring is essentially depended on quality and spatial resolution of input data than the methodology of prediction.(Jiao et al., 2016), concluded that VCI is provids strong correlation between data derived and in situ drought condition based on the information derived from MODIS images of 250 m of spatial resolution. (Javed et al., 2019), pointed out that the VCI is the better indicator

than other (such as NDVI) is when it connected with precipitation indices. This conclusion is obtained from the application considering MODIS images over China during 1982 and 2017.

Recently, Researchers is motivated to examine the VCI in evaluation drought in Iraq as the advantages of this indicator.

(Zoljoodi et al., 2013), linked between VCI and dust storm effected on Iraq, Syria and Iran during the period from 1980 to 2009depended on driving VCI from MODIS data of 5 km spatial resolution. The study concluded that dust storms that hit Iraq, Syria and Iran are highly related to vegetation cover along Iraqi-Syrian borders. Moreover, the frequency of dust storms were significantly increased in dry seasons as the vegetation cover in the lowest levels at these conditions. Based on MODIS images of 5 km spatial resolution, (Almamalachy, 2017), mapped agricultural drought from 2003 to 2015 over Iraq. The study showed that the drought coverd about 37% of vegetation cover. Furthermore, the year 2008 was found the most drought year over monitoring period flowed by years 2012, 2011 and 2009. The study recommended developing nationwide monitoring system to reduce the negative effects of drought. (Gaznayee et al., 2021)examined ten districts of the Erbil Governorate (Kurdistan Region), Iraq, another study was conducted to evaluate the severity of the drought and its links to several ecological variables over 20 years (1998-2017). The findings showed that Erbil experienced droughts frequently. Precipitation, the Digital Elevation Model (DEM), and latitude were all significantly associated with the Landsat time series based on (VCI). Extreme VCI-based drought area percentages of 43.4%, 67.9%, 43.3%, and 40.0%, respectively, were noticed in 1999, 2000, 2008, and 2011. Due to low precipitation rates, the largest crop output drop in the study area mostly happened in 2000, 2008, and 2012.(Alwan et al., 2022), studied the drought monitoring using Landsat images of 30 m spatial

resolution during growing season of winter vegetation for the period from 1988 to 2018 by using VCI as indicator of drought condition in the region southern and western of Iraq. The study indicated to significant drought (both agriculturally and meteorologically) in several parts of Iraq specifically in the Middle Euphrates region. In comparison to a drought-free period, the research area's overall percentage of drought found to be increased, according to the final data. In 1988, 2000, and 2018, the percentage of areas without drought fluctuated from 8% to 17%. Furthermore, the study concluded that drought significantly increased especially in the southern and western parts of Iraq.(Mukhlif & Al-Rifai, 2022), monitored the drought condition and the efficiency of geospatial technologies for the period starting in 1999 and continuing through 2019, a variety of indices, including the VCI, were used to track the drought status for soils in the Mohammed Sakran Region of western Iraq's desert. The findings of the agricultural drought indices VCI, which were grouped into five types whose areas of influence changed with the study's chosen years, concurred with other data in terms of the regions affected by the condition of drought, with a high incidence of severe dry cases.

2.2.3 The Modified Soil-Adjusted Vegetation Index (MSAVI)

Currently, the Modified Soil-Adjusted Vegetation Index (MSAVI) is very interested to quantify the main characteristics of spatiotemporal condition of vegetation cover, since this indicator takes in to consideration the effect of soil noise elimination and atmosphere spectrum. The MSAVI performed high sensitivity for vegetation due to accounting vegetation signal and soil noise ratio (Qi et al., 1994). The MSAVI showed high sensitivity to soil color and soil brightness. Moreover, the indicator performed better in monitoring vegetation densities on global level (Gilabert et al., 2002). (Ren & Feng, 2015), showed that MSAVI is better tool to quantify the vegetation over soil surface in arid and semi-arid region when the selected pixel in validation

processing taken closed to the center of training points.(Rhyma et al., 2020), illustrated that the correlation between NDVI and MSAVI approach to 0.991 in describing vegetation cover extracted from SPOT images. Moreover, image background can be eliminated in MSAVI that helps in increasing the accuracy of monitoring.

The MSAVI were applied in wide range over Middle East, such as Turkey and Iran, (origin of Tigris and Euphrates Rivers) as indicator to understand the drought events over this geographical extend.(Saleh, 2015), linked between the Landsat-7 ETM+ images with soil properties in Diyala Provence east of Iraq. The study indicated to the difficulty establishing the relationship between reflectance and soil properties such as texture and chemical elements. However, they concluded that MSAVI showed more sensitivity to vegetation density compared with NDVI. Furthermore, there is no significant correlation between MSVI and NDVI in the studied area due to atmosphere and geological conditions.(Gaznayee & Al-Quraishi, 2019), discussed the severe agricultural drought that affected Erbil Province using geo-information technology from 1998 to 2017. The findings showed that the drought decreased crop yield, especially in the years 2000, 2008, and 2012. In addition, the MSAVI2-based vegetation cover area significantly decreased in each of the aforementioned years by 22.3, 15.8, and 15.7%. Moreover, in its southern and western regions, Erbil Province experienced severe to exceptional agricultural drought spells in the years 2000, 2008, and 2012.(Nasery & Kaan, 2020), examined the MSAVI in determining forest fires in southern Turkey (closed Iraqi borders) based on data collected from Sentinal-2 images. The finding showed that MSAVI performed better description of recognize the burned and not burned areas as this indicator take into consideration only overland vegetation reflectance.(Mzuri et al., 2021), investigated the vegetation cover over Duhok Province located far north of Iraq based on Landsat images, metrological data and latitudes

produced by NASA. The study considers the MSAVI as an indicator of vegetation during the period from 2000 to 2019. The main findings of this study were indicated that the MSAVI in average is 0.36 and tends to increase in about 78% of the region. Moreover, the vegetation cover in lower elevation lands (less than 2000 m) tend to decrease compared with high elevations lands (more than 2000 m) and there is a positive relationship between MSAVI (on side) and precipitation and temperature (in other side). (Salman & Al Ramahi, 2022), analyzed Landsat images produced from 1999-2021 in order to evaluate the land cover change in Baghdad, capital of Iraq considering MSAVI and other indicators in this analysis. The study, pointed out that the water bodies and vegetation cover were significantly decreased due to urbanization. However, the migration from areas around Baghdad may play crucial role in this decreasing. Whereas, the building area reached the peak in 2021 with 1882 km^2 compared with 782 km^2 in 1999.

2.2.4 The Land Surface Temperature (LST)

The Land Surface Temperature (LST) is considered as an important indicator in evaluation of land surface energy. The LST value serve to understand the emitted long wave radiation as heat flux between atmosphere and land surface can be represented by remote sensing specifically by thermal data extracted from infrared part of electromagnetic energy (Trigo et al., 2008). The wave length of LST is usually located between 8 and 15 µm, this microwave received by sensors connected by satellite that measures the radiance of Top of Atmosphere (TOA). This radiance the transformed into LST after correction processes like angular effects, spectral emissivity and atmosphere attenuation. The LST helps to understand the urban heat and island measurements (Tomlinson et al., 2011). However, the LST is difficult or impossible to detect in coarser resolution data, because the thermal effects may be missed due to the mixing and thermal reflectance may be smaller

than related pixel (Zhan et al., 2013). (Yeneneh et al., 2022), examined the effects of spatiotemporal changes in land cover/land use (LCLU) on LST in the Suha watershed in the northwest highlands of Ethiopia. The classified Landsat images by GIS, applying controlled classification and accuracy evaluation for the time span (1989–2019). These satellite temperature bands are helpful in producing LST.

The LST was widely used in monitoring the land surface temperature over various locations of Iraq. (Ibrahim, 2017), investigated the impact of land cover and urbanization change on the land surface temperature in Dohuk City northern of Iraq. The study, implemented Landsat images collected during 1990, 2000 and 2016. The results showed that the water bodies and urbanization increased by 0.1 and 12%, respectively. Moreover, the study concluded that the bare land and urban are significantly increase the reflected temperature. Furthermore, the LST showed high sensitivity to vegetation cover and soil moisture. (Mejbel Salih et al., 2018), validated thermal infrared band produced by Landsat images with observed infrared by thermo camera. The training points was collected in Babylon province located in central of Iraq. The correlation coefficient of validation processes was 0.7 and 0.89 for the band 10 and 11, respectively. Moreover, the finding showed that the water bodies performed high LST compared with other land covers. The study, indicated that LST I s significantly sensitive by shadow of trees and buildings. (Beg, 2018), examined the land surface variation over Baghdad based on Landsat images produced in 1989, 2000, 2006 and 2016. The images validated by ground observations in 0.5 m above land surface utilizing ArcGIS 10.3 and ERDAS 2014 in processing and classification. The showed that the maximum temperature can be observed on bare land of temperature ranged between 26 and 41 ^{o}C. However, there is an inverse correlation between vegetation cover and estimated LST. Whereas, the urban land increased by 23% and green lands decreased by 6 to 16%. (Gaznayee,

2020) applied the LST in drought monitoring in northern of Iraq. The results indicated an increase in the intensity and frequency of drought, especially between 2000 and 2008. Since the afflicted severity region was 38.3% and 55% in both 2008 and 2000, the southwest and southeast regions were impacted more by the increase in LST for severe drought (> 40 °C). Moreover, Dukan and Darbandikhan lakes had the greatest decrease in 2009, at 41.3% and 72.3%, respectively. According to the study, drought events have increased over the past 20 years, and the amount of precipitation and surface area of water bodies have decreased while the temperature of the land has risen.(Abed et al., 2021), monitored the ecosystem change in Hor Al Dalmaj marshland south of Iraq using Landsat 8 images. The study showed that the highest temperatures were of 43, 50, 56, 62.6 C° for range land, mudflat, arid and desert lands, respectively. Moreover, a negative correlation was found between NDVI and LST. However, the LST is significantly related day time of image collection. The results, also, showed that vegetation cover has essential effects on distribution of surface temperatures.(Al-Masaodi & Al-Zubaidi, 2022), examined the spatiotemporal change of LST and vegetation cover over Babylon Province. Based on analysis done by QGIS software and Landsat images taken during 2013 to 2020, the results showed the average, maximum and minimum temperatures over bar land were 50, 62 and 30 C°, respectively. However, the vegetation cover, represented 10 to 22% of area and land surface temperature distribution, is effected by urbanization development. (Gaznayee et al., 2022) examined the classified NDVI and LST values in the northern of Iraq in 2022. The results demonstrated an increase in drought frequency and severity over the course of the research considered time, mainly during 2000 and 2008 years, which were characterized by elevated LST, decreased plant cover, and precipitation that was below average.

2.3 The Reconnaissance Drought Index (RDI)

The Reconnaissance Drought Index (RDI) firstly suggested by (Tsakiris et al., 2007)for drought assessment. The RDI refers to reconnaissance of drought based on precipitation and evapotranspiration. The index showed many advantages in drought evaluation such as; 1) physically based in deficit between precipitation and evaporation, 2) the index can be estimated for any month of year, 3) helpful in agricultural drought, 4) high related to climate condition, 5) useful in climate variation that generates water scarcity (Tsakiris et al., 2007).(Zarch et al., 2011), pointed out that the RDI resolved more climate variables like evapotranspiration with considering of water losses in specific watershed and RDI which is valuable index in drought monitoring. (Vangelis et al., 2013), concluded that the method applied evapotranspiration estimation in semiarid regions is not highly related on RDI calculation. The decline trend of RDI is highly related by lower value of precipitation and decreased RDI means increasing trend of drought as reported by (Kousari et al., 2014), when investigated the drought trend in Iran using RDI.(Tigkas et al., 2015), simplified the calculation of RDI by development the DrinC software to show the intersection between drought indices. The software is successfully applied in arid and semi-arid regions for drought monitoring, spatial extent of drought and assessment of various scenarios of drought and climate conditions.(Ullah et al., 2019), used the RDI developed a new climate map for Pakistan based on RDI. The study, suggested that RDI is helpful to construct mitigation and adaptation plans, water resources management and drought monitoring.

(Mohammed & Scholz, 2019)examined spatiotemporal characteristics of drought and aridity on climate variability in GZRB northern of Iraq as example of arid and semi-arid region. The study showed that an increase in average temperature consequently evapotranspiration and declined in precipitation over the studied region. Furthermore, the dry years is

significantly increased specifically after year 1995. The study, found that significant relationship between climate variation in side and drought and aridity on the other side.(Al-Khafaji & Al-Ameri, 2021), evaluated the correlation between drought indices for frequency of drought in Upper Tigris River watershed. The study utilized the meteorological data provided by Climate Forecast System Reanalysis (CFSR) for the period from 1979-2013. The results extracted from DrinC indicated that the evapotranspiration is most sensitive factor affected by drought amount. The RDI showed more dryness periods than other indices due to physically based of RDI in balanced of precipitation and evapotranspiration. The study showed that the period from 1979 to 1990 was considered as wet period and the reminder period was drier. (Mahdi et al., 2022), investigated the drought in Najaf Province western of Iraq for the future period from 2021 to 2050 based on RDI and impact of climate change. The study considered the duration, intensity and frequency as basic pattern in evaluation drought monitoring. The results showed that the average and maximum drought will mild and extremely drought. A severe drought is expected on the years 2021, 2034 and 2038. Using the RDI, (Alwan et al., 2022), monitored droughts affecting both agriculture and the environment. The ratio of moderate to mild droughts in the area was higher than the ratio of severe to extreme droughts. The area is extremely dry, especially in its southern and western regions, because of the lack of surface water sources and reliance on some wells with high salinities and unsuitable water for agriculture.

2.4 Climate Change Scenarios

(The Intergovernmental Panel on Climate Change (IPCC), 2014), suggested four greenhouse gases emissions scenarios until year 2100 based on global economy, energy consumptions, land use, population and adaptation plans. These scenarios called Reprehensive Concentration Pathways (RCP). The RCPs2.6, 4.5, 6 and 8.5 scenarios represent an increase

of global temperature of 1, 1.8, 2.1 and 4 °C by the year 2100, respectively. Many agencies and research centers developed the Global Climate Models (GCMs) to simulate impact of anthropic actions on climate variables in the current century. These models temporally updated based on Coupled Model Intercomparison Project (CMIP) to improve GCMs predictions. The five phases of CMIP developed by World Climate Research Program (WCRP) that presented more analysis on climate change (Taylor et al., 2012). The climate models projected climate variables and presented valuable information on future drought. Furthermore, these confirmed that the Middle East region tends to have more aridity during current century (Dai, 2010). In general, the severity and frequency of regional drought is expected to increase due to increase evaporation and deceased precipitation (Sheffield et al., 2012). (Trenberth et al., 2013), argued that the global warming may not lead to global drought and the frequency and intensity of drought are expected to increase.

A few studies forecasted the future drought over Iraq considering climate change scenarios. However, (Al-Faraj et al., 2014), concluded that drought on Diyala River Basin extremely linked to hydrological and meteorological drought based on analysis of RDI (Eklund & Seaquist, 2014), studied spatiotemporal drought on Duhok Province during the years 2007 and 2009 based on enhanced vegetation index. The study concluded that the precipitation declined by 50%, consequently, the vegetation cover decreased by 62%.

2.5 Summery

Drought monitoring plays a crucial role in water resources management. Drought leads to negative impact on economic, ecosystem and lifestyle. The indices developed to drought monitoring termed in different bases including remote sensing and physically base. However, one index may not serve as

drought monitoring due to the limited data in spatial or temporal scale. Therefore, analysis multiplied indices present valuable information in drought assessment. Moreover, future forecasting of future provides frameworks to future plans for land and water management.

In Recent years, the Middle East, including Iraq, is highly vulnerable to the effects of drought, in addition to, climate change is absolutely increasing the dryness in arid and semi-arid regions. Moreover, desertification, vegetation cover decreases and land degradation expected in future. Rising temperatures and reduced precipitation in the region could lead to water shortages, affecting water availability and demand, exacerbated by population growth. As a result, environmental challenges expected, with an increase in extreme events further worsening the situation.

Understanding the fluctuations in NDVI, VCI, and MSAVI, and how these spectral drought indices relate to land surface temperature (LST), Digital Elevation Model (DEM), precipitation (P), and other indices, is essential. This assessment and knowledge of vegetation cover play a pivotal role in executing effective measures for vegetation conservation and restoration in agricultural practices and water resource management.

Most previous works focused on one indicator of drought of a single base with small attention on other indices of different bases of driven. Therefore, in this study, the multi-meteorological drought indices were considered to present comprehensive understand on drought which effect on study area.

CHAPTER THREE

MATERIALS AND METHODS

3.1 Study Area

The Greater Zab River (GZR) is a significant branch of the Tigris River as a water source. After traveling approximately 372 km, the river joins the Tigris River after beginning in Turkey and flowing through northern Iraq, as shown in Figure (3.1). The GZR and its rivers are located between 36° and 38° N latitude and 43.3° and 44.3° E longitude. 26.330 km^2 is the approximate surface area and an altitude range of 180–4000 meters above sea level (masl) defines the GZR catchment (GZRC) (R. Mohammed & Scholz, 2019). Water erosion has deposited sandstone, gravel, and conglomerates throughout the catchment. The GZR passes through various ecological and climatic regions, experiencing diverse conditions. The average and maximum river discharge measures 419 and 1320 m^3/s, respectively, (UN-ESCWA, 2013). The annual rainfall ranges from 350 to 1000 mm. Winter and spring typically have the highest GZRC precipitation rates. Precipitation percentages for four seasons are roughly 48.9, 37.5, 12.9, and 0.7 percent, in that order. With a peak discharge in May and a relatively small stream between July and December, the GZRC flow regime exhibits significant seasonal changes (UN-ESCWA, 2013)Numerous springs in the catchment are used as sources for irrigation plans.

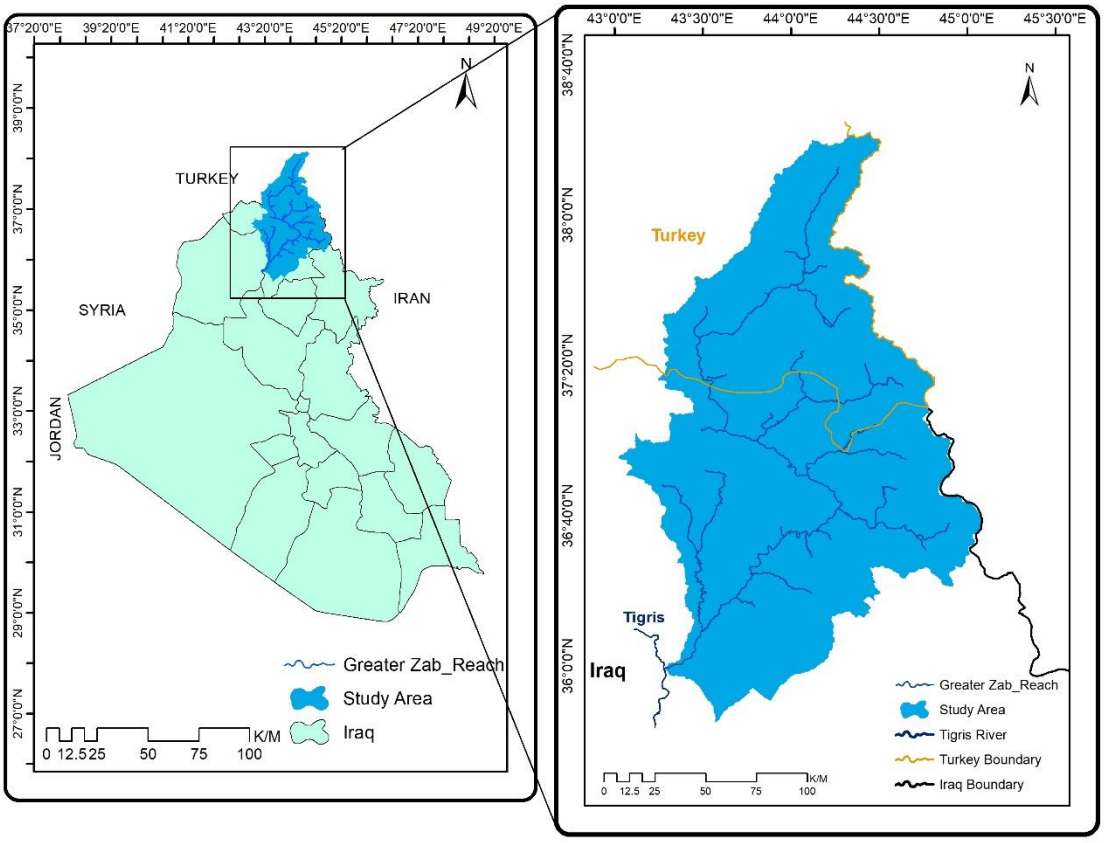

Figure (3.1): Location map of the GZRB

3.2 Geographical information

The GZRB shape files and Iraqi boundaries ,shown in Figure (3.1) have been retrieved from the Global and Land Cover Facility (Herrmann & Bucksch, 2014) and Global Administrative Areas (Robert J. Hijmans, 2012) databases, respectively. with a World Geodetic System reference 1984 (WGS84) and UTM project in 38N.

3.3 Satellite Data Acquisition

For research purposes, a total of 64 Landsat images were obtained from the USGS's Earth Explorer website (*Https://Earthexplorer.Usgs.Gov*) in September 2022 for the period 1990 to 2022. These images were collected during May of each year, which is the period when vegetation experiences its most rapid growth in the basin. The data span from 1990 to 2022, focusing on this timeframe to capture the study area experienced the most extreme drought ever recorded. The remotely sensed datasets, acquired from various

sensors including L5 (TM, Thematic Mapper), L8 (OLI, Operational Land Imager), and others, had a spatial resolution of 30 m. The images covered specific areas defined by (Path/Row, 170/34, 170/35, 169/35, and 169/34), and Table (3.1) provides a collection of free, cloudless, and geo-referenced images for analysis, (Hussain & Karuppannan, 2021).

Note: The Landsat image of 2012 not included because it is not available in the USGS website.

Table (3.1): Earth observation images data for the GZRC.

Collected date		Satellite image	Sensor	Spatial resolution	Bands	Source
Month	year					
May	1990 1992 1994 1996 1998 2000 2002 2004 2006 2008 2010	Landsat4 &5 TM*	TM*	30	1 to7	USGS (Https://Earthexplorer.Usgs.Gov)
	2014 2016 2018 2020 2022	Landsat8 OLI**	OLI-TIRs***	30,15	1 to11	

Path/row=169/34, 169/35, 170/34, 170/35

Note: The panchromatic band 8 for Landsat 8 employs a spatial resolution of 15m.

(*Thematic Mapper; **Operational Land Image; ***Operational Land Image and Thermal Infrared Sensor)

3.4 Topographic Data

The LANDSAT Shuttle Radar Topography Mission Version 3.0 of the (SRTM) DEM, which has a spatial resolution of 1.0 arc. second (30mx30m) was used to represent the basin topography, The US website provides free downloads of these images. Geological Survey (USGS) webpage via the internet from ESRI satellites (*Https://Earthexplorer.Usgs.Gov*) using Tag Image File Format tiff with a World Geodetic System reference 1984 (WGS84) and UTM project in 38N.

As shown in Table (3.2), in January 2023, eight raster files of the DEM were downloaded. Composed elements, mosaic, and extract on shape file of the study area, "the shape files of the Iraqi borders and GZRC were obtained from Global Administrative Areas" (Robert J. Hijmans, 2012) and Access to Data on the world and on land cover (Herrmann & Bucksch, 2014) databases and represented a UTM projection 38N as a single set of raster lines as shown in Figure (3.2).

Table (3.2) The sensor, as well as the date and time of the scene, are captured from USGS for DEM(USGS website ,January 2023)

Path/row	Date
n35_e043	23/09/2014
n35_e044	23/09/2014
n36_e042	23/09/2014
n36_e043	23/09/2014
n36_e044	23/09/2014
n36_e045	23/09/2014
n37_e042	23/09/2014
n37_e043	23/09/2014
n37_e044	23/09/2014
n37_e045	23/09/2014
n38_e042	23/09/2014
n38_e043	23/09/2014
n38_e044	23/09/2014

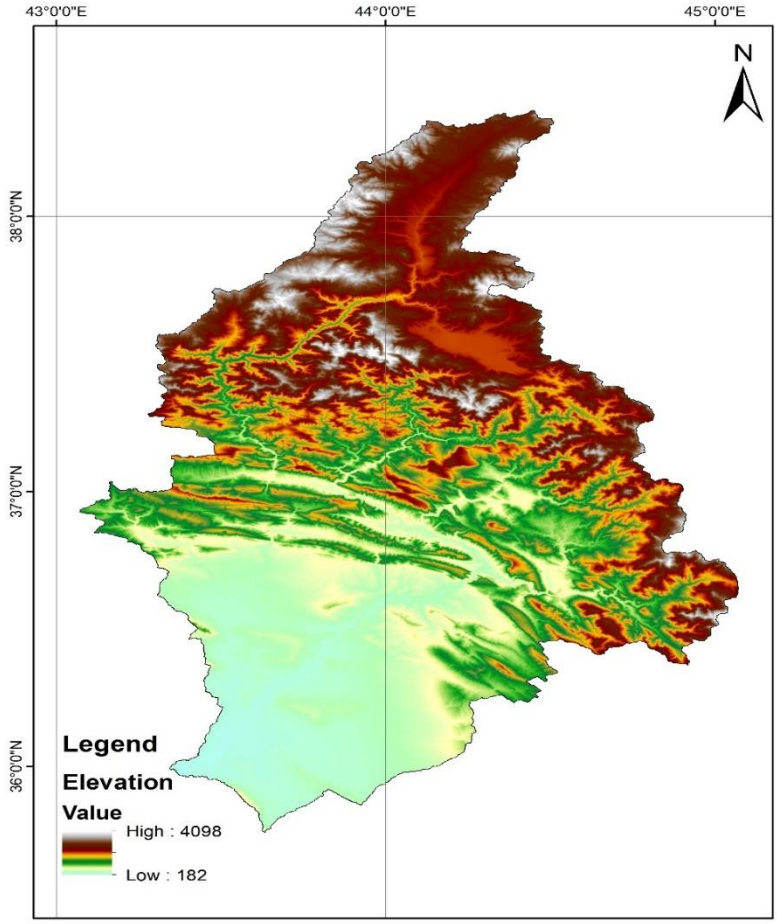

Figure (3.2): Digital Elevation Model for the GZRB with a resolution of 30 m (USGS website, January 2023).

3.5 Meteorological Data

Climate data from thirteen meteorological stations covering 1990 to 2022 was collected for the study area included Razi, Koozerash, Ravand urmia, Mirbad, Soran, Duhook, Aqra, Piranshahr, Salahddin, Bashur, Mousl, Erbil and Makhmoor .as shown in Table (3.3). These data included annual precipitation amounts downloaded from Climate Hazards Group InfraRed Precipitation with Station data (CHIRPS) (*Https://App.Climateengine.Org/ClimateEngine*) ,in march 2023. Figure (3.3) and the maximum and minimum air temperatures, were downloaded from *(Https://Power.Larc.Nasa.Gov/Data-Access-Viewer/)*,in August 2022. Stations range in altitude from 223 to 1980 m are dispersed inside and beyond the GZRB (R. Mohammed & Scholz, 2019) .

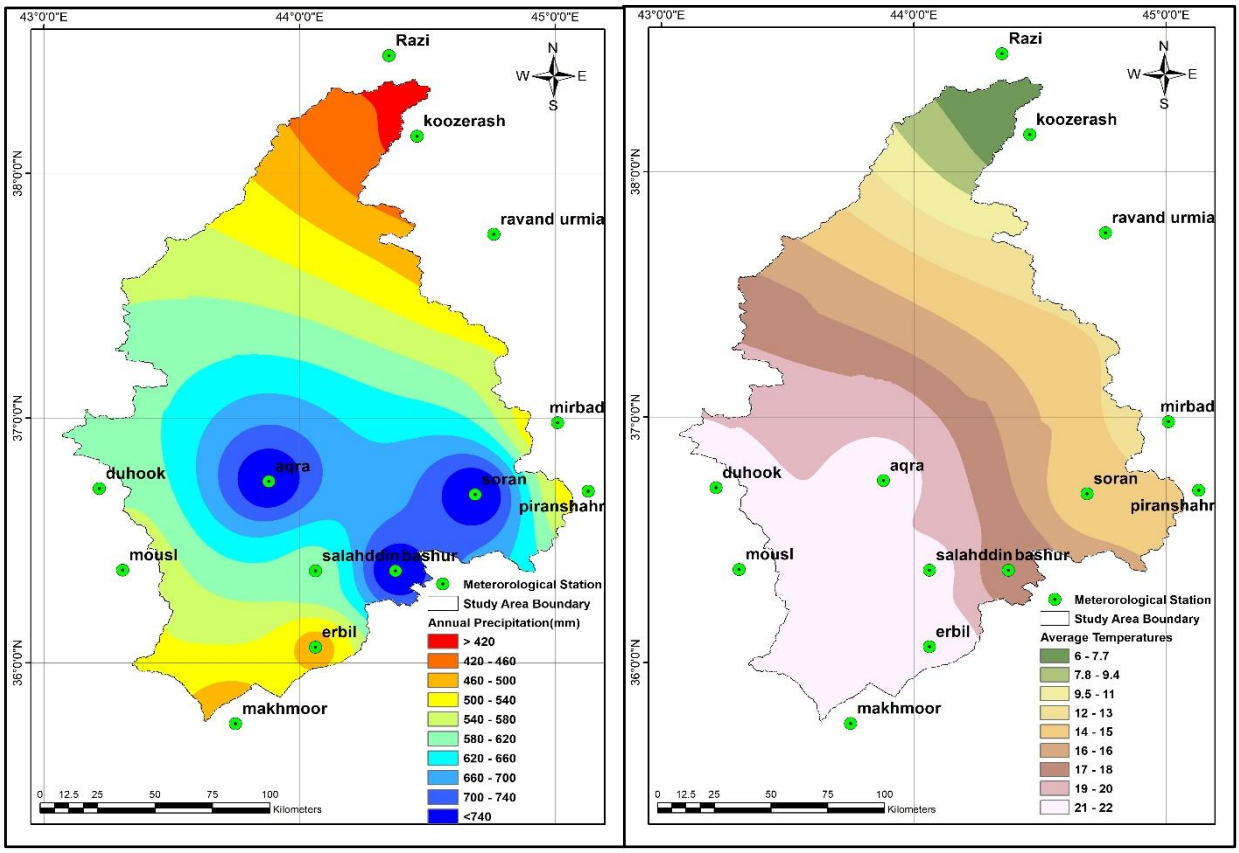

Figure (3.3): A- Spatial distribution of the annual precipitation (mm/year) in GZRB, B- Spatial distribution of average temperature (°C) in GZRB.

Table (3.3) : Longitude, latitude, and elevation for the selected stations GZRB.

Station Name	Longitude (°)	Latitude (°)	Dem (m)	Annual precipitation (mm/year)	Average Temp.(°C)
Razi	44.35	38.48	1980	406.18	5.49
Koozerash	44.46	38.15	1344	408.38	6.06
Ravand urmia	44.76	37.75	1290	426.54	12.24
Mirbad	45.01	36.98	1650	476.17	10.47
Soran	44.69	36.69	1154	789.29	13.39
Duhook	43.13	36.69	436	617.14	20.91
Aqra	43.88	36.74	505	780.47	20.75
Piranshahr	45.13	36.70	1350	502.71	13.39
Salahddin	44.06	36.37	507	601.27	20.54
Bashur	44.38	36.37	977	781.65	17.28
Mousl	43.13	36.37	233	429.24	20.91
Erbil	44.06	36.06	439	481.45	21.60
Makhmoor	43.75	35.75	306	462.87	21.61

3.6 Digital Data and Pre-Processing

ERDAS IMAGINE 2014 has established a DNS based on information in metadata files that allow for modified Landsat images and has converted the resulting imagery into a surface reflection. Then, using WGS 84, Landsat images were georeferenced to region 38 N (UTM). Due to the scale and quality of the problem, images of a specific year that covered the entire basin for a similar period were not available. Different rows and trajectories were considered to obtain a Landsat image simultaneously.

3.7 Methodology of Producing Maps

3.7.1 ARC GIS

A Geographic Information System (GIS) is a set of tools for analyzing, showing, and making sense of spatial and geographic data. ArcGIS version 10.8 is now used as a tool in many engineering projects. The user was able to analyze the data with the help of a few menus and tools. With the help of a tool called "model builder," ArcGIS lets users make their own models. Model Builder is a language used to develop geo-processing workflows. It is a visual computer language.

It lets the user creates, changes, and manages workflows that link geo-referenced processing tools in a certain order and feed the output of one tool into other inputs. This makes it easier for the user to do repetitive tasks in one step. Figure (3.4) shows methodology of NDVI, VCI, MSAVI, and LST at GZRB.

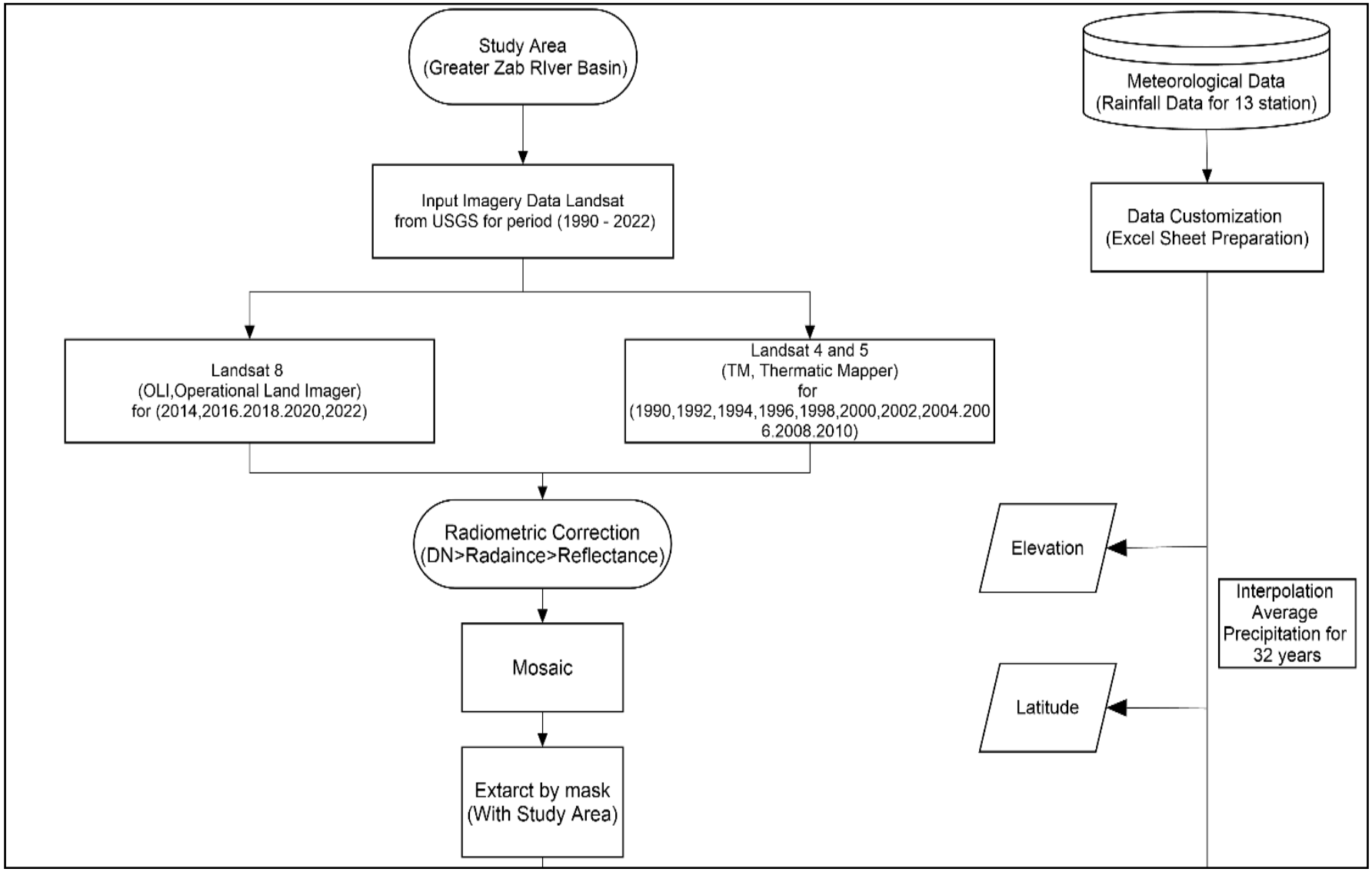

Figure (3.4): Methodology for this study

continued →

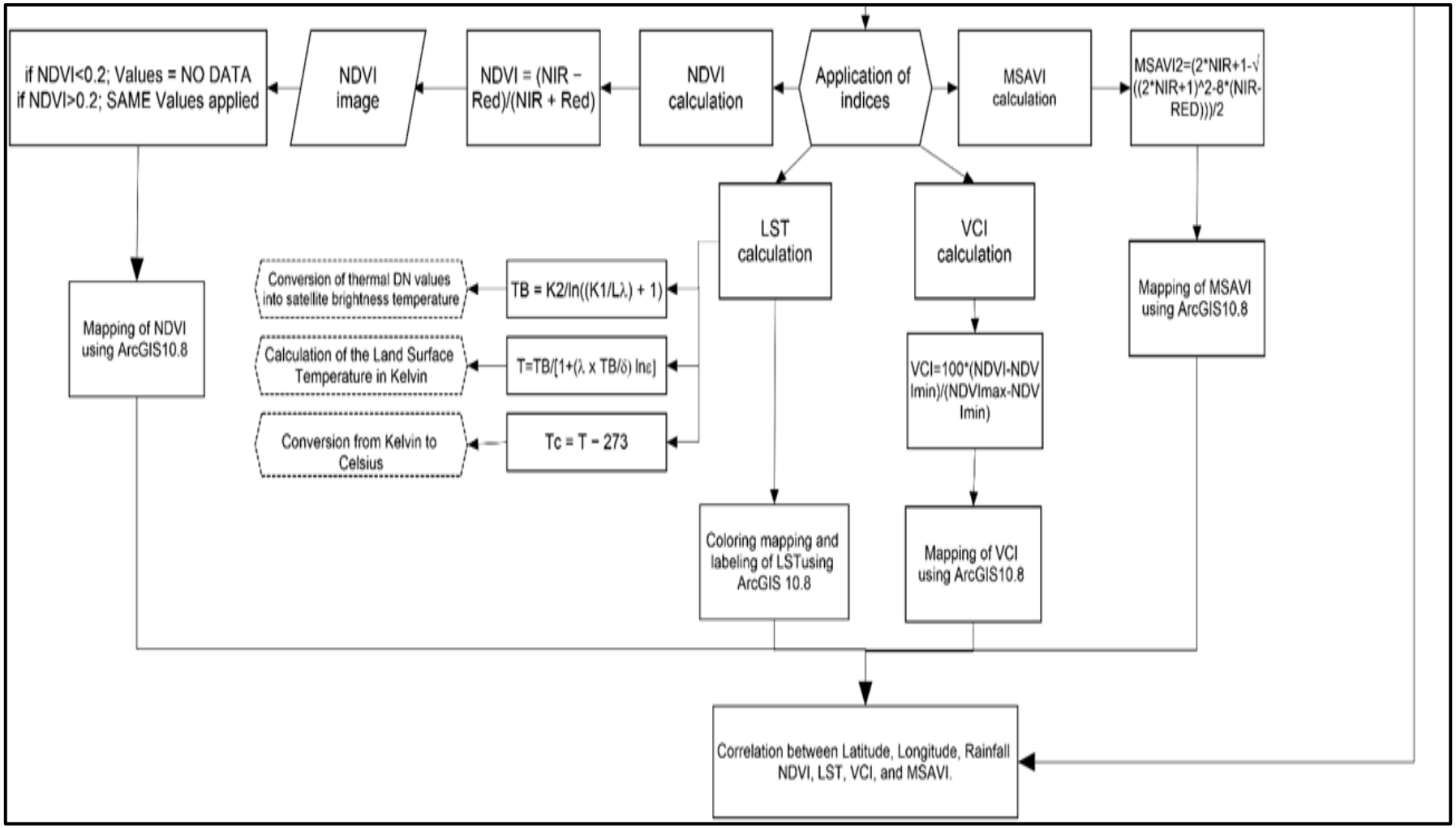

Figure (3.4): Continue...

3.7.2 SPSS Software

The software SPSS stands for Statistical Package for Social Science. It is statistical software that makes data compilation and analysis easier. It was used in this thesis to calculate the coefficients of correlation between latitude, longitude, altitude, precipitations and (LST, NDVI, MASVI, RDI, and VCI) from 1990 to 2022 (33 years on average).

3.7.3 DrinC

The Drought Index Calculator (DrinC 1.7) is an easy-to-use program designed to calculate climatic indices, including the Reconnaissance Drought Index (RDI) and the Streamflow Drought Index (SDI), as well as the Standardized Precipitation Index (SPI) and the Precipitation Deciles (PD), which are well-known measures.

Only RDI was calculated in this study. The primary aspects of this indicator are that it requires very little data to calculate and that the results are easy to understand and apply. With approaches based on minimum, maximum temperatures and annual precipitation, DrinC provides a module for estimating potential evapotranspiration. Hydrological data must be prepared over 30-year water time series least to describe drought (Tigkas et al., 2015).

3.7.4 The Weather Generator model (LARS-WG)

The utilization of the Long Ashton Research Station Weather Generator (LARS-WG) has proven effective in simulating weather variables at specific locations, encompassing current as well as projected climate scenarios. This tool was developed to generate daily time series data and investigated the impacts of climate change on various phenomena,(Wilby, 1999).To lessen uncertainty surrounding climate projections and downscaling temperatures and precipitation, five general circulation models GCMs being provided in Table (3.4) along with a new version of LARS-WG (6.0). Climate

predictions from the Coupled Model Intercomparison Project 5 (CMIP5) ensemble, which were utilized in the Intergovernmental Panel on Climate Change (IPCC's) fifth report, are included in version 6.0 , The model's accuracy in predicting climatic conditions has shown its results in a variety of global locations,(Z. M. Mohammed & Hassan, 2022; Semenov et al., 2013).Even though LARS-WG 6.0 has 19 CMIP5 models for predicting climate, only five of them were be used in this study. Based on a study done in Iraq, five models have been chosen as the best ones for predicting climate change in the future (Khalaf et al., 2022),Table (3.4). Using all of the CMIP5 GCMs for climate change forecast and effect assessment is not practical due to limitations in human and computing resources.

In this thesis, the LARS-WG was employed to make projections concerning precipitation levels and temperature trends. The Weather Generator analyzes daily weather data from specific locations to derive a set of parameters that govern the correlations and probability distributions of meteorological variables. (Semenov & Stratonovitch, 2010) provide additional information about the LARS-WG6 model and its use.

The LARS-WG modelling process is summarized in the stages below: Two input files must contain the data that the model needs. The second file is a site file that contains information on each station's location, including CO2 levels, its name, and its location. The main file contains observed daily climate data for each station in the examined basin region. Before proceeding to the following step, these files were prepared and verified for each of the thirteen stations.

Analytical process: Three location variable files are created for every place using the observed data once it has been processed. The place data file is located in the first file, "*.wgx". The third file, "*.tst," comprises the findings of statistical analyses that match recorded data with created data. Further statistics are contained in the second file, "*.stx."

Table (3.4): Situation of the climate places in the GZRB, northern Iraq, and integration of the Five Assessment Report (AR5) of the Intergovernmental Panel on Climate Change (IPCC) into the Long Ashton Research Station Weather Generator (LARS-WG6)

Sub-basin	Station name	Latitude (°)	Longitude (°)	Altitude (m)	Length of Records
Upstream	Koozerash	38° 9' 0"	44° 27' 36"	1344	1990 – 2022
	Mirbad	36° 58' 48"	45° 0' 36"	1650	1990 – 2022
	Piranshahr	36° 42' 0"	45° 7' 48"	1350	1990 – 2022
	Ravand urmia	37° 45' 0"	44° 45' 36"	1290	1990 – 2022
	Soran	36° 41' 24"	44° 41' 24"	1154	1990 – 2022
	Razi	38° 28' 48"	44° 21' 0"	1980	1990 – 2022
Downstream	Aqra	36° 44' 24"	43° 52' 48"	505	1990 – 2022
	Bashur	36° 22' 12"	44° 22' 48"	977	1990 – 2022
	Duhook	36° 41' 24"	43° 7' 48"	436	1990 – 2022
	Erbil	36° 3' 36"	44° 3' 36"	439	1990 – 2022
	Makhmoor	35° 45' 0"	43° 45' 0"	306	1990 – 2022
	Mousl	36° 22' 12"	43° 7' 48"	233	1990 – 2022
	Salahddin	36° 22' 12"	44° 3' 36"	507	1990 – 2022
GCM Models	Organization				Spatial Resolution
CanESM2	Canadian Centre for Climate Modeling and Analysis, Canada				2.8◦ × 2.8◦
CSIRO-Mk3.6.0	Commonwealth Scientific and Industrial Research Organization, Australia				1.8◦ × 1.8◦
HadGEM2-ES	Met Office Hadley Center, United Kingdom				1.2◦ × 1.8◦
MIROC5	Atmosphere and Ocean Research Institute (The University of Tokyo), National Institute for Environmental Studies, and Japan Agency for Marine-Earth Science and Technology, Japan				1.4◦ × 1.4◦
NorESM1-M	Norwegian Climate Center, Norway				2.0◦ × 2.0◦

3.8 Satellite-Based Indices

3.8.1 The Normalized Difference Vegetation Index (NDVI)

The Normalized Difference Vegetation Index (NDVI), which measures vegetation cover, is the most widely used. Depending on the grouping of the R band and NIR band wavelengths, the following equation can be used to estimate the near-infrared (Z. A. Mahdi & Mohammed, 2022)

$$NDVI = \frac{NIR\text{-}RED}{NIR+RED} \quad (3.1)$$

where NDVI stands for Normalized Difference Vegetation Index, NIR stands for the near-infrared band, and RED is the electromagnetic spectrum (EMS) by chlorophyll and other pigment absorption (0.76–0.9 m). In the EMS's NIR section, it has a high reflectance, though. Its digital number values between -1 and 1 represent non-vegetative features like the bare surface, populated areas, and water bodies; values between -1 and 0 represent vegetative cover characteristics. As shown in Table (3.5), there are three main NDVI classifications.

Table (3.5): NDVI classification values drought (Al-Quraishi et al., 2021)

Drought Classification	NDVI values
Extremely Low NDVI	NDVI ≤0.2
Low to Moderate NDVI	0.2 < NDVI ≤ 0.6
Moderate to High NDVI	0.6 < NDVI ≤ 1.0

Remote sensing phenology data from the USGS shows that areas with NDVI values less than 0.1 indicate bare rock, sand, or snow. NDVI values between 0.2 and 0.6 may specify modest plants, like grasslands and shrubs. NDVI values greater than 0.6 mean Dense vegetation, such as that found in temperate regions and tropical forests, or during the prime growth phases of crops. (Sun & Kafatos, 2007). The red band (0.63-0.69 m) In the visible range of the electromagnet, healthy vegetation reflects less.

3.8.2 Vegetation Condition Index (VCI)

It was developed to distinguish between environmental and meteorological NDVI factors and assess the condition of the vegetation(Gaznayee et al., 2021). It can be calculated using Equation (3.2).

$$VCI = \frac{NDVI - NDVI_{min}}{NDVI_{max} - NDVI_{min}} \times 100 \quad (3.2)$$

(Kogan, 1986) proposed a VCI based on the change in NDVI relative to the past NDVI minimum value. The VCI links the recent NDVI readings to those taken during similar periods in earlier years. The terms $NDVI_{min}$ and $NDVI_{max}$, which stand for the observation's minimum and maximum NDVI values, respectively, denote the NDVI value for the most recent month and the overall NDVI value.

Numerous studies used VCI as a tool to measure drought, but using just VCI values provided an insufficiently precise explanation of the state of the water shortage (Wan and Wang, 2004). According to the classification created by (Heydari et al., 2018)and (Karim et al., 2018), VCI values are classified in Table (3.6).

Table (3.6): Vegetation Condition Index (VCI) classification values in terms of drought (Gaznayee et al., 2021)

Drought Classification	VCI values
Extreme drought	VCI ≤ 10
Severe drought	10 < VCI ≤ 20
Moderate drought	20 < VCI ≤ 30
Mild drought	30 < VCI ≤ 40
No drought	VCI > 40

3.8.3 The Modified Soil-Adjusted Vegetation Index (MSAVI)

The MSAVI values range from -1 to 1, with -1 to 0 denoting non-vegetative features like bare ground, populated areas, and water bodies, and values greater than 0 indicate vegetative cover. By calculating a soil brightness correction factor more quickly and precisely, MSAVI is accurate for high-degree exposed soil areas (Gaznayee & Al-Quraishi, 2019) .

The key objective of this stage is to have a simply vegetated zone, which is calculated per pixel using the formula (3.5), and to conceal non-vegetated areas like home sites and roads.

$$MSAVI = \frac{\left(2\times NIR+1-\sqrt{\left((2\times NIR+1)^2-8\times(NIR-RED)\right)}\right)}{2} \quad (3.3)$$

3.8.4 The Land Surface Temperature (LST)

The L5 TM sixth band and the band 10–11 L8 TIRS were used to create the Landsat LST fraction images. Top-of-atmosphere radiances from TIR sensors can be used to calculate brightness temperature using Plank's law (Wan et al., 2010).

First, for the study basin five types of droughts, changes over the following 33 years were projected. The five types of dryness were then contrasted, and the dominant category was determined by which category differed most noticeably from the other four. The percentage of land that experiences each type of drought is then calculated for each period to show how the periods of drought have changed over time.

Digital values are converted into land surface temperatures using thermal DN numbers and satellite brightness temperature TB conversion equations.

$$TB = \frac{K_2}{Ln\left(\frac{K_1}{L_\lambda}+1\right)} \quad (3.4)$$

where K_1 = thermal conversion constant for a certain band (in Watts/m^2 × srad × μm); K_2 = thermal conversion constant that is band-specific (in kelvin); L_λ is the spectral radiance at the sensor's caperture, measured in watts/ (m^2 × star × μm).

Calculating the Kelvin value of LST:

$$T = TB/\left[1+\left(\frac{\lambda \times TB}{\rho}\right)\ln\varepsilon\right] \quad (3.5)$$

in which λ= the radiance's wavelength; $\rho = \frac{h \times c}{\sigma\ (1.438\ \times 10^{-2}\ \mathrm{m.K})}$;

h = 6.626 × 10^{-34} J.s (Plank's constant); σ = 1.38 × 10^{-23} J/K (Boltzmann's constant); c = light velocity (2.998 × 10^{8} m/s); ε = emissivity = 1.009 + 0.047 ln (NDVI). Kelvin to degree of Celsius conversion:

$$T_c = T - 273 \qquad (3.6)$$

where T is the temperature at the land's surface in Kelvin and T_c is the temperature at the same location in Celsius.

3.9 The Reconnaissance Drought Index (RDI)

The RDI can be expressed in standard (RDI_{st}), normalized (RDI_n), and initial (RDI_k) terms. In general, the standardized form is used to assess the severity of drought, while the initial form is employed as an aridity index.

The aridity index is primarily determined by accumulated precipitation and evapotranspiration potential. (R. Mohammed & Scholz, 2019; Tigkas et al., 2015). The estimation of RDI_{st} can be used to gauge how severe the drought is. This technique is popular, especially in arid and semi-arid areas of the world (Vangelis et al., 2013).

To calculate the $RDI_{\alpha k}$, the following equation is generally employed. (R. Mohammed & Scholz, 2019):

$$RDI_{i_{\alpha k}} = \frac{\sum_{j=1}^{12} P_{ij}}{\sum_{j=1}^{12} PET_{ij}} \qquad i=1 \text{ to } N \quad \text{and } j=1 \text{ to } 12 \qquad (3.7)$$

P_{ij} and PET_{ij} represent precipitation (mm) and potential evapotranspiration (mm), respectively, for the jth month of the ith hydrological year, which begins in October in Iraq.

N is the total number of years for the meteorological data. K is the time step being analyzed. For a variety of time scales under consideration, the RDI_k values match the gamma and lognormal distributions at various points. (Tigkas et al., 2015). Equation can be used to calculate RDI_{st} by using the

prior distribution (R. Mohammed & Scholz, 2019)

$$RDI_{st}^{i} = \frac{y_i - \bar{y}}{\hat{\sigma}} \quad (3.8)$$

where yi = ln (RDIαk) , ȳ it is algebraic mean and $\hat{\sigma}$ is the equivalent standard deviation.

Drought severity may be classified as shown in Table (3.7), (Ashraf et al., 2022).

Table (3.7): Drought classes for RDI

Drought classes		RDI_{st} value
wet	Severely	1.99 to 1.50
	Moderately	1.49 to 1.00
-	Normal	0.99 to 0.00
	Near normal	0.00 to -0.99
dry	Moderately	-1.00 to -1.49
	Severely	-1.50 to -1.99
	Extremely	≤ -2.00

CHAPTER FOUR
RESULTS AND DISCUSSIONS

4.1 Landsat Image Pre-Processing

All the Landsat (5 and 8) images were successfully mosaicked after converting them to top-of-atmosphere spectral reflectance values using ERDAS IMAGINE 2014 as shown in Figure (4.1) (as a sample). All of the Landsat (5 and 8) mosaic images were subtracted to extract the study area as shown in Figure (4.2).

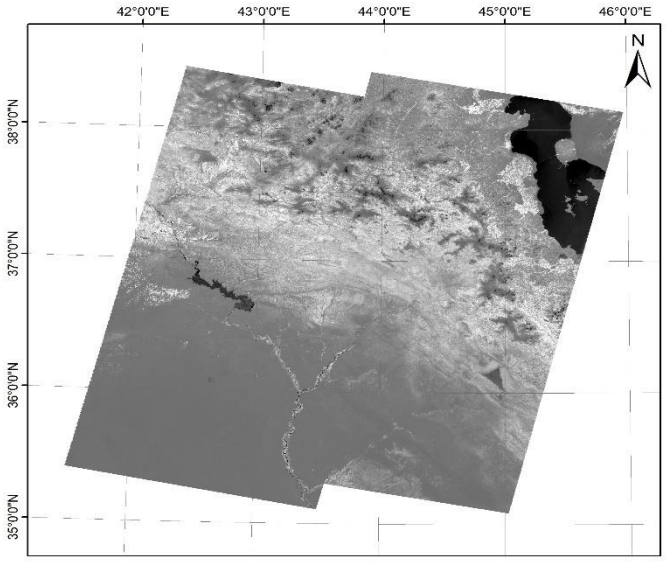

Figure (4.1): Mosaic Landsat 8 images (2020**)**

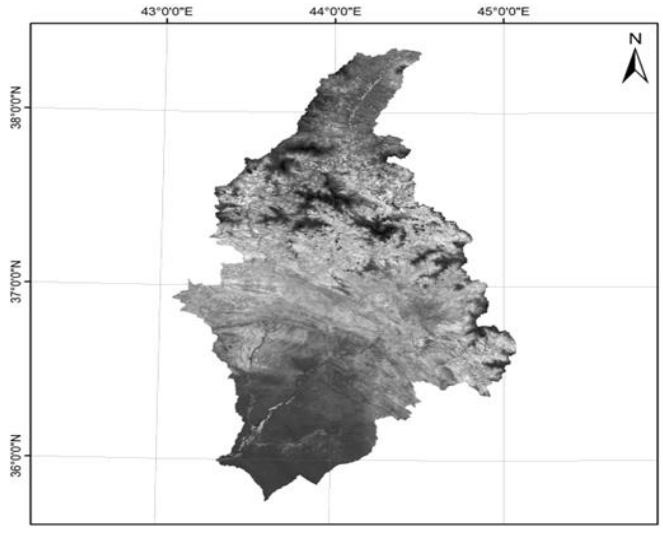

Figure (4.2): Study area of Greater Zap River (2020)

4.2 Indices-Based Drought Investigation

4.2.1 Spatio-Temporal Variation in NDVI

Equation (3.2) was used to compute the NDVI, for Landsat 8 where NIR is band 5 and RED is band 4, whereas used for Landsat 4 and 5 where NIR is band 4 and RED is band 3. For the period 1990 to 2022, each two-year's variation in spatio-temporal distribution of NDVI within the GZRB was illustrated in Figure (4.3) and (4.4). Also, statist of measures of NDVI values and vegetation density (VD) classes are depicted in Table (4.1). As was mentioned, the severe and extreme years of drought that hit Iraq caused a reduction in the area of vegetation cover, which resulted in significant decreases in the vegetation cover in the GZRC from 2000 to 2008. In 2000 and 2002, the total area covered by vegetation was 21500.7 km^2 (81.7%), and 20587.0 km^2 (78.2%) of the total area of GZRB respectively. Such deterioration can be mostly recognized by the severe drought events that hit the country, together with the GZRB in 2000 and 2008, besides a noticeable decline in mean precipitation.

Conversely, the maximum extent of high VD (class 3) was measured in 2020 at 4736.6 km^2 (18.5%). The lowest NDVI is computed in 2000, 2002, and 2008, with values of 0.2, 4.3, and 0.1. Are shown in Table (4.1), according to the findings of low VD (class 1), the biggest areas of this class were computed in 2000 and 2008, which is 11131.6 km^2 (51.8%) and 11837.7 km^2 (47.9%), respectively. However, Areas of moderate VD (class2) were computed in 2000 and 2008, measuring 10335.0 km^2 (48.1%) and 12872.8 km^2 (52.1%), respectively. These areas had values of NDVI between 0.2 and 0.6. It can be noted that while the drought had little to no (or barely any) impact in the northeastern parts of the basin, it had a significant impact on some southern GZRB areas.

The severity of the drought in the GZRB increased gradually as one moved southwest. There are numerous ongoing Class 1 drought areas (value

= 0.2). Actual drought episodes observed in the GZRB in 2000, 2002, and 2008 are revealed in Table (4.1) and Figure (4.3). In the three years of the drought, the NDVI-based low-vegetation class, in particular, increased, reaching 11131.6 km^2 (51.8%), 9531.6 km^2 (44.8%), and 11837.7 km^2 (47.9%), respectively, in 2000, 2002, and 2008. According to the maps in Figure (4.3), the driest years for the region, particularly in the southern part of the basin, occurred between 2000 and 2008.

Table (4.1): The NDVI-Based Vegetation Density Classes, Area of Vegetation Cover (VC), and the statistical Properties of NDVI Values in GZRB between 1990 and 2022

Years	Max[1]	Min[2]	Mean	SD[3]	Class 1[a]		Class 2[b]		Class 3[c]	
					Area		Area		Area	
					km^2	%	km^2	%	km^2	%
1990	1	-1	0.30	0.20	7856.1	31.3	15739.1	62.7	1514.3	6.0
1992	0.85	-0.75	0.24	0.19	9427.9	38.3	14803.0	60.2	372.6	1.5
1994	0.84	-0.64	0.33	0.20	5734.2	22.9	17090.2	68.4	2163.9	8.7
1996	0.96	-1	0.25	0.19	9680.0	39.3	14001.9	56.8	956.6	3.9
1998	0.88	-0.54	0.31	0.22	6903.4	28.1	14921.8	60.8	2701.0	11.0
2000	0.85	-1	0.15	0.15	11131.6	51.8	10335.0	48.1	34.1	0.2
2002	1	-1	0.17	0.25	9531.6	46.3	10170.1	49.4	885.3	4.3
2004	0.9	-0.62	0.32	0.18	7959.2	30.5	16090.3	61.6	2076.5	7.9
2006	0.93	-1	0.30	0.19	8157.7	32	15527.9	60.9	1813.6	7.1
2008	0.8	-0.45	0.20	0.14	11837.7	47.9	12872.8	52.1	12.5	0.1
2010	0.93	-1	0.30	0.17	8663.3	33.4	16118.6	62.2	1131.8	4.4
2014	1	-1	0.36	0.2	6202.8	23.8	16562.3	63.6	3261.4	12.5
2016	1	-1	0.38	0.20	5288.8	20.3	16662.5	63.9	4107.2	15.8
2018	1	-1	0.38	0.19	5968.6	22.8	16332.3	62.5	3837.8	14.7
2020	1	-1	0.39	0.20	3628.6	14.2	17211.0	67.3	4736.6	18.5
2022	1	-1	0.34	0.18	7091.2	27.0	16580.0	63.2	2566.1	9.8

[1]Maximum; [2]Minimum; [3]Standared deviation; [a] NDVI values < 0.2 (very low) ; [b] 0.2 < NDVI values < 0.6 (low to moderately low); [c] 0.6 < NDVI values < 1 (moderately high to high); Total basin area = 26330.2 km2

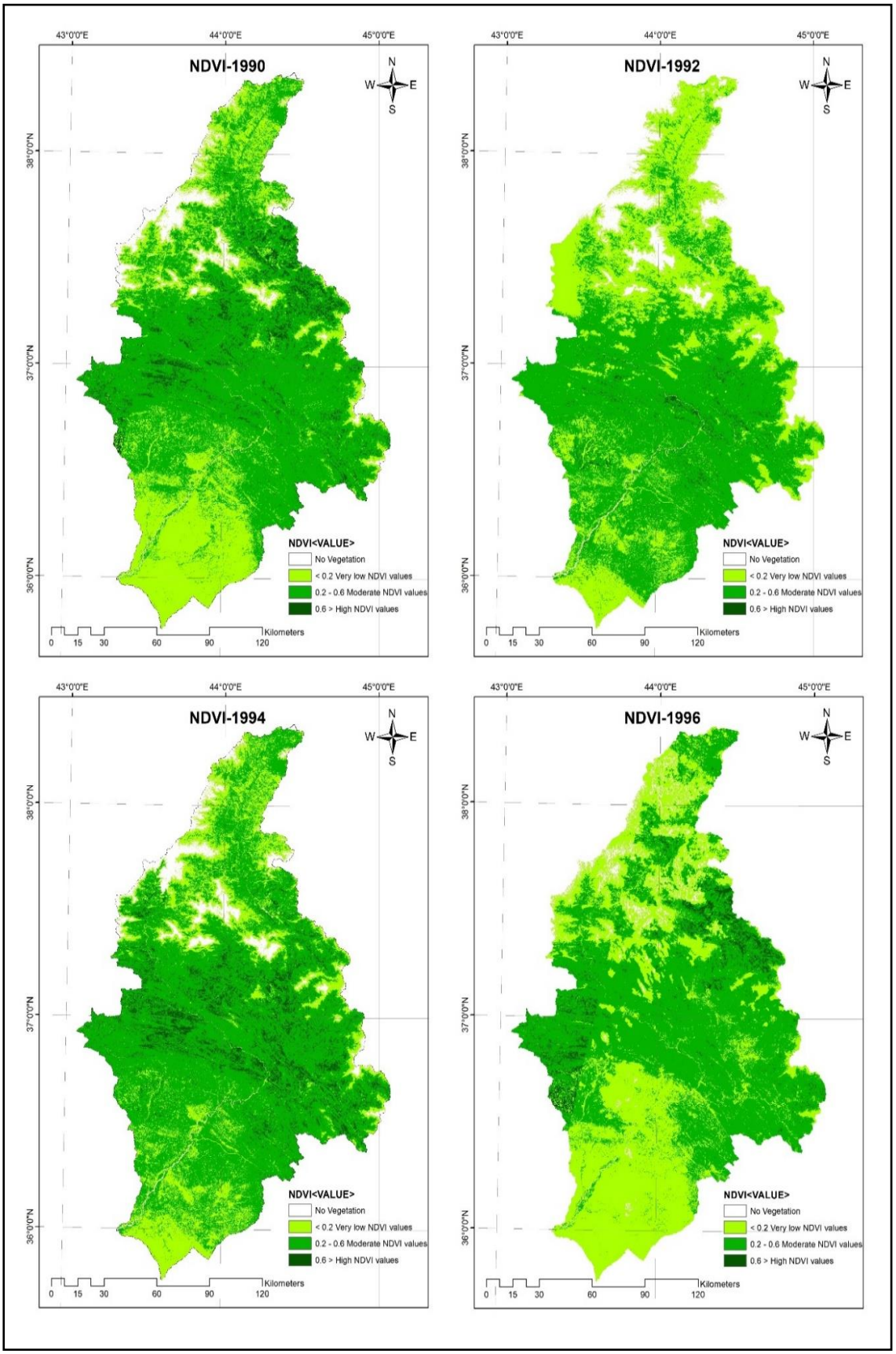

Figure (4.3): Spatial variation of NDVI-based within the GZRB for the period between 1990 and 2022

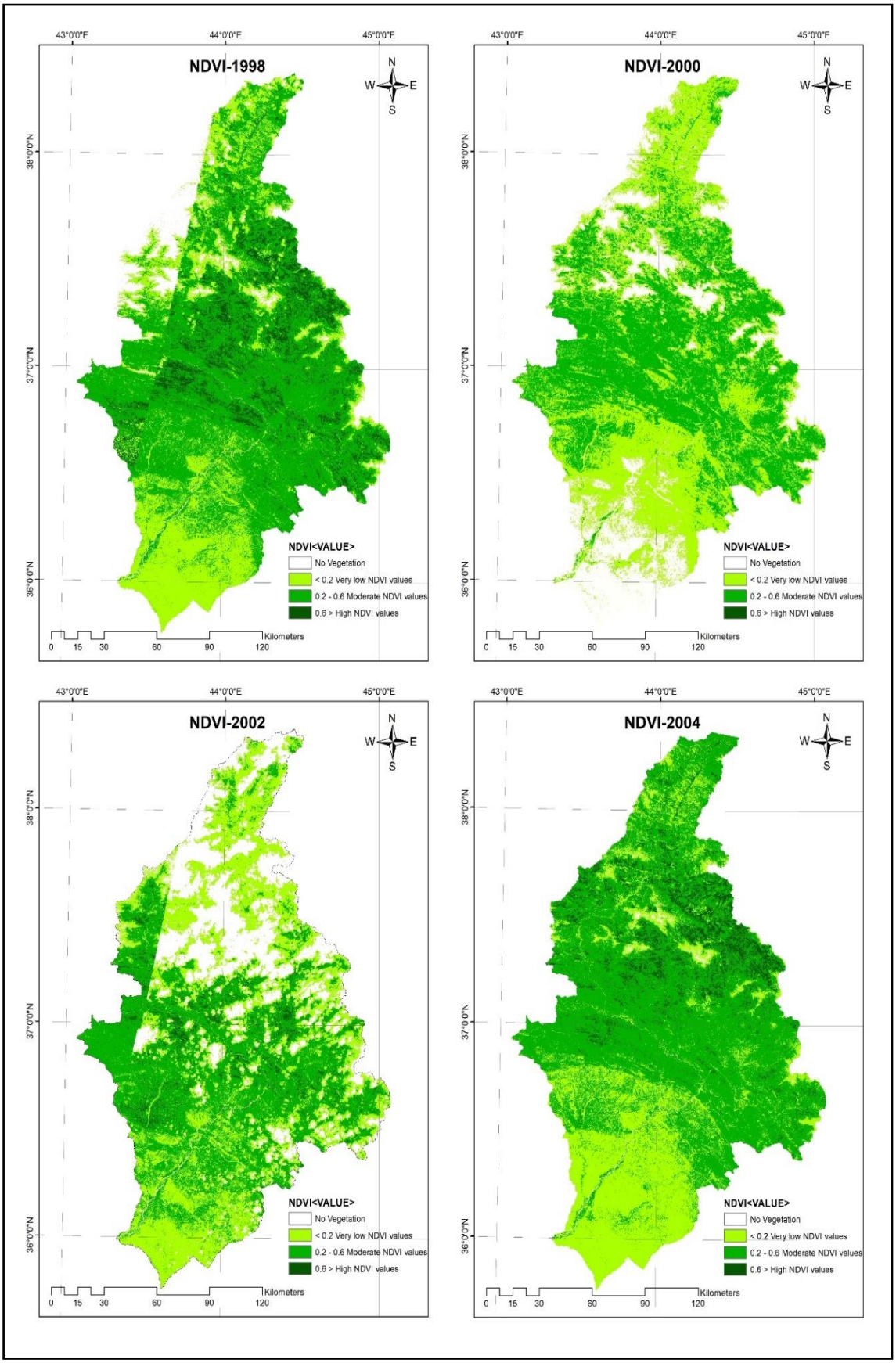

Figure (4.3) Continue…

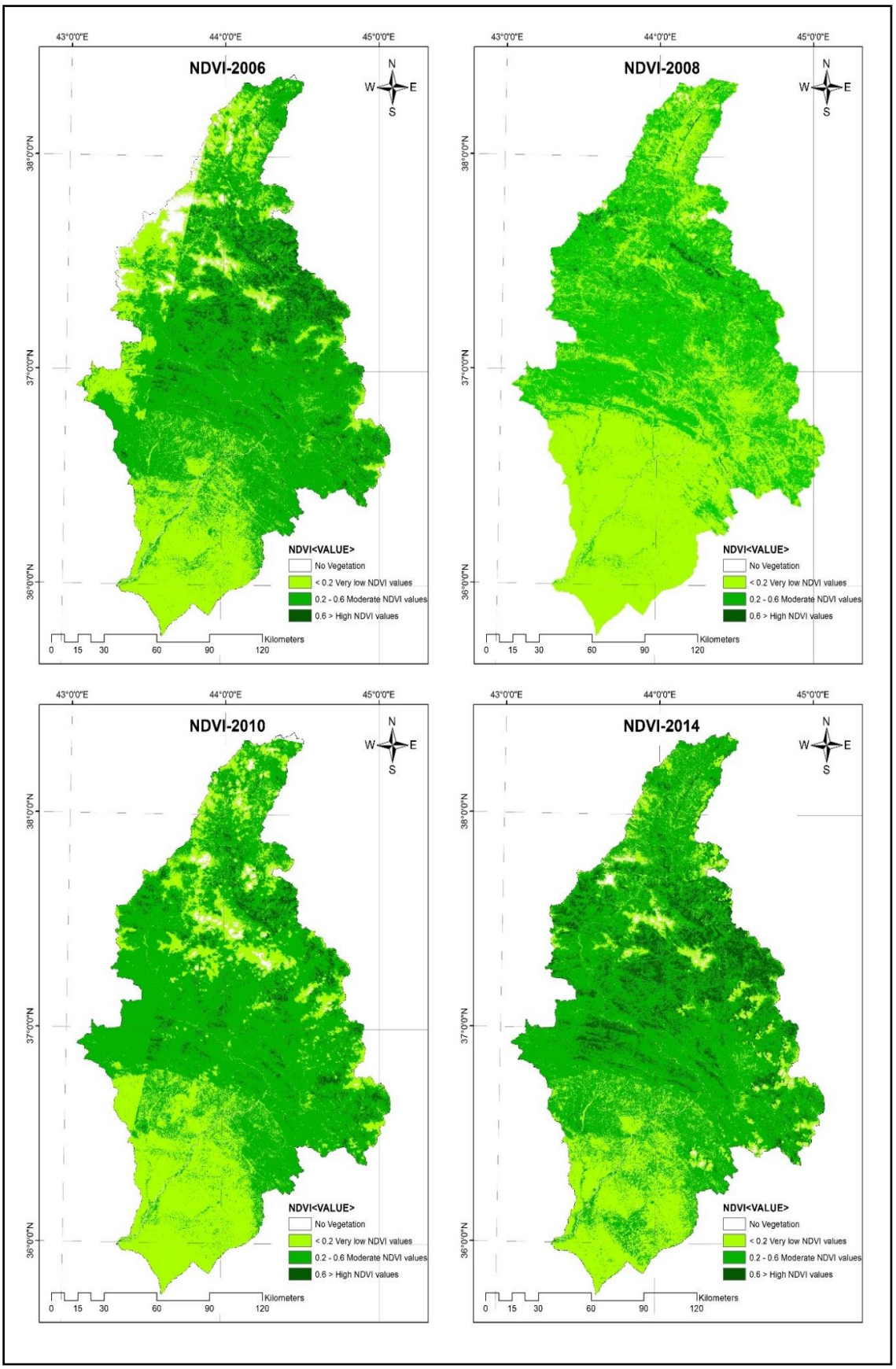

Figure (4.3) Continue…

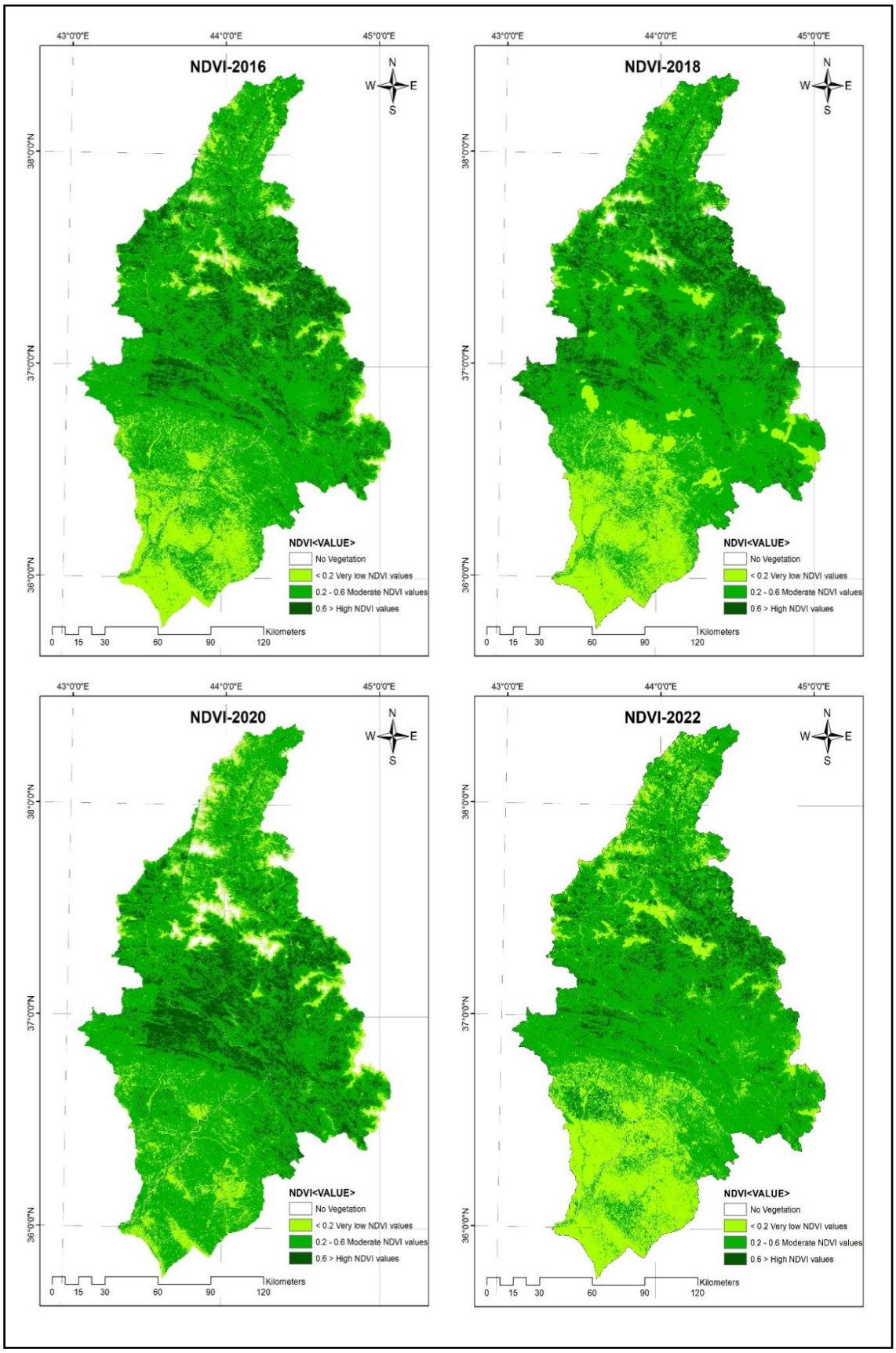

Figure (4.3) Continue…

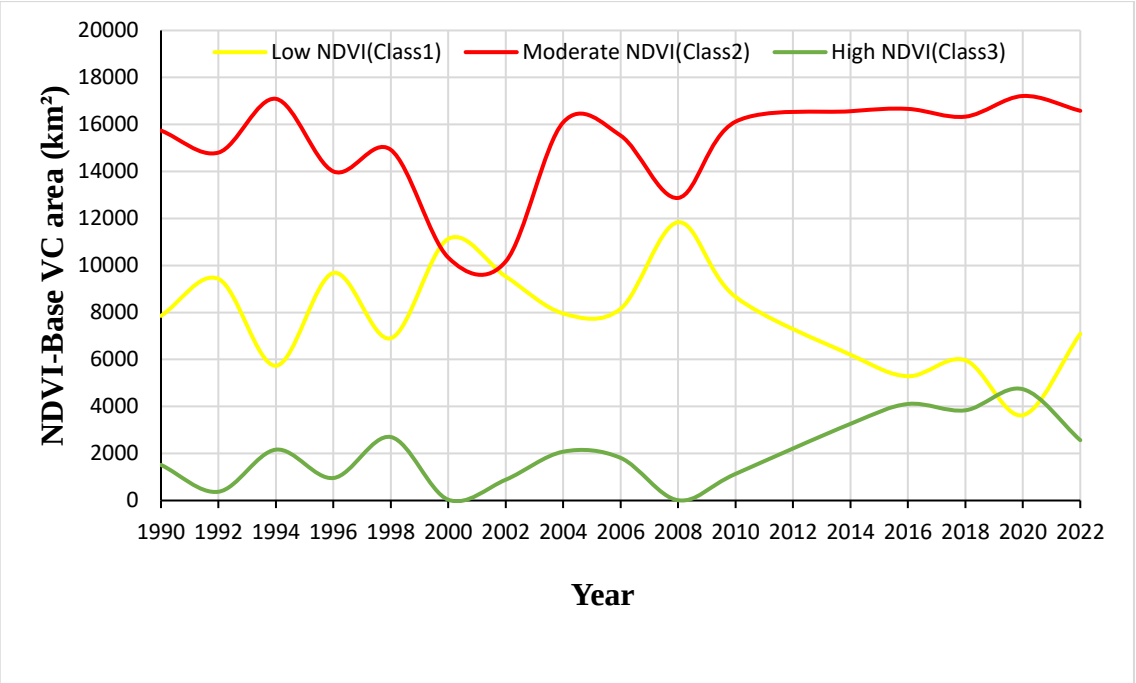

Figure (4.4): Temporal variation in NDVI-Based VC with the GZRB for the period (1990-2022)

4.2.2 Spatio-Temporal Variation in VCI

Equation 3.4 was used to compute VCI, see Figures (4.5) and (4.6) According to the VCI findings, severe drought events happened in 1996, 2000, 2004, and 2008 as shown in Table (4.2). The four years with the highest likelihood of experiencing a drought according to the VCI index, were 1996, 2000, 2004, and 2008. Values for the VC went from 0 (no vegetation) to 40 (dense vegetation). It was noticeably lower than the other years in the investigated period. 2000 was the driest year in the considered period because it was the year when the drought reached its worst point. The area experienced moderate to severe drought during 1996, 2000, 2004, and 2008, especially in 2000 and 2008. Except for a few small northern patches, 2008 was a worst year for drought, with severe conditions throughout the studied region.

North, east, center, and south of the GZRB, the combined areas of severe and extremely severe drought were 8110.3 km^2 (39.4%), 5,544.6 km^2 (26.9%), 3,314.6 km^2 (16.1%), and 1,848.6 km^2 (9%), respectively. The south and

middle parts of GZRB typically experienced the most extreme droughts, according to the VCI as in Figures (4.5) and (4.6) and Table (4.2).

Extreme, severe, moderate, mild, and no drought conditions covering 3050.1 km^2 (11.6%), 2,964.4 km^2 (11.3%), 3,634.0 km^2 (13.8%), and 4,194.6 km^2 (15.9%) and 12,487.4 km^2 (47.4%) of the total area, were all experienced by the GZRB in 2008. The largest (class 1) area was recorded in 2000, when the extreme drought area increased by 11972.7 km^2 (45.5%), according to the Extreme Drought Class (VCI≤10) results.

Table (4.2): The VCI-Based Vegetation Density Classes, Area of Vegetation Cover, and the statistical Properties of VCI Values in GZRB between 1990 and 2022

Years	Class 1[a]		Class 2[b]		Class 3[c]		Class 4[d]		Class 5[e]	
	Area		Area		Area		Area		Area	
	km^2	%	km^2	%	km^2	%	km^2	%	km^2	%
1990	880.1	3.3	757.9	2.9	1278.1	4.9	2322.5	8.8	21091.6	80.1
1992	4031.1	15.3	1878.2	7.1	2056.8	7.8	2677.9	10.2	15686.2	59.6
1994	708.4	2.7	722.0	2.7	856.5	3.3	1363.9	5.2	22679.6	86.1
1996	3317.2	12.6	2501.8	9.5	3361.3	12.8	3527.2	13.4	13613.7	51.7
1998	2196.1	8.3	1023.8	3.9	1328.0	5.0	1951.8	7.4	19830.7	75.3
2000	11972.7	45.5	2309.1	8.8	2467.4	9.4	2665.0	10.1	6916.3	26.3
2002	10451.5	39.7	1279.9	4.9	1174.9	4.5	1652.8	6.3	11771.1	44.7
2004	1275.6	4.8	2291.2	8.7	2964.6	11.3	2803.4	10.6	16995.4	64.5
2006	1780.4	6.8	1455.7	5.5	2043.3	7.8	2756.1	10.5	18294.7	69.5
2008	3050.1	11.6	2964.4	11.3	3634.0	13.8	4194.6	15.9	12487.0	47.4
2010	1470.6	5.6	2106.5	8.0	2473.9	9.4	2567.5	9.8	17677.0	67.2
2014	692.3	2.6	650.7	2.5	1408.3	5.3	2270.0	8.6	21309.1	80.9
2016	323.7	1.2	608.5	2.3	1059.7	4.0	1624.0	6.2	22714.6	86.3
2018	685.5	2.6	930.4	3.5	1521.6	5.8	1746.9	6.6	21446.1	81.4
2020	425.6	1.6	465.6	1.8	628.2	2.4	849.4	3.2	23961.6	91.0
2022	612.4	2.3	1339.0	5.1	2093.3	8.0	2483.0	9.4	19802.9	75.2

[a] VCI values ≤ 10 (extreme); [b] 10 < VCI values ≤ 20 (severe); [c] 20 < VCI values ≤ 30 (moderate); [d]30 < VCI values ≤ 40 (mild); [e] VCI values > 40 (no)

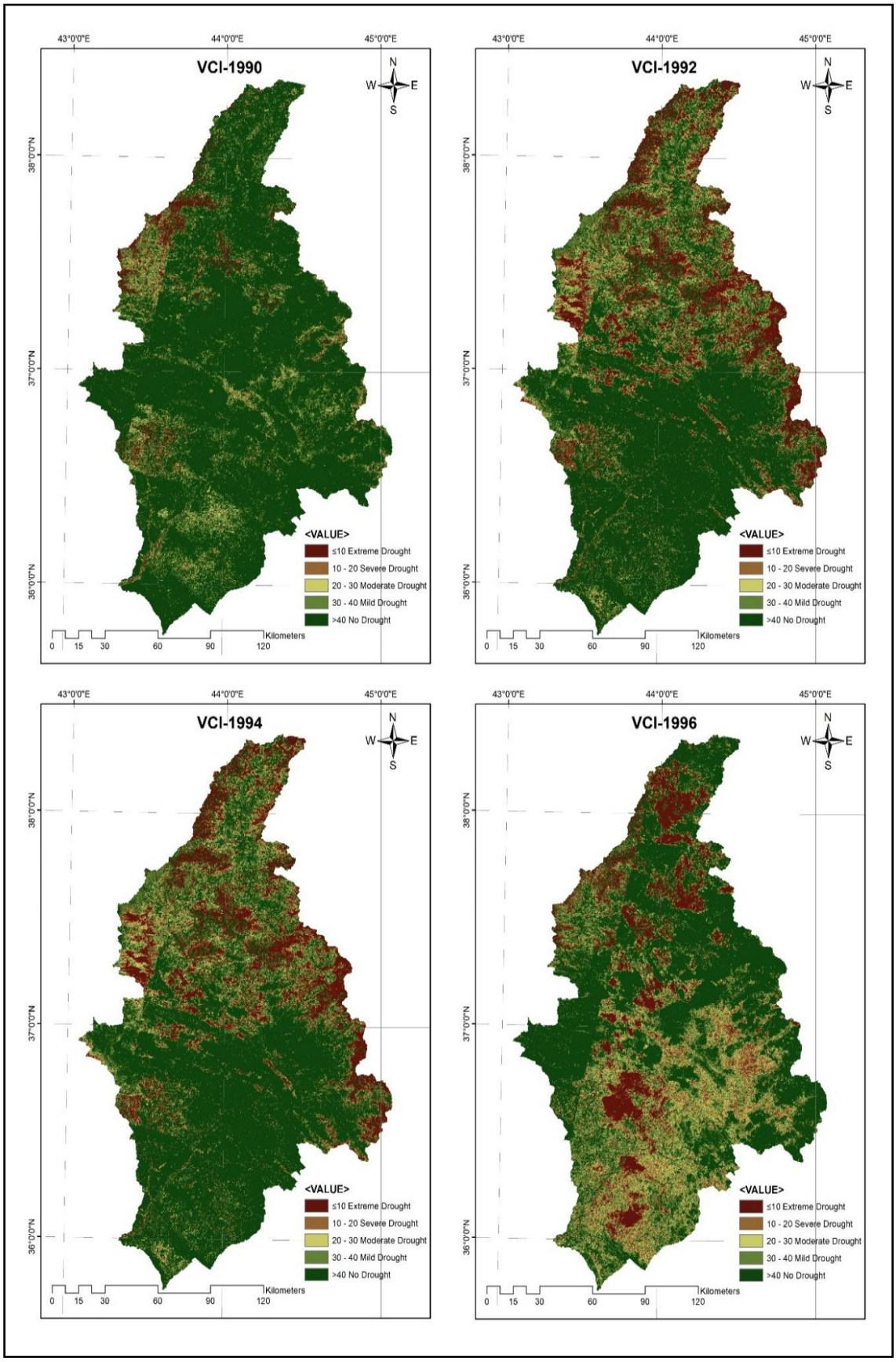

Figure (4.5): Spatial variation of VCI within the GZRB for the period 1990 and 2022.

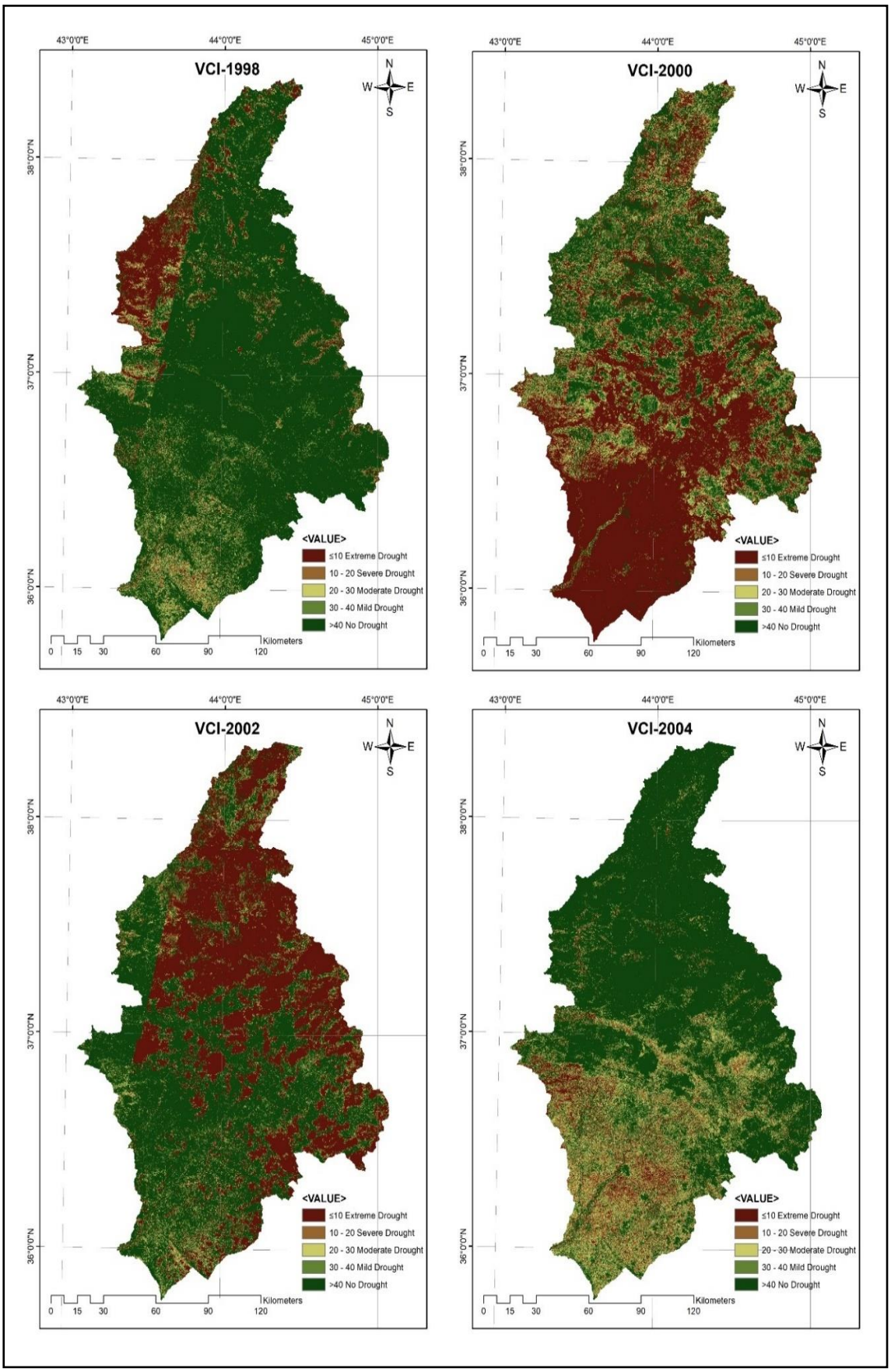

Figure (4.5) Continue…

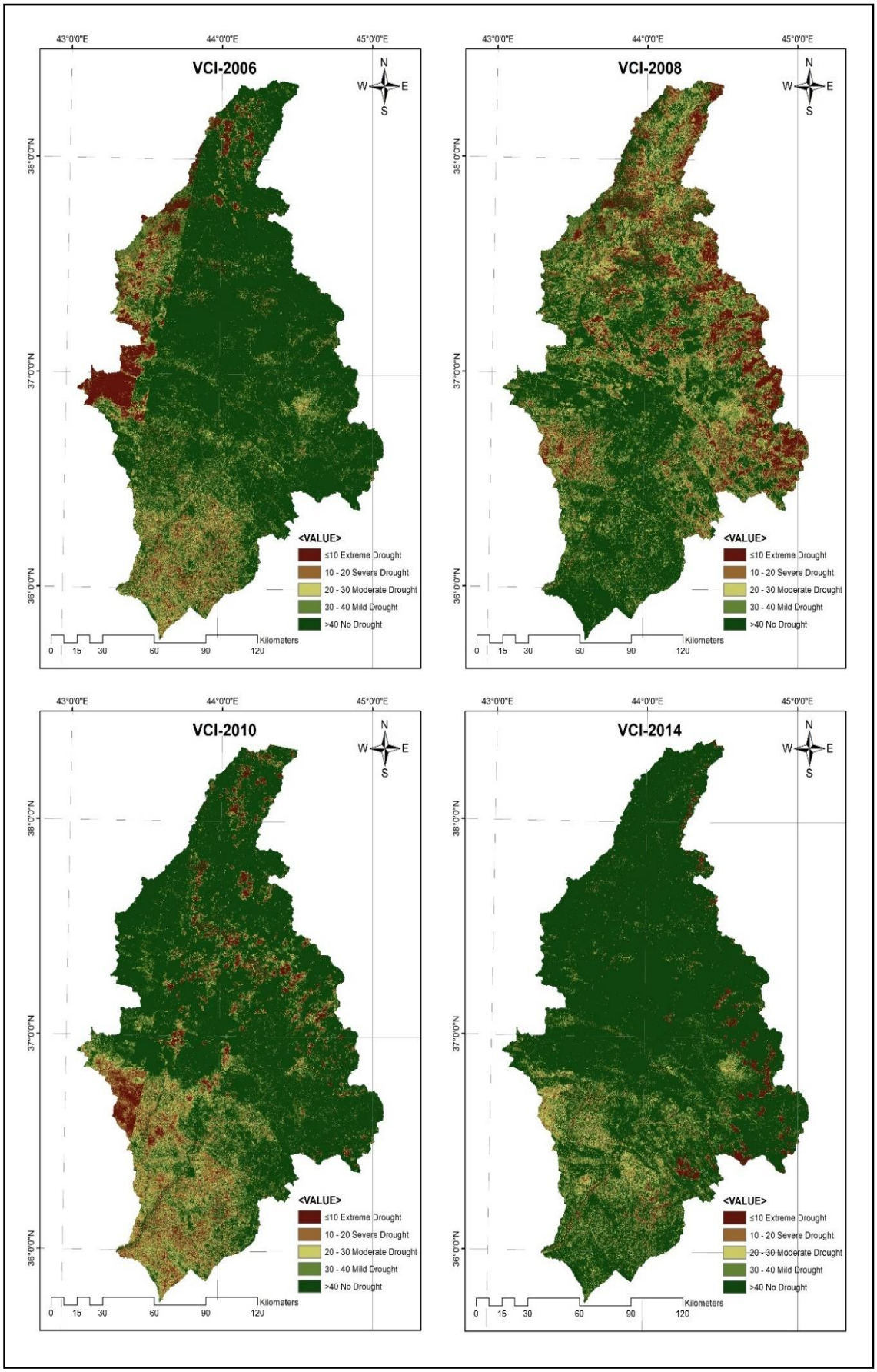

Figure (4.5) Continue…

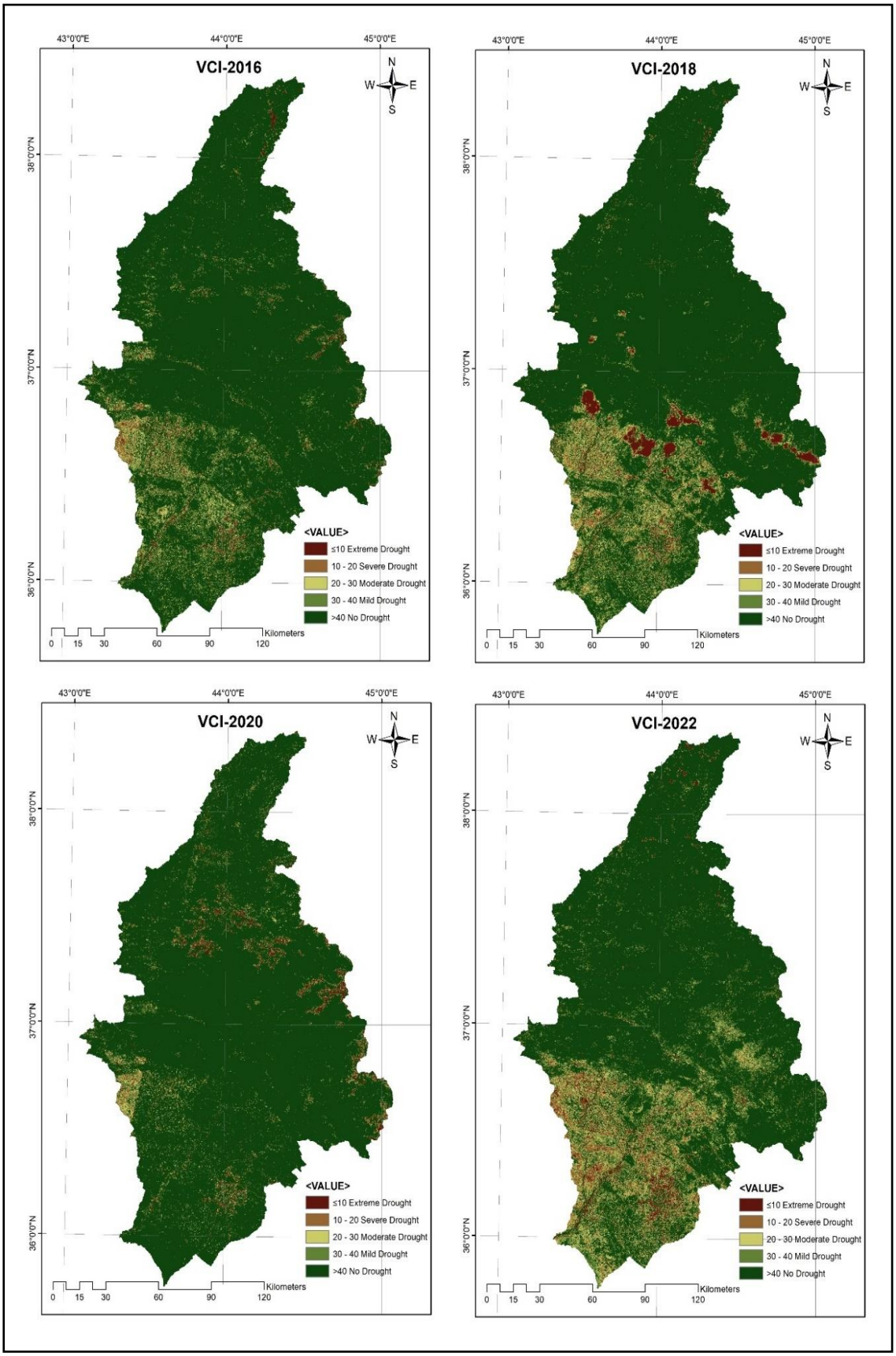

Figure (4.5) Continue…

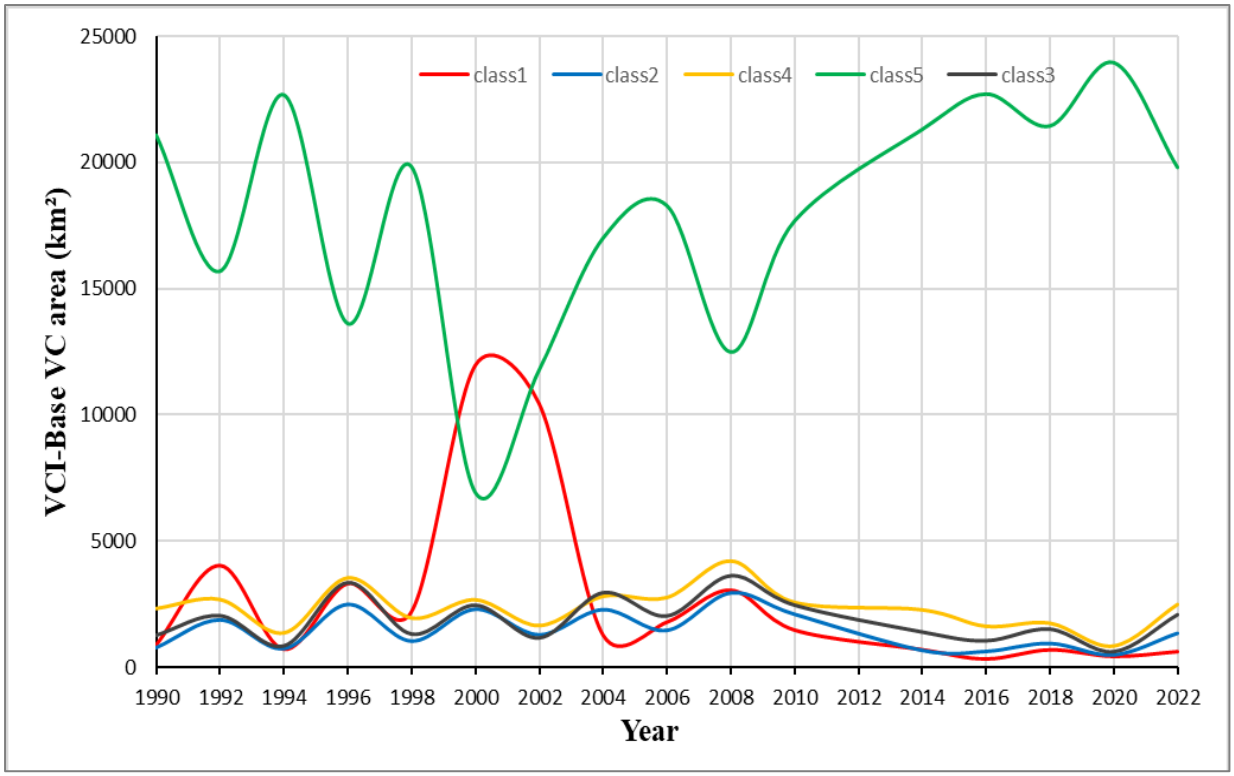

Figure (4.6): Temporal variation in VCI-Based VC with the GZRB for the period (1990-2022)

4.2.3 Spatio-Temporal Variation in MSAVI

Equation 3.5 was used to compute MSAVI, for Landsat 8 NIR is band 5, RED is band 4, and for Landsat 4 and 5 NIR is band 4, and RED is band 3, see Figure (4.7) and (4.8).

The MSAVI, as well as its variations, and derivatives, are beneficial for monitoring droughts. Table (4.3) provides statistics for the years 1990 through 2022. The findings revealed that the MSAVI's lowest mean values for 2002 were 0.08.

The decrease in values referred to annual rainfall, which is regarded as a critical factor influencing vegetation cover growth in the basin. The MSAVI reached its highest mean value of 0.24 in 2016, 2018, and 2020; a high value indicates healthy vegetation. MSAVI is near or equal to zero, which refers to arid land without vegetation.

Figure (4.7) presents during the thesis period. Almost every site in the basin was impacted by the drought during the growing season. The growing

seasons of 2002 show the greatest reduction in MSAVI-based vegetation cover during that season. According to Table (4.3), the entire zone of severe drought in the basin with MSAVI mean values less than 0.2 was 13667.5 km^2 or 66.5% of the overall part. The northern areas of the province's research area show a decline in vegetation. This decrease may also be related to a difference between normal precipitation and plant needs during the critical growing phase.

Table (4.3): The MSAVI-Based Vegetation Density Classes, Area of Vegetation Cover, and the statistical Properties of MSAVI Values in GZRB between 1990 and 2022

Years	Max[1]	Min[2]	Mean	SD[3]	Class 1[a]		Class 2[b]		Class 3[c]	
					Area		Area		Area	
					km^2	%	km^2	%	km^2	%
1990	0.82	-0.71	0.19	0.15	13560.0	54.0	11521.5	45.9	28.0	0.1
1992	0.72	-0.95	0.15	0.15	15524.6	63.1	9078.5	36.9	0.2	0.0
1994	0.74	-0.67	0.20	0.15	12070.0	48.3	12909.3	51.7	9.0	0.0
1996	0.95	-1	0.15	0.15	16238.5	65.9	8349.3	33.9	50.6	0.2
1998	0.82	-0.72	0.19	0.17	12804.3	52.2	11618.7	47.4	103.1	0.4
2000	0.79	-0.68	0.17	0.11	13035.7	60.6	8460.3	39.3	4.8	0.0
2002	0.98	-1	0.08	0.23	13667.5	66.5	6881.1	33.5	13.9	0.1
2004	0.85	-0.70	0.20	0.12	14597.1	55.9	11393.3	43.6	132.3	0.5
2006	0.95	-1	0.19	0.15	13688.0	53.9	11600.3	45.7	90.9	0.4
2008	0.63	-0.69	0.12	0.10	19798.5	80.1	4904.5	19.9	0.0	0.0
2010	0.95	-1	0.19	0.12	14739.4	56.9	11125.3	42.9	43.4	0.2
2014	0.99	-0.19	0.22	0.12	13124.3	50.4	12727.8	48.9	188.8	0.7
2016	0.88	-0.22	0.24	0.13	11501.2	44.1	14283.4	54.8	274.3	1.1
2018	0.92	-0.16	0.24	0.13	11354.7	43.4	14555.7	55.7	229.0	0.9
2020	0.90	-0.19	0.24	0.13	9960.5	38.9	15516.2	60.7	99.6	0.4
2022	0.87	-0.19	0.22	0.12	12933.0	49.3	13068.6	49.8	239.2	0.9

[1]Maximum; [2]Minimum; [3]Standared deviation; [a] MSAVI values < 0.2 (very low); [b] 0.2 < MSAVI values < 0.6 (low to moderately low); [c] 0.6 < MSAVI values < 1 (moderately high to high); Total basin area = 26330.2 km^2

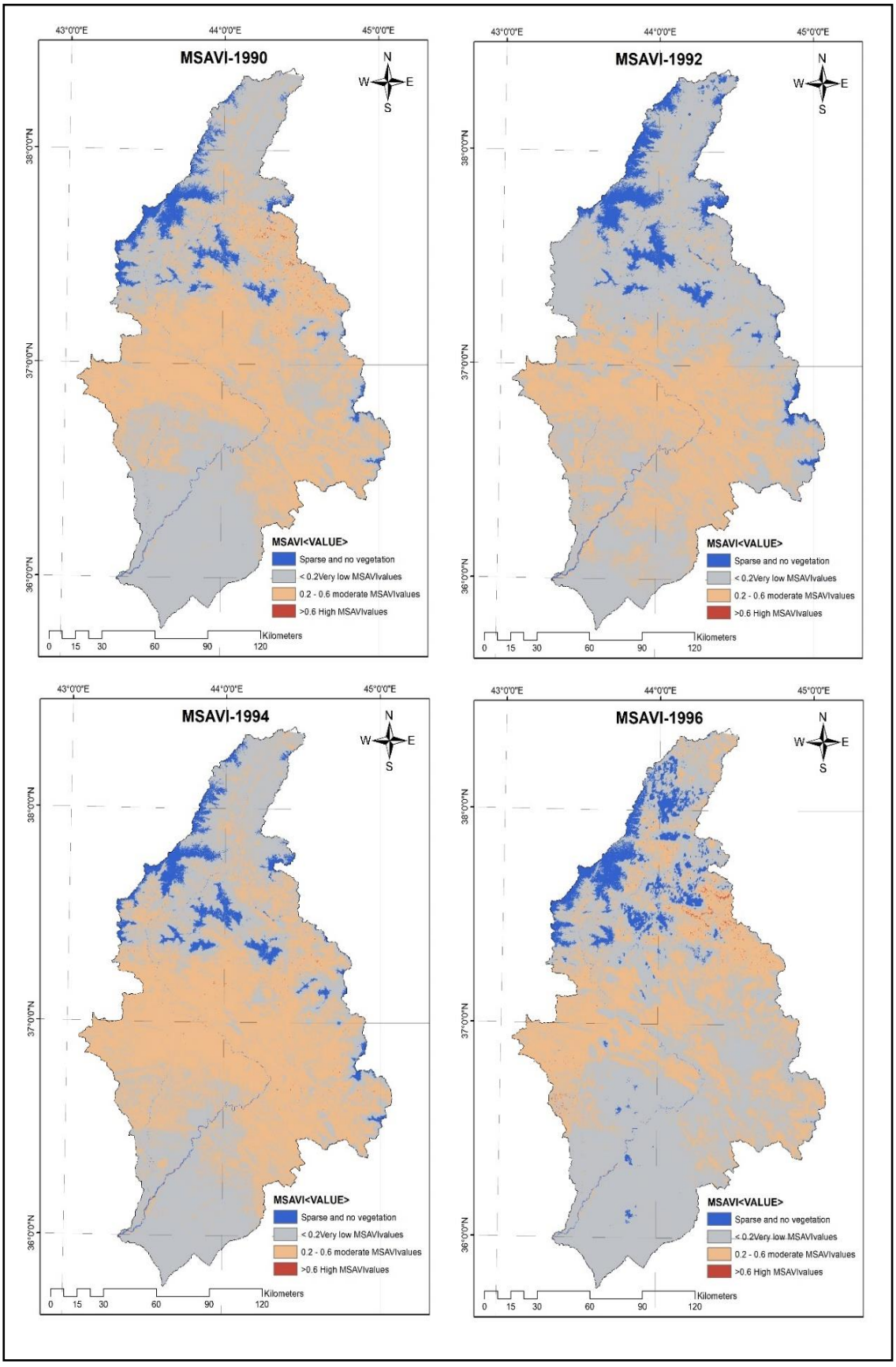

Figure (4.7): Spatial variation of MSAVI within the GZRB for the period between 1990 and 2022

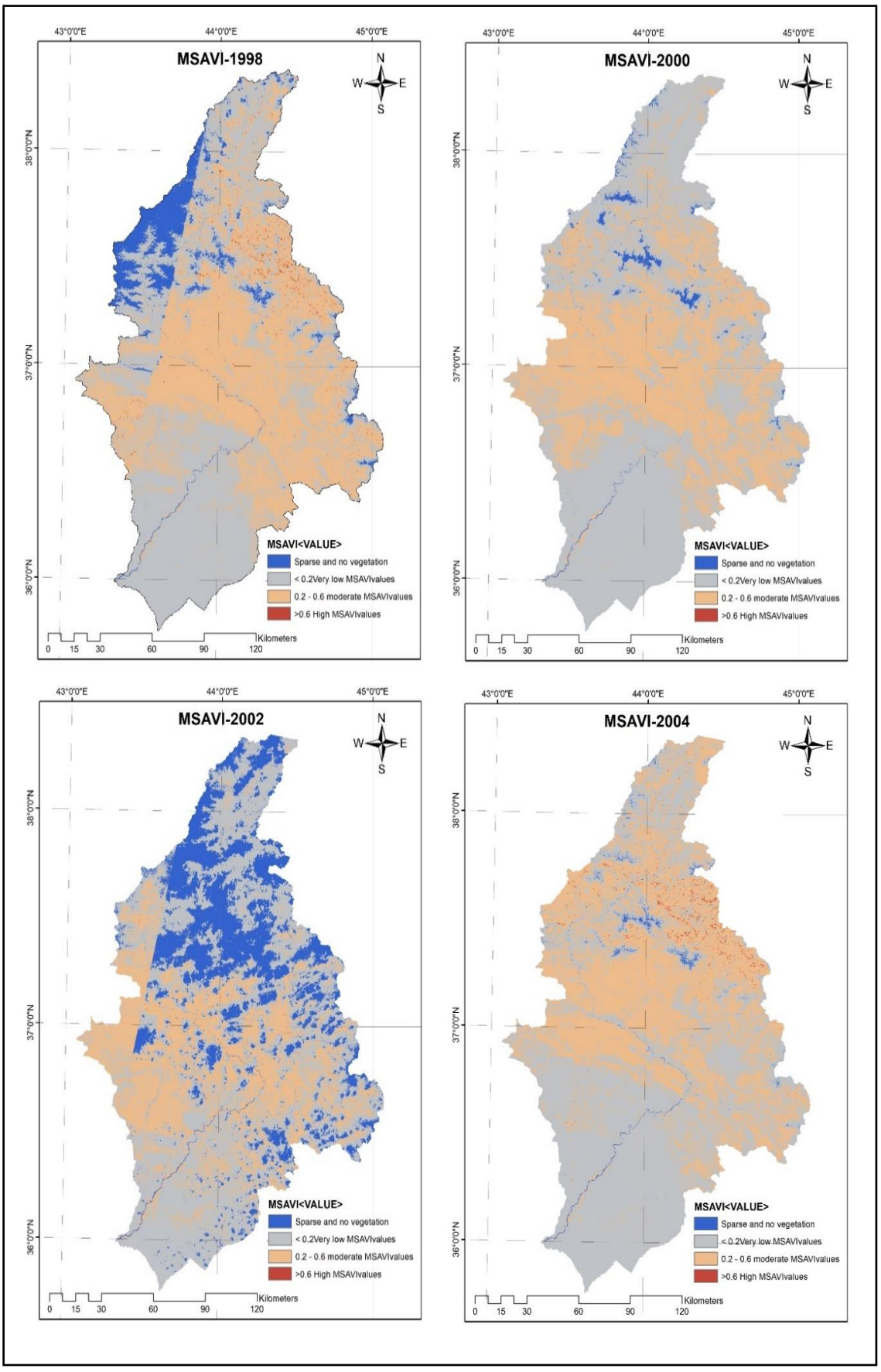

Figure (4.7) Continue…

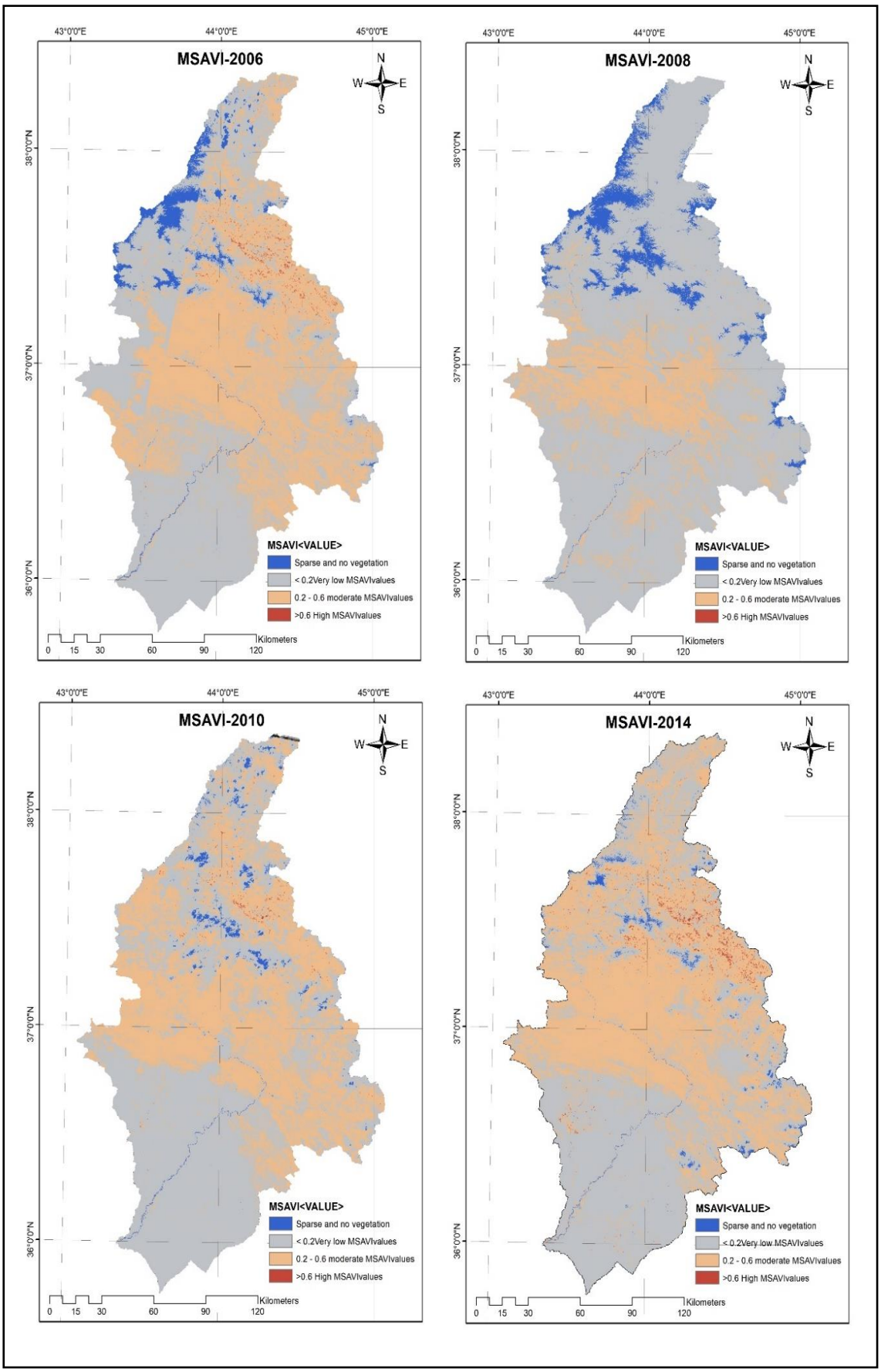

Figure (4.7) Continue…

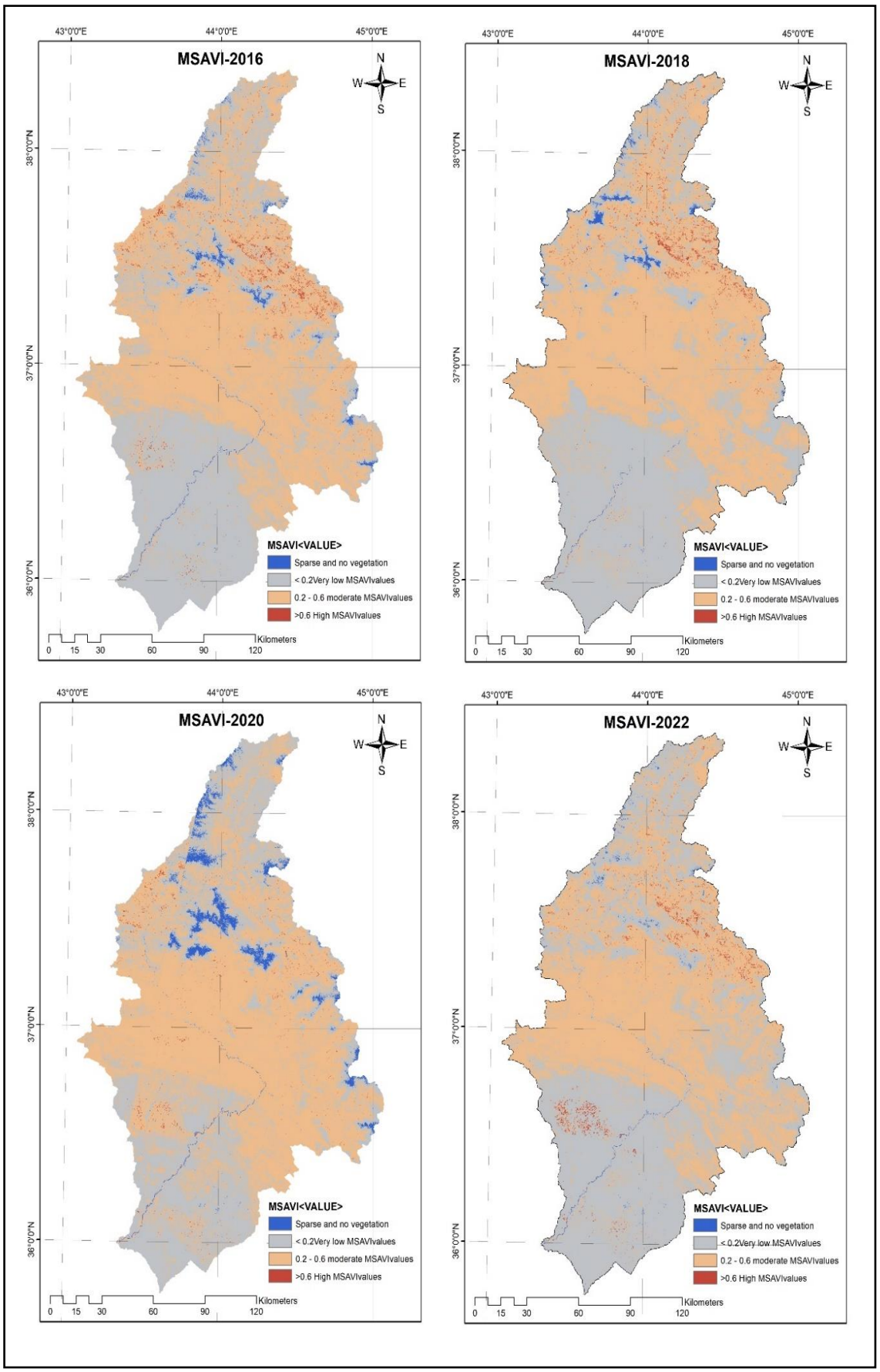

Figure (4.7) Continue…

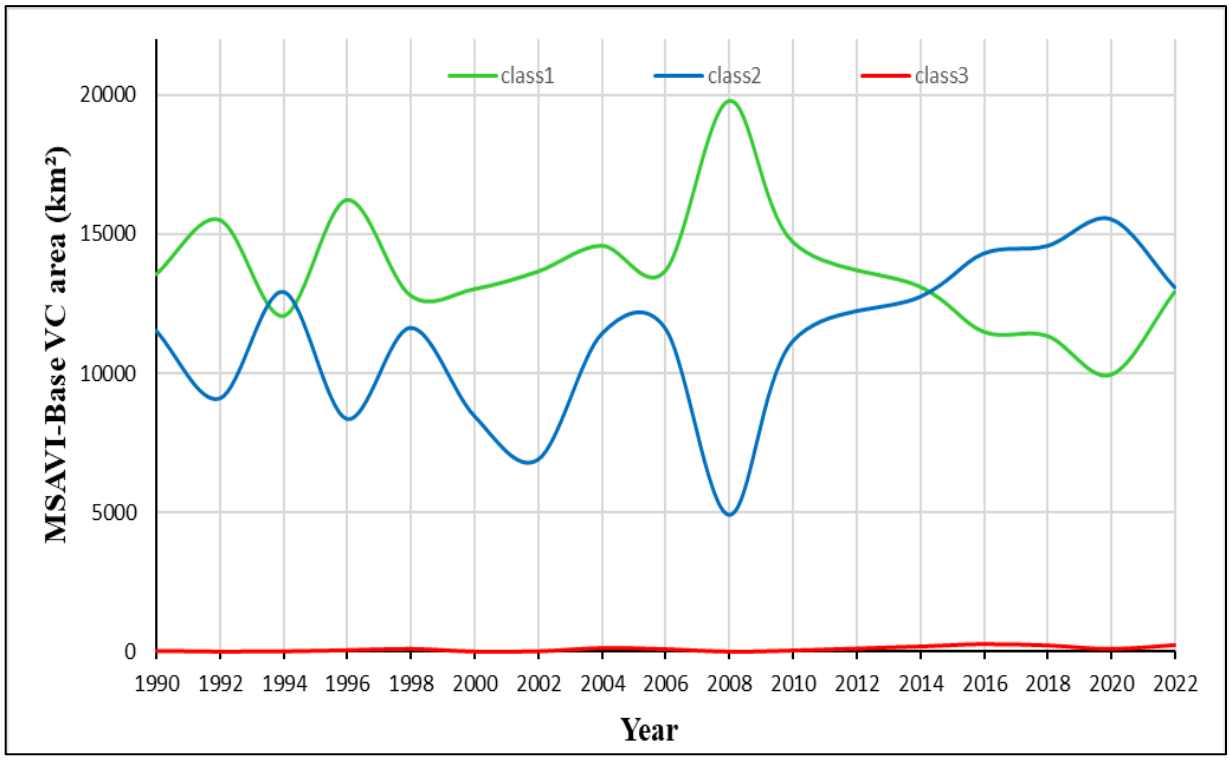

Figure (4.8): Temporal variation in MSAVI-Based VC with the GZRB for the period (1990-2022)

4.2.4 Spatio-Temporal Variation in LST

Equations (3.6, 3.7 and 3.8) were used to compute LST, for Landsat 8 is band 10 and Landsat 4 and 5 is band 6, see Figures (4.10) and (4.11) and Table (4.4). The thermal infrared data of the Landsat agreement can be used to express the LST and specify the presence of drought, which was used to create the LST fraction images. Figures (4.10), show the LST status of the basin from 1990 to 2022. First, the modifications in the five drought classes in the study area over 32 years were determined. The variations among the five types of droughts were contrasted.

Comparing the category that had the biggest change to the other four categories, it was found that the treatment was comparative. The temporal changes were then calculated for each drought category area. Figure (4.9) compares the LST average over the 32 years in the GZRB between 1990 and 2022 with the LST mean values every year during the studied period. Despite a cooling trend, for 2002 (17.8°C) and 2018 (18.2°C), GZR's temperature

rate steadily increased. In 2014, the LST temperature was 37.56°C. The rate of the LST significantly rose in the period and surpassed that of 2002. The class 5 region, with an LST value area greater than 40°C between 2004 and 2014, had the highest LST value. In class 5 (40°C), 11193.6 km^2 (42.6%) of the basin was impacted by a severe drought. Only 0.1% of the study area had the coldest temperatures in 1994, 1998, 2002, 2018, and 2022.

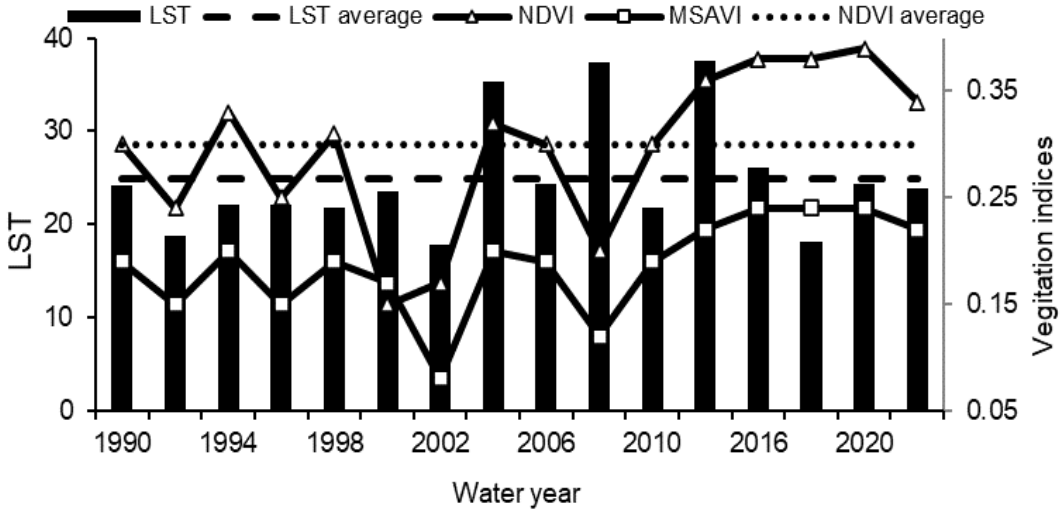

Figure (4.9): Average annual values of LST, NDVI and MSAVI over the GZRB for the period between 1990 and 2022

Over the past 32 years, very severe drought episodes have affected significant portions of the southern regions of the GZRB, whereas most of the other areas of the study area have only experienced mild to moderate droughts depending on LST as shown in Figure (4.10). The study area's southern regions were warmer than its other regions. The highest mean LST fluctuated between 37.28°C in 2008 and 37.56°C in 2014.

The area covered by vegetation, which was primarily found in lower-elevation lands, decreased due to a lack of precipitation, which also resulted in a lack of moisture and a rise in LST. The drop in vegetation cover in the southeast and southwest is one impact of the rise in LST, as shown by the NDVI of the basin. This illustrates the detrimental effects of high LST on the

vegetation-growing atmosphere, which resulted in a reduction in the area covered by vegetation (NDVI).

Only a few locations in the northeast of the basin had a rise in precipitation rates and a decrease in LST values that was reflected in the increased vegetation (NDVI) at those locations in Figures (4.4 and 4.10).

Table (4.4): Drought severity area based on LST and the categories of LST generated from Landsat Thermal Bands in the GZRB between 1990 and 2022

Year	Mean	Class 1[a]		Class 2[b]		Class 3[c]		Class 4[d]		Class 5[e]	
		Area		Area		Area		Area		Area	
		km^2	%	km^2	%	km^2	%	km^2	%	km^2	%
1990	24.18	3267.0	12.4	3159.2	12.0	11484.0	43.6	8139.8	30.9	280.3	1.1
1992	18.76	5172.7	19.6	5889.2	22.4	11799.6	44.8	3468.8	13.2	0.3	0.0
1994	22.12	2042.2	7.8	6168.7	23.4	14404.8	54.7	3713.2	14.1	1.3	0.0
1996	22.18	4804.0	18.3	3126.8	11.9	10024.8	38.1	8299.5	31.5	66.1	0.3
1998	21.74	3376.3	12.8	5895.3	22.4	10984.2	41.7	6074.4	23.1	0.1	0.0
2000	23.55	1653.7	6.3	6383.0	24.2	12149.6	46.1	5655.9	21.5	488.1	1.9
2002	17.8	4867.7	18.5	9060.3	34.4	10433.9	39.6	1931.8	7.3	36.5	0.1
2004	35.29	317.8	1.2	527.8	2.0	6741.3	25.6	10297.1	39.1	8446.2	32.1
2006	24.37	4427.4	16.8	2386.7	9.1	8607.7	32.7	8369.6	31.8	2538.9	9.6
2008	37.2	383.0	1.5	494.8	1.9	4677.5	17.8	9980.0	37.9	10778.8	41.0
2010	21.78	4739.2	18.0	4654.2	17.7	9019.3	34.6	7320.6	27.8	506.8	1.9
2014	37.56	891.5	3.4	676.9	2.6	4401.2	16.7	9166.9	34.9	11193.6	42.6
2016	26.10	1125.1	4.3	2912.7	11.1	14031.8	53.3	8247.4	31.3	13.5	0.1
2018	18.2	5299.5	20.1	5848.4	22.2	10285.2	39.1	4897.2	18.6	0.2	0.0
2020	24.26	2180.0	8.3	2500.9	9.5	15396.6	58.5	6252.6	23.7	0.3	0.0
2022	23.85	884.5	3.4	6320.6	24.0	13374.3	50.8	5743.2	21.8	7.8	0.0

[a] LST values < 10 °C; [b] 10 °C < LST values < 20 °C; [c]20 °C < LST values < 30 °C; [d]30 °C < LST values < 40 °C; [e] LST values > 30 °C

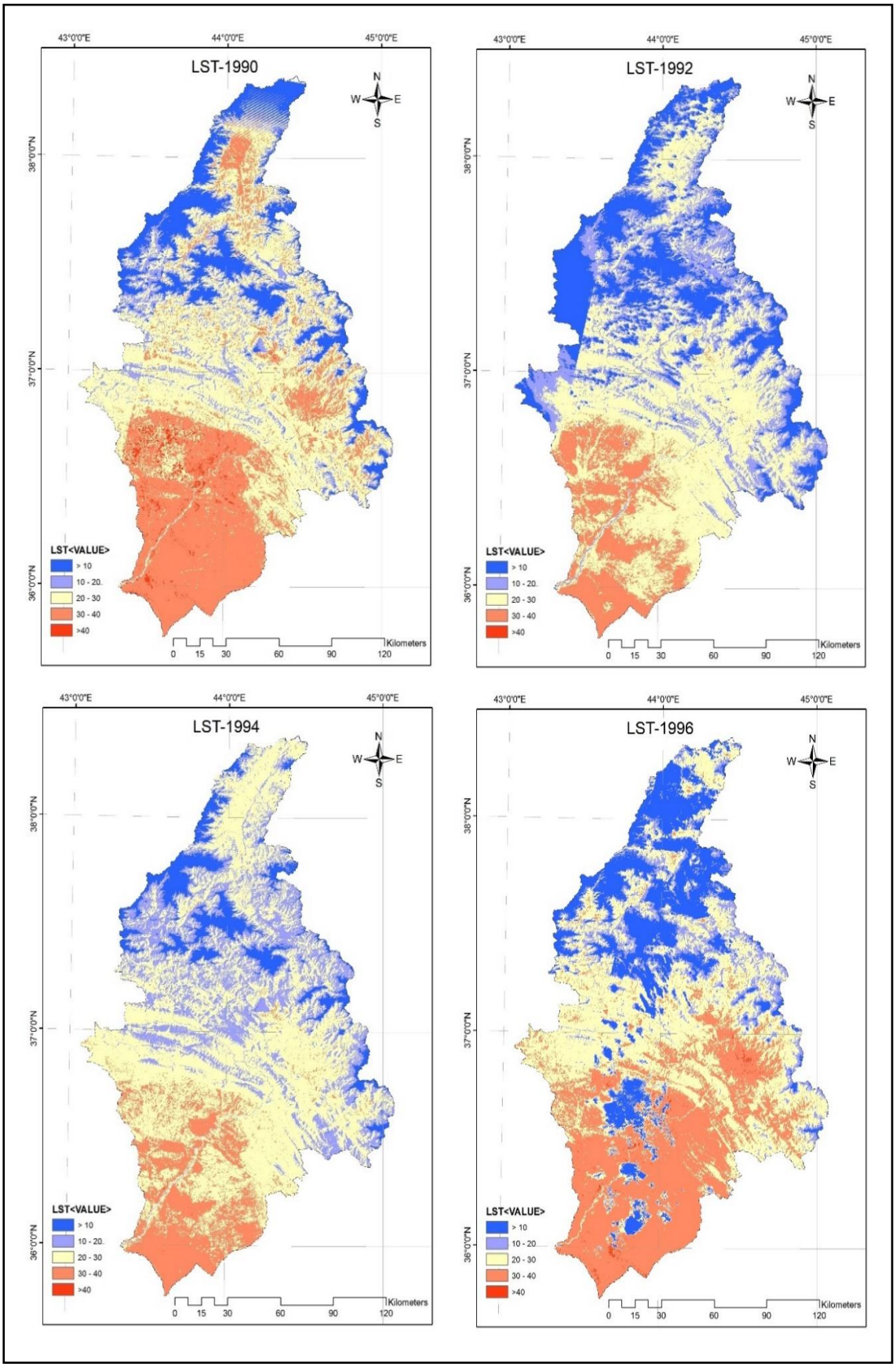

Figure (4.10): Spatial variation of LST within the GZRB for the period between 1990 and 2022

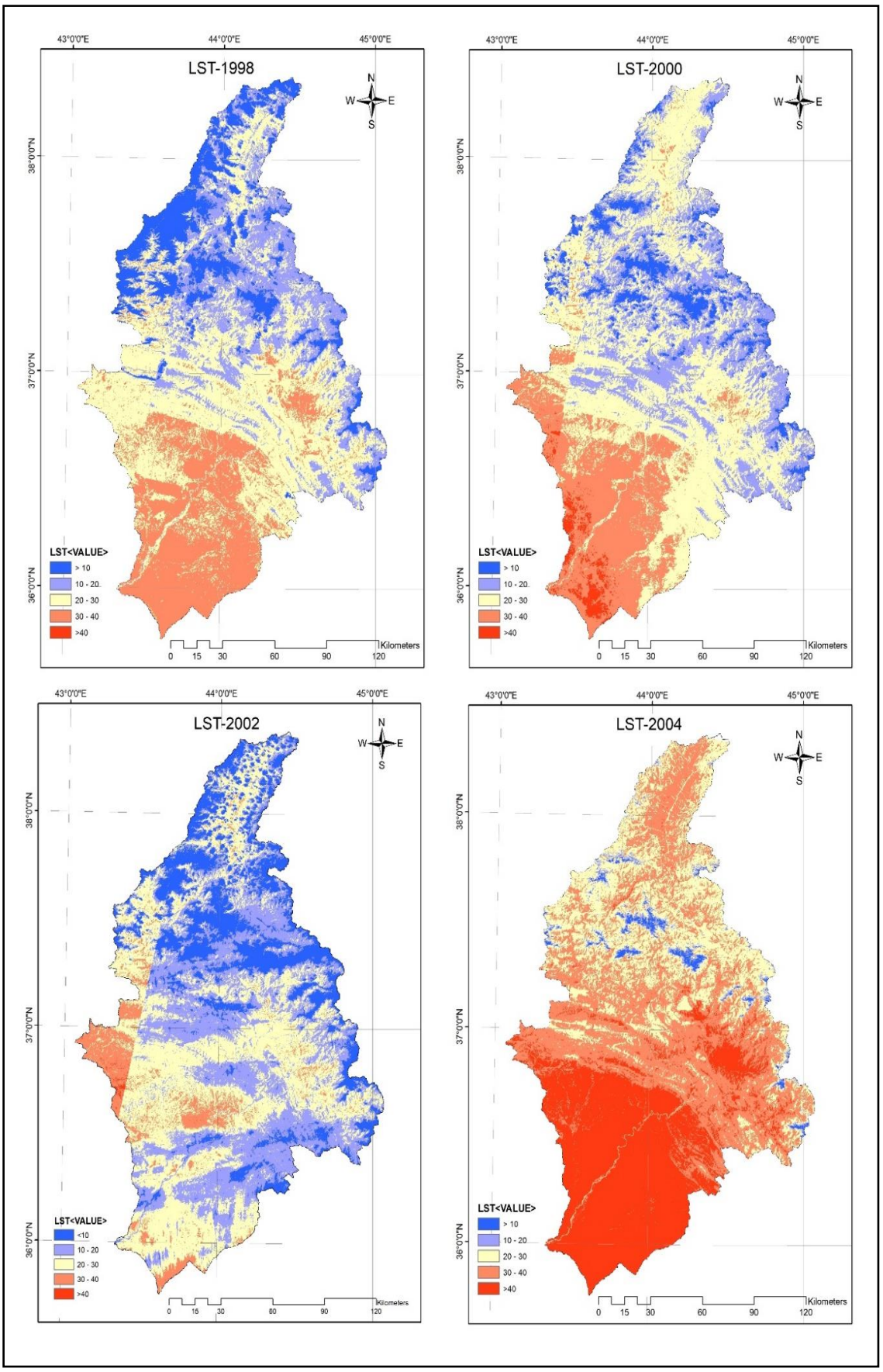

Figure (4.10) Continue…

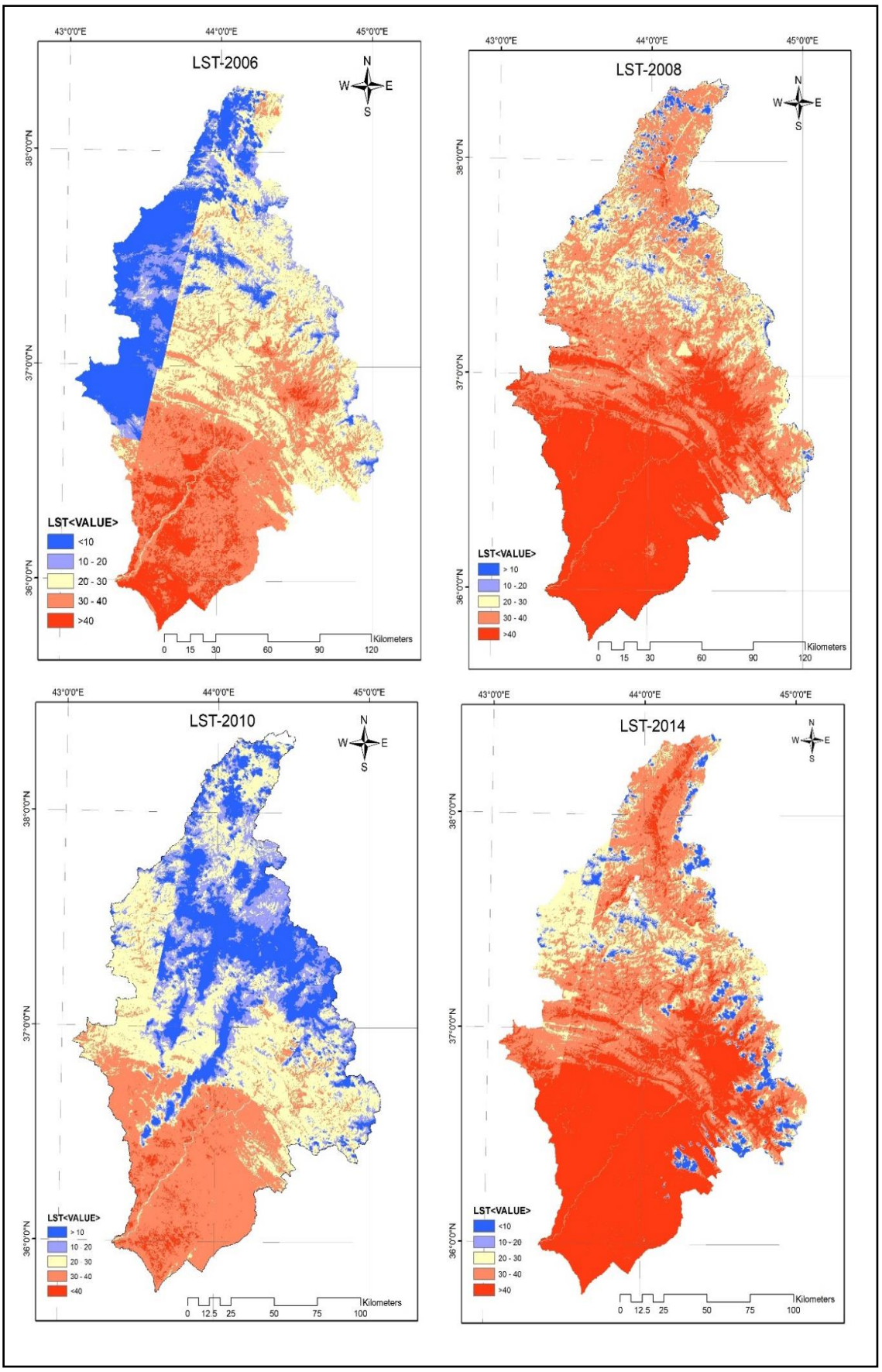

Figure (4.10) Continue…

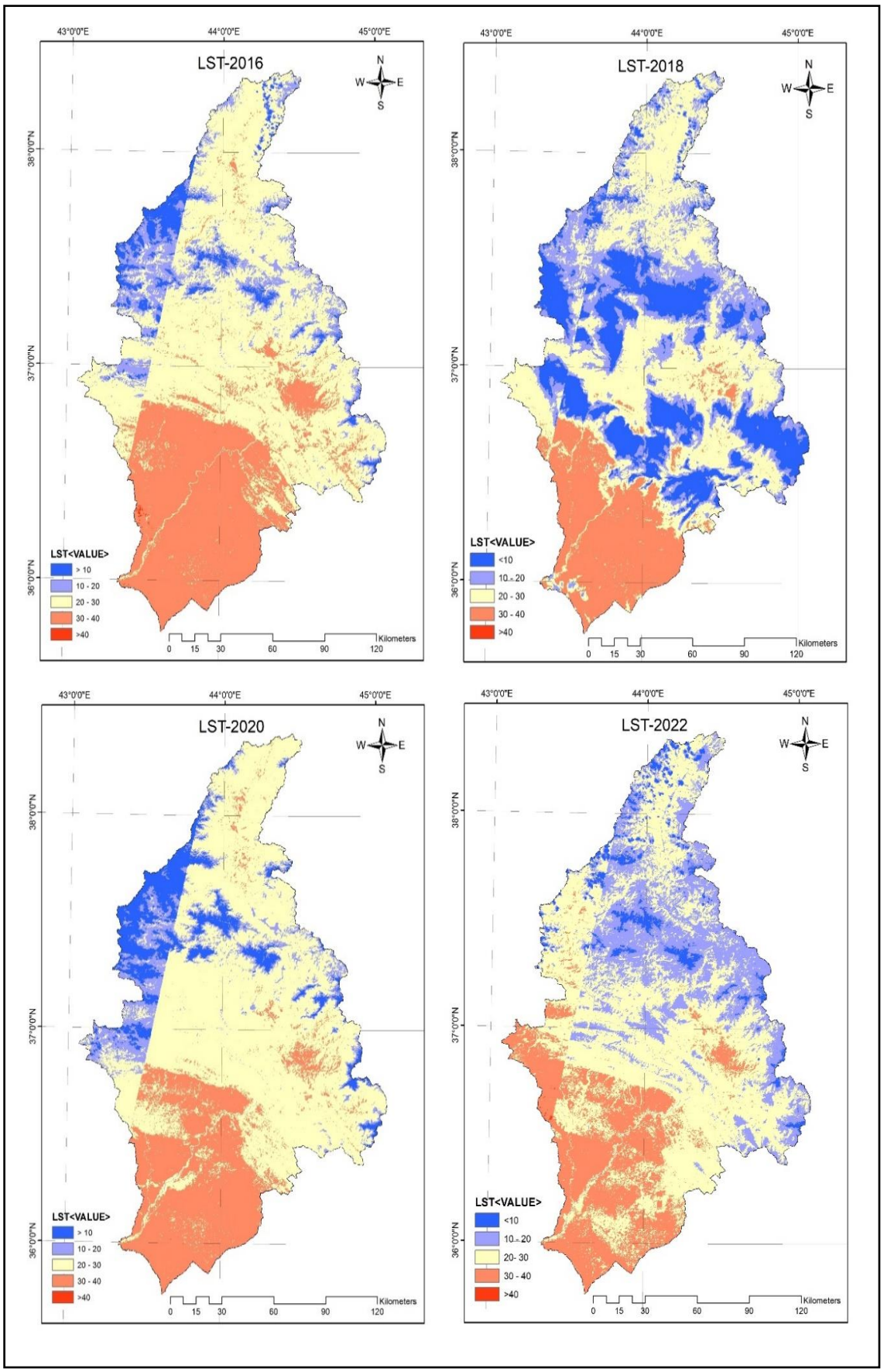

Figure (4.10) Continue…

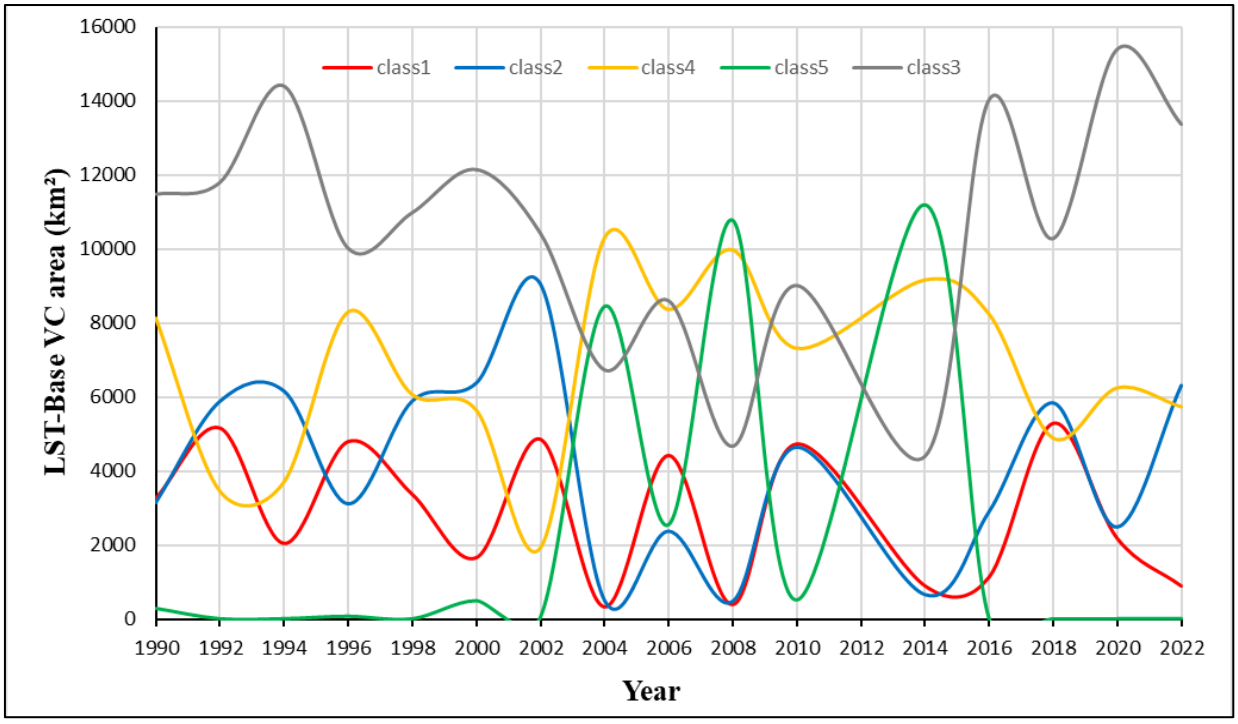

Figure (4.11): Temporal variation in MSAVI-Based VC with the GZRB for the period (1990-2022)

4.3 Calibrating and Validation of the Model's

The calibration and validation of LARS-WG6 involved utilizing daily climate data for the baseline period at thirteen meteorological locations spanning from 1990 to 2022. The model evaluation entailed several mathematical tests and graphical comparisons. The Kolmogorov-Smirnov (K-S) test was employed to assess the resemblance between periodic distributions of wet/dry series (WDSeries), daily rainfall (RainD), daily minimum temperature (TminD), and daily maximum temperature (TmaxD) obtained from both observed and downscaled data. The K-S test generated a "p-value" to confirm or reject whether two datasets originated from a similar distribution, indicating the presence of significant differences between the recorded and simulated weather data for that parameter.

Any generated weather data with a very low p-value and a high K-S value, indicating a lack of resemblance to real weather, was excluded from consideration. While the conventional significance threshold for statistical

analysis is typically set at 0.05, it was recommended to adopt a more stringent threshold of 0.01 as an acceptable level of significance (Semenov et al., 2013).

The primary factors contributing to the notable disparities between observed and simulated data were attributed to the smoothing effect of the LARS-WG model on observed data, inaccuracies in the recorded data, random fluctuations in the recorded data, and exceptional climate phenomena at specific weather stations that significantly influenced weather patterns for certain years.

The impact analysis incorporated the results of the downscaling simulation, focusing on reviewing the daily precipitation distribution for each month and the yearly variations in wet and dry spells. Tables (4.5) and (4.6) presented the outcomes of the K-S test from the validation stage, demonstrating an excellent fit of the wet/dry spells series with the seasonal distribution, ranging from perfect to very good (p-value > 0.7). Evaluation of LARS-WG6's ability to fit dry/wet period series distributions during the spring season (MAM) yielded very good (p-value > 0.70) to perfect (p-value = 1.0) results. However, during the summer season (June, July, and August), some variations in the weather generator's performance were observed. The model moderately fit the wet spell distribution (0.70 < p-value < 0.40) and poorly fit the dry spell distribution (p-value < 0.40) during this season. This poor outcome was attributed to the dry JJA season, which experienced little to no rainfall, causing the model's inability to capture rainy spells. Additionally, Table (4.5) indicates that LARS-WG6's performance in simulating daily rain distributions ranged from very good to perfect, except during the summer season. This summer performance issue could be attributed to a similar cause as the previously noted problem with simulating cyclical distributions.

In general, the model exhibited exceptional performance in accurately predicting daily precipitation, Tmin, and Tmax in the basin. Therefore, considering the five groups of GCM and SRA2 scenario, it is feasible to use the model for forecasting daily climatic data in the basin for the future period from 2021 to 2040.

Table (4.5): The outcomes of the Kolmogorov-Smirnov (K-S) test were analyzed to assess the distributions of dry and wet years series for the base period from 1990 to 2022 using the LARS-WG model.

Sub-basin	Site name	Seasons for wet years							
		DJF[a]		MAM[b]		JJA[c]		SON[d]	
		K-S	*p-value*	K-S	*p*-value	K-S	*p-value*	K-S	*p-value*
US[e]	Koozerash	0.036	1.000[1]	0.062	1.000[1]	0.015	1.000[1]	0.016	1.000[1]
	Mirbad	0.015	1.000[1]	0.025	1.000[1]	0.098	1.000[1]	0.010	1.000[1]
	Piranshahr	0.056	1.000[1]	0.048	1.000[1]	0.000	1.000[1]	0.035	1.000[1]
	Ravand urmia	0.023	1.000[1]	0.065	1.000[1]	0.021	1.000[1]	0.071	1.000[1]
	Soran	0.025	1.000[1]	0.036	1.000[1]	0.087	1.000[1]	0.021	1.000[1]
	Razi	0.208	0.649[3]	0.025	1.000[1]	0.006	1.000[1]	0.015	1.000[1]
DS[f]	Aqra	0.219	0.584[3]	0.040	1.000[1]	0.087	1.000[1]	0.051	1.000[1]
	Bashur	0.040	1.000[1]	0.243	0.449	0.000	1.000[1]	0.064	1.000[1]
	Duhook	0.029	1.000[1]	0.045	1.000[1]	0.087	1.000[1]	0.022	1.000[1]
	Erbil	0.014	1.000[1]	0.200	0.697[3]	0.000	1.000[1]	0.141	0.964[2]
	Makhmoor	0.009	1.000[1]	0.065	1.000[1]	0.037	1.000[1]	0.055	1.000[1]
	Mousl	0.009	1.000[1]	0.024	1.000[1]	0.217	1.000[1]	0.062	1.000[1]
	Salahddin	0.037	1.000[1]	0.016	1.000[1]	0.131	0.982[2]	0.037	1.000[1]

continued

Sub-basin	Site name	Seasons for dry years							
		DJF[a]		MAM[b]		JJA[c]		SON[d]	
		K-S	*p-value*	K-S	*p-value*	K-S	*p-value*	K-S	*p-value*
US[e]	Koozerash	0.046	1.000[1]	0.113	0.997[2]	0.093	1.000[1]	0.078	1.000[1]
	Mirbad	0.038	1.000[1]	0.076	1.000[1]	0.061	1.000[1]	0.060	1.000[1]
	Piranshahr	0.135	0.976[2]	0.087	1.000[1]	0.174	0.842[2]	0.095	1.000[1]
	Ravand urmia	0.066	1.000[1]	0.036	1.000[1]	0.138	0.971[2]	0.053	1.000[1]
	Soran	0.058	1.000[1]	0.057	1.000[1]	0.087	1.000[1]	0.059	1.000[1]
	Razi	0.072	1.000[1]	0.103	0.999[2]	0.099	1.000[1]	0.100	1.000[1]
DS[f]	Aqra	0.047	1.000[1]	0.088	1.000[1]	0.130	0.984[2]	0.145	0.954[2]
	Bashur	0.091	1.000[1]	0.065	1.000[1]	0.131	0.982[2]	0.089	1.000[1]
	Duhook	0.046	1.000[1]	0.067	1.000[1]	0.218	0.589[3]	0.091	1.000[1]
	Erbil	0.091	1.000[1]	0.070	1.000[1]	0.305	0.193[4]	0.087	1.000[1]
	Makhmoor	0.052	1.000[1]	0.073	1.000[1]	0.066	1.000[1]	0.054	1.000[1]
	Mousl	0.067	1.000[1]	0.086	1.000[1]	0.305	0.193[4]	0.054	1.000[1]
	Salahddin	0.049	1.000[1]	0.061	1.000[1]	0.131	0.982[2]	0.067	1.000[1]

[a]Winter (Dec, Jan, Feb); [b]Spring (Mar, Apr, , May); [c]Summer , (Jun, Jul, , Aug); [d]Autumn , (Sep, Oct, , Nov);
[e]Upstream; [f]Downstream; [1]Perfect fit (*p-value* = 1); [2]Very good fit ($0.7 \leq$ *p-value* < 1); [3]Good fit($0.4 \leq$ *p-value* < 0.7);
[4]Poor fit (*p-value* <0.4).

Table (4.6): The data used to validate the daily rainfall distribution during the reference period of 1990–2022 were obtained from the Long Ashton Research Station. The validation process involved performing the Kolmogorov-Smirnov (K-S) test.

Sub-basin	Site Name	January		February		March		April	
		K-S	*p-value*	K-S	*p-value*	K-S	*p-value*	K-S	*p-value*
Upstream	Koozerash	0.071	1.000[1]	0.083	1.000[1]	0.064	1.000[1]	0.063	1.000[1]
	Mirbad	0.065	1.000[1]	0.065	1.000[1]	0.071	1.000[1]	0.069	1.000[1]
	Piranshahr	0.130	0.984[2]	0.065	1.000[1]	0.065	1.000[1]	0.132	0.981[2]
	Ravand urmia	0.130	0.984[2]	0.063	1.000[1]	0.065	1.000[1]	0.061	1.000[1]
	Soran	0.130	0.984[2]	0.136	0.974[2]	0.065	1.000[1]	0.064	1.000[1]
	Razi	0.062	1.000[1]	0.065	1.000[1]	0.079	1.000[1]	0.064	1.000[1]
Downstream	Aqra	0.065	1.000[1]	0.130	0.984[2]	0.065	1.000[1]	0.064	1.000[1]
	Bashur	0.065	1.000[1]	0.068	1.000[1]	0.065	1.000[1]	0.064	1.000[1]
	Duhook	0.065	1.000[1]	0.130	0.984[2]	0.065	1.000[1]	0.064	1.000[1]
	Erbil	0.065	1.000[1]	0.130	0.984[2]	0.065	1.000[1]	0.070	1.000[1]
	Makhmoor	0.073	1.000[1]	0.059	1.000[1]	0.077	1.000[1]	0.068	1.000[1]
	Mousl	0.116	0.996[2]	0.130	0.984[2]	0.065	1.000[1]	0.063	1.000[1]

continued

	Salahddin	0.130	0.984[2]	0.065	1.000[1]	0.130	0.984[2]	0.064	1.000[1]
Sub-basin	Site Name	May		June		July		August	
		K-S	*p-value*	K-S	*p-value*	K-S	*p-value*	K-S	*p-value*
Upstream	Koozerash	0.069	1.000[1]	0.127	0.987[2]	0.200	0.697[3]	0.087	1.000[1]
	Mirbad	0.077	1.000[1]	0.065	1.000[1]	0.080	1.000[1]	0.131	0.982[2]
	Piranshahr	0.141	0.964[2]	0.261	0.359[4]	0.391	0.043[4]	1.000	0.000[4]
	Ravand urmia	0.136	0.974[2]	0.190	0.755[2]	0.174	0.842[2]	0.261	0.359[4]
	Soran	0.065	1.000[1]	0.392	0.042[4]	0.652	0.000[4]	(-)*	(-)*
	Razi	0.066	1.000[2]	0.110	0.998[2]	0.130	0.984[2]	0.066	1.000[1]
Downstream	Aqra	0.064	1.000[1]	0.652	0.000[4]	1.000	0.000[4]	0.652	0.000[4]
	Bashur	0.134	0.978[2]	0.158	0.913[4]	(-)*	(-)*	(-)*	(-)*
	Duhook	0.063	1.000[1]	0.218	0.589[3]	(-)*	(-)*	1.000	0.000[4]
	Erbil	0.072	1.000[1]	0.217	0.595[3]	(-)*	(-)*	(-)*	(-)*
	Makhmoor	0.070	1.000[1]	0.073	1.000[1]	0.064	1.000[1]	0.123	0.991[2]
	Mousl	0.065	1.000[1]	0.305	0.193[4]	(-)*	(-)*	(-)*	(-)*
	Salahddin	0.063	1.000[1]	0.261	0.359[4]	(-)*	(-)*	(-)*	(-)*
Sub-basin	Site Name	September		October		November		December	
		K-S	*p-value*	K-S	*p-value*	K-S	*p-value*	K-S	*p-value*

Upstream	Koozerash	0.067	1.000[1]	0.064	1.000[1]	0.063	1.000[1]	0.068	1.000[1]
	Mirbad	0.177	0.826[2]	0.079	1.000[1]	0.064	1.000[1]	0.080	1.000[1]
	Piranshahr	0.304	0.196[4]	0.083	1.000[1]	0.066	1.000[1]	0.145	0.954[2]
	Ravand urmia	0.140	0.966[2]	0.070	1.000[1]	0.072	1.000[1]	0.126	0.988[2]
	Soran	0.072	1.000[1]	0.071	1.000[1]	0.066	1.000[1]	0.064	1.000[1]
	Razi	0.065	1.000[1]	0.128	0.986[2]	0.064	1.000[1]	0.141	0.964[2]
Downstream	Aqra	0.217	0.595[3]	0.127	0.987[2]	0.075	1.000[1]	0.126	0.988[2]
	Bashur	0.174	0.842[2]	0.173	0.847[2]	0.198	0.709[2]	0.124	0.990[2]
	Duhook	0.348	0.096[4]	0.082	1.000[1]	0.198	0.709[2]	0.063	1.000[1]
	Erbil	0.870	0.000[4]	0.089	1.000[1]	0.175	0.837[2]	0.063	1.000[1]
	Makhmoor	0.150	0.940[2]	0.081	1.000[1]	0.064	1.000[1]	0.128	0.986[2]
	Mousl	0.391	0.043[4]	0.123	0.991[2]	0.128	0.986[2]	0.062	1.000[1]
	Salahddin	0.217	0.595[3]	0.164	0.888[2]	0.127	0.987[2]	0.140	0.966[2]

* Below the maximum that can be seen; [1]Perfect fit (p-value = 1); [2]Very good fit ($0.7 \leq$ p-value < 1); [3]Good fit ($0.4 <$ p-value ≤ 0.7); [4]Poor fit (p-value < 0.4)

4.4 Estimation of the Weather Variables

Using RCP8.5 and RCP4.5, two important emission scenarios created by the five designated GCMs, the weather generator model works well in the future (2021− 2040), depending on the findings of the calibration procedure and validation of the study.

For the Northern and Southern parts, the Tmax and precipitation were downscaled using the outputs from five GCM models, which are CSIRO-MK3.6.0, MIROC5, HadGEM2-ES, CanESM2, and NorESM1-M. Figures (4.12) and (4.13) display predicted temperatures and precipitation, respectively. The range of five chosen GCMs is shown in Figure (4.12), along with the mean monthly Tmax for future times. Plots of the mean monthly Tmax across the Northen and Southern parts revealed that the summer months (July and August) saw the largest rises, whereas the winter months (Dec. and Jan.) saw the minimum rises. Between the observed and anticipated RCP scenarios, the graphs likewise show a steady drop in Tmax. HadGEM2-ES reported at the Southern part in July that the Tmax predicted by the model by RCP8.5 (about 44.5°C).

Figure (4.12) displays the annual average expected Tmax difference from the time of observation for each of the five GCM models considered in this study. According to the results, the average annual Tmax under RCP4.5 drops to 6.20 and 5.78 °C for the Northern and Southern part. Under RCP8.5, the temperature reduction ranges from 6.10 to 5.58 °C for the Northen and Southern parts, respectively.

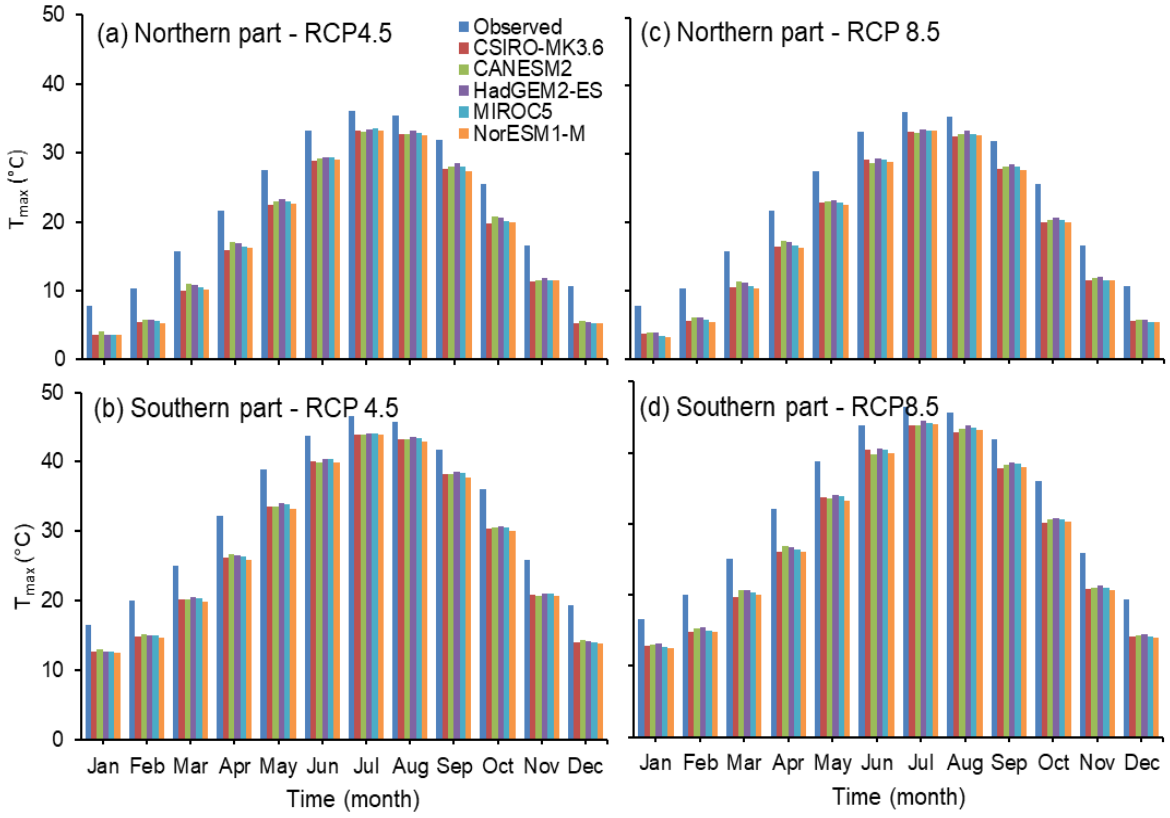

Figure (4.12): Comparison of the RCP4.5 and RCP8.5 scenarios' predictions with the actual average monthly maximum temperatures observed for the period (1990–2021) using five GCMs (2021–2040).

The precipitation forecasts for the two RCP4.5 and RCP8.5 scenarios are displayed in Figure (4.13), which shows that the Northern and Southern parts of the five selected GCMs have different predicted. This is because there are days with no data since precipitation does not occur continuously throughout the year. This makes it difficult to anticipate future precipitation. Figure (4.13) demonstrates that for each of the five chosen GCMs across the chosen future period, there are different forecast trends. Because of the possibility of each GCM model producing a different projection, these variations show the challenges and related uncertainty in forecasting rainfall values using a single GCM model.

In contrast to other models such as NorESM1-M and MIROC5, the CANESM2 model predicts an increase in precipitation between the two sub-basins in a variety of seasons, with the total changing depending on the RCP

8.5. Other models, however, like NorESM1-M and MIROC5, predict a minor reduction or rise in precipitation, or that there won't be any appreciable rainfall variation in the future.

The Northen sub-basin experienced the largest increase in precipitation (14.10 mm) according to the CanESM2 model in the winter (DJF) season. The MIROC5 model during winter (DJF) at the Northern part produced the largest decrease in precipitation (9.44 mm). The aforementioned findings are in line with climate change studies in Iraq and other surrounding countries, which show that this region in northern Iraq is experiencing an altered trend of variations in precipitation.

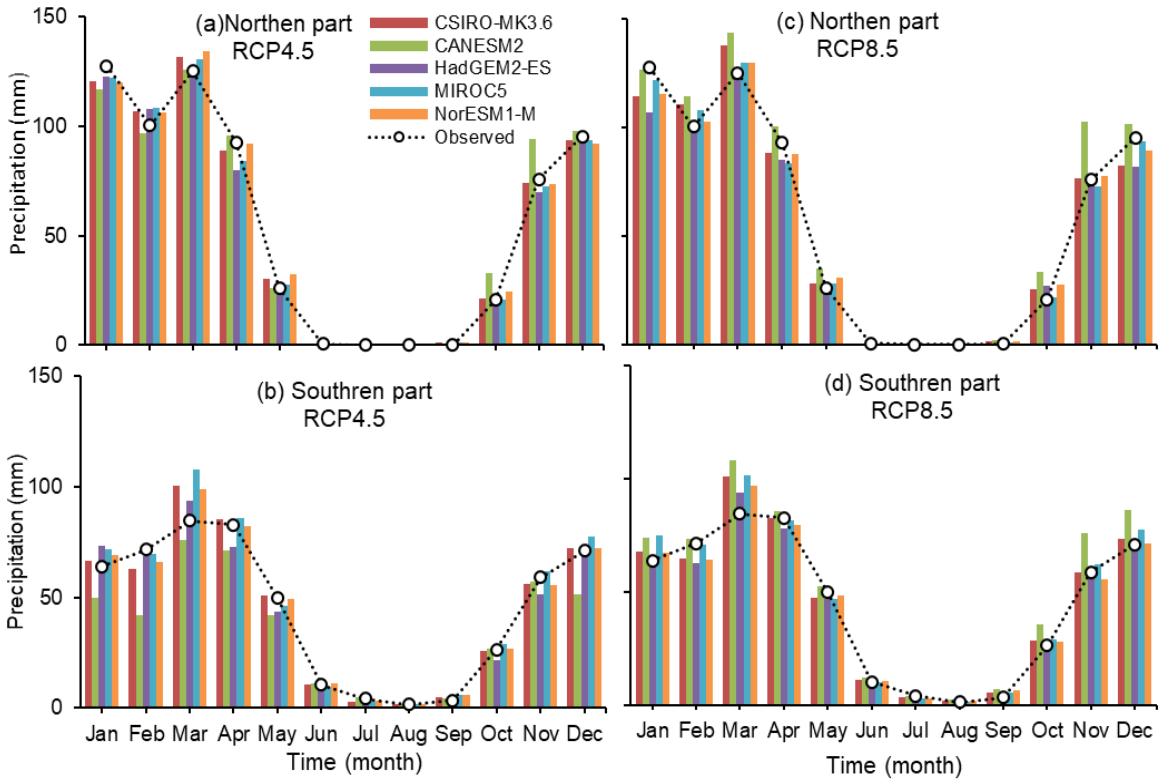

Figure (4.13): Comparison of the monthly mean precipitation values observed (1990–2022) and the projected by scenarios (RCP4.5) and (RCP8.5) Appling five General Circulation Models (GCM) for the years (2021–2040) in the Northern and Southern parts of GZRB

4.5 Variation of Drought

According to Figure (4.14), the Southern sub-basin is currently categorized as almost normal to moderately dry, whereas the Northen parts has been categorized as severely and moderately wet-normal. However, over the following twenty years, they are predicted to change from extremely moderately wet to moderately dry and from moderately wet to severely dry, respectively.

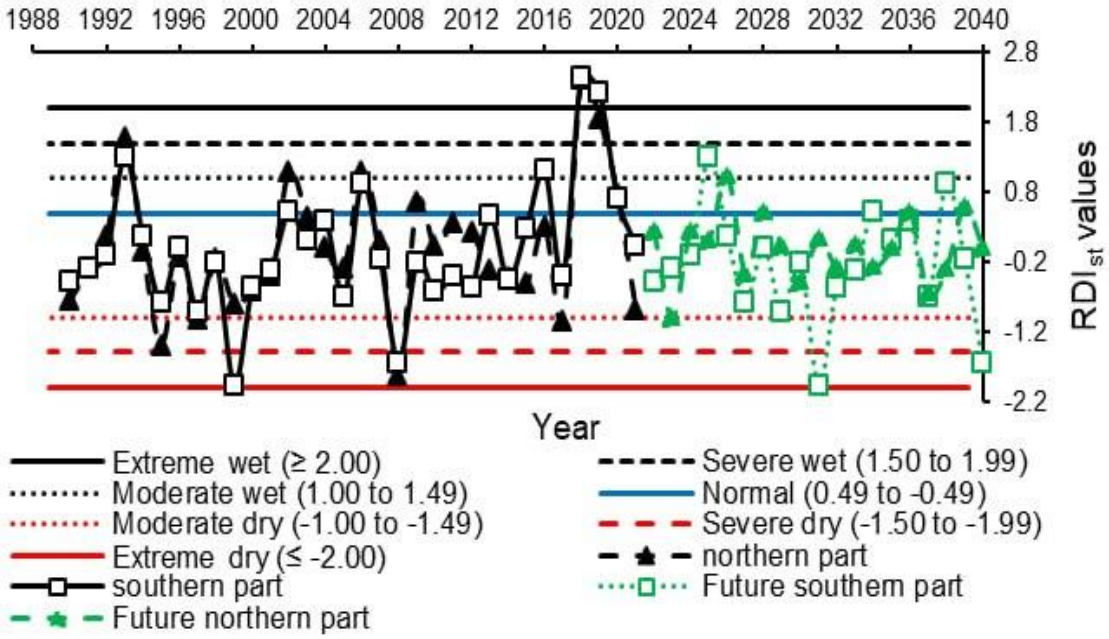

Figure (4.14): Temporal variation of the annual values of the standardized reconnaissance drought index (RDIst) estimated (1990–2021) and the projected by scenarios (RCP4.5) and (RCP8.5) using five General Circulation Models (GCM) for the years (2021–2040) in the Northern and Southern parts of GZRB

The temporal evolution of the RDIst index for GZRB from 1990 to 2021 and from 2022 to 2040 is depicted in Figure (4.14). The findings revealed an inconsistent cycle of dry and wet periods throughout the research period. The hydrological years 1999–2000 and 2007–2008 both saw droughts, although there were some variances between the Northern and Southern parts. Droughts normally start at the beginning of the rainy season, either as a result

of a delay or a reduction in rainfall. The Southern sub-basin experienced the worst levels of drought, with average RDIst values of -1.97 and -1.64, respectively, in the years 1999–2000 and 2007–2008. In addition, moderate to severe droughts with average RDIst values of -0.81 and -1.84, respectively, also affected the Northern part stations in 1999–2000 and 2007–2008.

CHAPTER FIVE

CONCLUSIONS AND RECOMMENDATIONS

5.1 Spectral Drought Indices

- According to the VCI, the most severe droughts are typically experienced in the southern and central regions of GZRB.
- The MSAVI's lowest mean values for 2002 were 0.08. The decrease in values referred to annual rainfall, which is regarded as a critical factor influencing vegetation cover growth in the basin.
- The MSAVI reached its highest mean value of 0.24 in 2016, 2018, and 2020; a high value indicates healthy vegetation.
- MSAVI is near or equal to zero, which refers to arid land without vegetation.
- Due to the uneven supply of precipitation and the effects of the basin's elevation, there was spatial variation in the LST and NDVI.
- The connection between precipitation, geographic elevation, latitude, and Landsat-based spectral drought indices displayed noteworthy correlations.
- The classification of land use demonstrates that, particularly in 2000 and 2008, climatic factors had an effect on the area covered by vegetation.
- Over the past few years, particularly in 2000 and 2008, the GZRB has observed an increase in the frequency and severity of droughts.

5.2 Drought and Climate Change

- According to the results, under both RCP scenarios, the Tmax is expected to rise by 2.27 to 3.71 °C at the northern part and southern part sub-basin locations for the future.

• The downscaled rainfall from the five GCM models shows different outlines for each sub-basin.

• The MIROC5 Model projected the greatest precipitation decrease (9.44 mm) at the upstream sub-basin under RCP8.5, while the CanESM2 Model predicted the largest precipitation increase (14.10 mm).

5.2 Recommendations

• It is advised to regularly conduct drought detection studies to:

  o Support various business objectives and address various environmental issues.

  o Fully understand the drought and its correlation with the features that influence it.

• Future studies may include data on agricultural output and surface evaporation to better understand how these variables interact during droughts.

References:

1- Abed, S. A., Ahmed, A. A., & Salim, M. A. (2021). Using ArcGIS Software and Remote Sensing Technology to Predict Land Surface Temperature (LST) for Monitoring Ecological and Climate Change in Hor Al-Dalmaj, Southern Iraq. *IOP Conference Series: Earth and Environmental Science*, *790*(1).

2- Al-Faraj, F. A. M., Scholz, M., & Tigkas, D. (2014). Sensitivity of surface runoffto drought and climate change: Application for shared river basins. *Water (Switzerland)*, *6*(10), 3033–3048.

3- Al-Khafaji, M. S., & Al-Ameri, R. A. (2021). Evaluation of drought indices correlation for drought frequency analysis of the Mosul dam watershed. *IOP Conference Series: Earth and Environmental Science*, *779*(1).

4- Al-Masaodi, H. J. O., & Al-Zubaidi, H. A. M. (2022). Spatial-temporal changes of land surface temperature and land cover over Babylon Governorate, Iraq. *Materials Today: Proceedings*, *xxxx*.

5- Al-Quraishi, A. M. F., Gaznayee, H. A., & Crespi, M. (2021). Drought trend analysis in a semi-arid area of Iraq based on Normalized Difference Vegetation Index, Normalized Difference Water Index and Standardized Precipitation Index. *Journal of Arid Land*, *13*(4), 413–430.

6- Al-Quraishi, A. M. F., Qader, S. H., & Wu, W. (2020). Drought Monitoring Using Spectral and Meteorological Based Indices Combination: A Case Study in Sulaimaniyah, Kurdistan Region of Iraq. *Springer Water*, 377–393.

7- Al-Timimi, Y. K., George, L. E., & Al-Jiboori, M. H. (2012). Drought Risk Assessment In Iraq Using Remote Sensing And GIS Techniques. *Iraqi Journal of Science*, *53*(4), 1078–1082.

8- Allawai, M. F., & Ahmed, B. A. (2020). Using Remote Sensing and GIS in Measuring Vegetation Cover Change from Satellite Imagery in Mosul City, North of Iraq. *IOP Conference Series: Materials Science and Engineering*, *757*(1), 012062.

9- Almamalachy, Y. (2017). *Utilization of Remote Sensing in Drought Monitoring Over Iraq by Yousif Almamalachy A thesis submitted in partial fulfillment of the requirements for the degree of Master of Science in Civil and Environmental Engineering Thesis Committee : Hamid Moradkhan*.

10- Alphan, H., & Derse, M. A. (2013). Change detection in Southern Turkey using normalized difference vegetation index (NDVI). *Journal of Environmental Engineering and Landscape Management*, *21*(1), 12–18.

11- Alwan, I. A., Ziboon, A. T., Khalaf, A. G., Pham, Q. B., Anh, D. T., & Khedher, K. M. (2022). Monitoring agricultural and meteorological

drought using remote sensing. *Arabian Journal of Geosciences 2022 15:2*, *15*(2), 1–15.
12- Ashraf, M., Ullah, K., & Adnan, S. (2022). Satellite based impact assessment of temperature and rainfall variability on drought indices in Southern Pakistan. *International Journal of Applied Earth Observation and Geoinformation*, *108*(January), 102726.
13- Baniya, B., Tang, Q., Xu, X., Haile, G. G., & Chhipi-Shrestha, G. (2019). Spatial and temporal variation of drought based on satellite derived vegetation condition index in Nepal from 1982–2015. *Sensors (Switzerland)*, *19*(2).
14- Beck, P. S. A., Atzberger, C., Høgda, K. A., Johansen, B., & Skidmore, A. K. (2006). Improved monitoring of vegetation dynamics at very high latitudes: A new method using MODIS NDVI. *Remote Sensing of Environment*, *100*(3), 321–334.
15- Beg, A. (2018). Assessment of land surface temperature variation over Rusafa side of Baghdad city, Iraq. *MATEC Web of Conferences*, *162*, 1–9.
16- Brown, J. F., Wardlow, B. D., Tadesse, T., Hayes, M. J., & Reed, B. C. (2008). The Vegetation Drought Response Index (VegDRI): A new integrated approach for monitoring drought stress in vegetation. *GIScience and Remote Sensing*, *45*(1), 16–46.
17- Dai, A. (2010). Drought under global warming: A review. *Wiley Interdisciplinary Reviews: Climate Change*, *2*(1), 45–65.
18- Dikici, M., & Aksel, M. *Evaluation of Two Vegetation Indices (NDVI and VCI) Over Asi Basin in Turkey* *. 2021–10995.
19- Eklund, L., & Seaquist, J. (2014). Meteorological, agricultural and socioeconomic drought in the Duhok Governorate, Iraqi Kurdistan. *Natural Hazards*, *76*(1), 421–441.
20- Eklund, L., & Thompson, D. (2017). Differences in resource management affects drought vulnerability across the borders between Iraq, Syria, and Turkey. *Ecology and Society*, *22*(4).
21- Fadhil, A. M. (2011). Drought mapping using Geoinformation technology for some sites in the Iraqi Kurdistan region.(3), 239–257.
22- Foody, G. M. (2003). Geographical weighting as a further refinement to regression modelling: An example focused on the NDVI-rainfall relationship. *Remote Sensing of Environment*, *88*(3), 283–293.
23- Gaznayee, H. A. A. (2020). Modeling Spatio-Temporal Pattern of Drought Severity Using Meteorological Data and Geoinformatics Techniques for the Kurdistan Region of Iraq. *Dissertation*, *1965*, 1–11.
24- Gaznayee, H. A. A., & Al-Quraishi, A. M. F. (2019). Analysis of agricultural drought, rainfall, and crop yield relationships in erbil province, the kurdistan region of iraq based on landsat time-series msavi2. *Journal of Advanced Research in Dynamical and Control*

Systems, *11*(12 Special Issue), 536–545.
25- Gaznayee, H. A. A., Al-Quraishi, A. M. F., Mahdi, K., & Ritsema, C. (2022). A Geospatial Approach for Analysis of Drought Impacts on Vegetation Cover and Land Surface Temperature in the Kurdistan Region of Iraq. *Water (Switzerland)*, *14*(6), 927.
26- Gaznayee, H. A. A., Fadhil Al-Quraishi, A. M., & Al-Sulttani, A. H. A. (2021). Drought Spatiotemporal Characteristics Based on a Vegetation Condition Index in Erbil, Kurdistan Region, Iraq. *Iraqi Journal of Science*, *62*(11), 4545–4556.
27- Ghaleb, F., Mario, M., & Sandra, A. N. (2015). Regional landsat-based drought monitoring from 1982 to 2014. *Climate*, *3*(3), 563–577.
28- Gholamnia, M., Khandan, R., Bonafoni, S., & Sadeghi, A. (2019). Spatiotemporal analysis of MODIS NDVI in the semi-arid region of Kurdistan (Iran). *Remote Sensing*, *11*(14), 8–12.
29- Gilabert, M. A., González-Piqueras, J., García-Haro, F. J., & Meliá, J. (2002). A generalized soil-adjusted vegetation index. *Remote Sensing of Environment*, *82*(2–3), 303–310.
30- Gu, Y., Brown, J. F., Verdin, J. P., & Wardlow, B. (2007). A five-year analysis of MODIS NDVI and NDWI for grassland drought assessment over the central Great Plains of the United States. *Geophysical Research Letters*, *34*(6).
31- Herrmann, H., & Bucksch, H. (2014). Global Land Cover Facility. In *Dictionary Geotechnical Engineering/Wörterbuch GeoTechnik* (pp. 612–612).
32- Heydari, H., Zoej, M. J. V., Maghsoudi, Y., & Dehnavi, S. (2018). An investigation of drought prediction using various remote-sensing vegetation indices for different time spans. *39*(6), 1871–1889.
33- *https://app.climateengine.org/climateEngine*. Retrieved July 27, 2023, from https://app.climateengine.org/login.
34- *https://earthexplorer.usgs.gov*. Retrieved July 27, 2023, from https://earthexplorer.usgs.gov/
35- *https://power.larc.nasa.gov/data-access-viewer/*. Retrieved July 27, 2023, from https://power.larc.nasa.gov/data-access-viewer/
36- Hussain, S., & Karuppannan, S. (2021). Land use/land cover changes and their impact on land surface temperature using remote sensing technique in district Khanewal, Punjab Pakistan.*7*(1), 46–58.
37- Ibrahim, G. R. F. (2017). Urban land use land cover changes and their effect on land surface temperature: Case study using Dohuk City in the Kurdistan Region of Iraq. *Climate*, *5*(1).
38- IPCC. (2014). *AR5 Synthesis Report: Climate Change 2014 — IPCC*. https://www.ipcc.ch/report/ar5/syr/
39- IPCC. (2022). *2022 Global Climate Report | National Centers for Environmental Information (NCEI)*.

https://www.ncei.noaa.gov/access/monitoring/monthly-report/global/2022

40- Javed, T., Yao, N., Chen, X., Suon, S., & Li, Y. (2019). Drought evolution indicated by meteorological and remote-sensing drought indices under different land cover types in China. *Environmental Science and Pollution Research*, *27*(4), 4258–4274.

41- Jiao, W., Zhang, L., Chang, Q., Fu, D., Cen, Y., & Tong, Q. (2016). Evaluating an enhanced vegetation condition index (VCI) based on VIUPD for drought monitoring in the continental United States. *Remote Sensing*, *8*(3).

42- Julien, Y., Sobrino, J. A., & Verhoef, W. (2006). Changes in land surface temperatures and NDVI values over Europe between 1982 and 1999. *Remote Sensing of Environment*, *103*(1), 43–55.

43- Karim, T. H., Keya, D. R., & Amin, Z. A. (2018). Temporal and spatial variations in annual rainfall distribution in Erbil province.*47*(1), 59–67.

44- Khalaf, R. M., Hussein, H. H., Hassan, W. H., Mohammed, Z. M., & Nile, B. K. (2022). Projections of precipitation and temperature in Southern Iraq using a LARS-WG Stochastic weather generator. *Physics and Chemistry of the Earth*, *128*(September), 103224.

45- Kogan, F. N. (1986). Climate constraints and trends in global grain production. *Agricultural and Forest Meteorology*, *37*(2), 89–107.

46- Kogan, F. N. (1995). Application of vegetation index and brightness temperature for drought detection. *Advances in Space Research*, *15*(11), 91–100.

47- Kousari, M. R., Dastorani, M. T., Niazi, Y., Soheili, E., Hayatzadeh, M., & Chezgi, J. (2014). Trend Detection of Drought in Arid and Semi-Arid Regions of Iran Based on Implementation of Reconnaissance Drought Index (RDI) and Application of Non-Parametrical Statistical Method. *Water Resources Management*, *28*(7), 1857–1872.

48- Liu, W. T., & Kogan, F. (2002). Monitoring Brazilian soybean production using NOAA/AVHRR based vegetation condition indices. *International Journal of Remote Sensing*, *23*(6), 1161–1179.

49- Mahdi, H. H., Musa, T. A., Al-Rammahi, Z. A. A., & Mahmood, E. J. (2022). Forecasting the Future Drought Indices Due to the Effects of Climate Change in Al Najaf City, Iraq. *IOP Conference Series: Earth and Environmental Science*, *961*(1).

50- Mahdi, Z. A., & Mohammed, R. (2022). Land use/land cover changing aspect implications: Lesser Zab River Basin, northeastern Iraq. *Environmental Monitoring and Assessment*, *194*(9), 1–16.

51- Mejbel Salih, M., Zakariya Jasim, O., I. Hassoon, K., & Jameel Abdalkadhum, A. (2018). Land Surface Temperature Retrieval from LANDSAT-8 Ther-mal Infrared Sensor Data and Validation with

Infrared Ther-mometer Camera. *International Journal of Engineering & Technology*, *7*(4.20), 601.

52- Mohammed, R., & Scholz, M. (2019). Climate Variability Impact on the Spatiotemporal Characteristics of Drought and Aridityin Arid and Semi-Arid Regions. *Water Resources Management*, *33*(15), 5015–5033.

53- Mohammed, Z. M., & Hassan, W. H. (2022). Climate change and the projection of future temperature and precipitation in southern Iraq using a LARS-WG model. *Modeling Earth Systems and Environment*, *8*(3), 4205–4218.

54- Mukhlif, H., & Al-Rifai, M. (2022). Using Geospatial Techniques to Study The Temporal Variability of Some Drought Indicators in The Sakran Region-Western Iraq. *Iraqi Journal of Desert Studies*, *12*(2), 1–17.

55- Mzuri, R. T., Omar, A. A., & Mustafa, Y. T. (2021). Spatiotemporal analysis of vegetation cover and its response to terrain and climate factors in duhok governorate, kurdistan region, iraq. *Iraqi Geological Journal*, *54*(1), 110–126.

56- Nasery, S., & Kaan, K. (2020). Burn Area Detection and Burn Severity Assessment Using Sentinel 2 MSI Data: The Case of Karabağlar District. *Turkish Journal of Geosciences*, *1*(2), 72–77.

57- Nielsen, T. T., & Adriansen, H. K. (2005). Government policies and land degradation in the Middle East. *Land Degradation and Development*, *16*(2), 151–161.

58- Qi, J., Chehbouni, A., Huete, A. R., Kerr, Y. H., & Sorooshian, S. (1994). A modified soil adjusted vegetation index. *Remote Sensing of Environment*, *48*(2), 119–126.

59- Ren, H., & Feng, G. (2015). Are soil-adjusted vegetation indices better than soil-unadjusted vegetation indices for above-ground green biomass estimation in arid and semi-arid grasslands? *Grass and Forage Science*, *70*(4), 611–619.

60- Rhyma, P. P., Norizah, K., Hamdan, O., Faridah-Hanum, I., & Zulfa, A. W. (2020). Integration of normalised different vegetation index and Soil-Adjusted Vegetation Index for mangrove vegetation delineation. *Remote Sensing Applications: Society and Environment*, *17*(December 2019), 100280.

61- Robert J. Hijmans. (2012). *Global Administrative Areas (GADM) | Geospatial Centre | University of Waterloo*. https://uwaterloo.ca/library/geospatial/collections/us-and-world-geospatial-data-resources/global-administrative-areas-gadm

62- Saleh, A. M. (2015). Relationship Betweenvegetation Indicesof Landsat-7 ETM+, MSS Data and Some Soil Properties: Case Study of Baqubah, Diyala, Iraq. *IOSR Journal of Agriculture and Veterinary Science Ver. II*, *8*(2), 2319–2372.

63- Salman, A. A., & Al Ramahi, F. K. M. (2022). Detection of Spectral Reflective Changes for Temporal Resolution of Land Cover (LC) for Two Different Seasons in central Iraq. *Iraqi Journal of Science*, *63*(12), 5589–5603.
64- Semenov, M. A., Pilkington-Bennett, S., & Calanca, P. (2013). Validation of ELPIS 1980-2010 baseline scenarios using the observed European Climate Assessment data set. *Climate Research*, *57*(1), 1–9.
65- Semenov, M. A., & Stratonovitch, P. (2010). Use of multi-model ensembles from global climate models for assessment of climate change impacts. *Climate Research*, *41*(1), 1–14.
66- Sheffield, J., Wood, E. F., & Roderick, M. L. (2012). Little change in global drought over the past 60 years. *Nature*, *491*(7424), 435–438.
67- Sun, D., & Kafatos, M. (2007). Note on the NDVI-LST relationship and the use of temperature-related drought indices over North America. *Geophysical Research Letters*, *34*(24).
68- Taylor, K. E., Stouffer, R. J., & Meehl, G. A. (2012). An overview of CMIP5 and the experiment design. *Bulletin of the American Meteorological Society*, *93*(4), 485–498.
69- Tigkas, D., Vangelis, H., & Tsakiris, G. (2015). DrinC: a software for drought analysis based on drought indices. *Earth Science Informatics*, *8*(3), 697–709.
70- Tomlinson, C. J., Chapman, L., Thornes, J. E., & Baker, C. (2011). Remote sensing land surface temperature for meteorology and climatology: A review. *Meteorological Applications*, *18*(3), 296–306.
71- Trenberth, K. E., Dai, A., Van Der Schrier, G., Jones, P. D., Barichivich, J., Briffa, K. R., & Sheffield, J. (2013). Global warming and changes in drought. *Nature Climate Change*, *4*(1), 17–22.
72- Trigo, I. F., Monteiro, I. T., Olesen, F., & Kabsch, E. (2008). An assessment of remotely sensed land surface temperature. *Journal of Geophysical Research Atmospheres*, *113*(17), 1–12.
73- Tsakiris, G., Pangalou, D., & Vangelis, H. (2007). Regional drought assessment based on the Reconnaissance Drought Index (RDI). *Water Resources Management*, *21*(5), 821–833.
74- Ullah, H., Akbar, M., & Khan, F. (2019). Construction of homogeneous climatic regions by combining cluster analysis and L-moment approach on the basis of Reconnaissance Drought Index for Pakistan. *International Journal of Climatology*, *40*(1), 324–341.
75- UN-ESCWA. (2013). *Inventory of Shared Water Resources in Western / United Nations Economic and Social Commission for Western Asia (UN-ESCWA) and Bundesanstalt fu¨r Geowissenschaften und Rohstoffe (BGR)*. Beirut
76- Vangelis, H., Tigkas, D., & Tsakiris, G. (2013). The effect of PET method on Reconnaissance Drought Index (RDI) calculation. *Journal of*

Arid Environments, *88*, 130–140.

77- Wan, Z., Wang, P., & Li, X. (2010). Using MODIS Land Surface Temperature and Normalized Difference Vegetation Index products for monitoring drought in the southern Great Plains, USA. *25*(1), 61–72.

78- Wilby, R. L. (1999). The weather generation game: A review of stochastic weather models. *Progress in Physical Geography*, *23*(3), 329–357.

79- Xu, Y., Yang, Y., Chen, X., & Liu, Y. (2022). Bibliometric Analysis of Global NDVI Research Trends from 1985 to 2021. *Remote Sensing*, *14*(16), 1–20.

80- Yeneneh, N., Elias, E., & Feyisa, G. L. (2022). Detection of land use/land cover and land surface temperature change in the Suha Watershed, North-Western highlands of Ethiopia. *Environmental Challenges*, *7*, 100523.

81- Zarch, M. A. A., Malekinezhad, H., Mobin, M. H., Dastorani, M. T., & Kousari, M. R. (2011). Drought Monitoring by Reconnaissance Drought Index (RDI) in Iran. *Water Resources Management*, *25*(13), 3485–3504.

82- Zhan, W., Chen, Y., Zhou, J., Wang, J., Liu, W., Voogt, J., Zhu, X., Quan, J., & Li, J. (2013). Disaggregation of remotely sensed land surface temperature: Literature survey, taxonomy, issues, and caveats. *Remote Sensing of Environment*, *131*(19), 119–139.

83- Zhou, X., Guan, H., Xie, H., & Wilson, J. L. (2009). Analysis and optimization of NDVI definitions and areal fraction models in remote sensing of vegetation. *International Journal of Remote Sensing*, *30*(3), 721–751.

84- Zoljoodi, M., Didevarasl, A., & Saadatabadi, A. R. (2013). Dust Events in the Western Parts of Iran and the Relationship with Drought Expansion over the Dust-Source Areas in Iraq and Syria. *Atmospheric and Climate Sciences 03*(03), 321–336.

الخلاصة

لقد تعرض العراق لنوبات جفاف شديدة خلال السنوات العشرين الماضية، وهي ظاهرة نموذجية في مناخ البلاد. يقع حوض الزاب الكبير في المنطقة شبه القاحلة في العراق، والتي كانت مواردها المائية شحيحة منذ عقود ويتم تقاسمها بشكل أساسي مع البلدان المجاورة الأخرى. تم استخدام الاستشعار عن بعد (RS) ونظم المعلومات الجغرافية (GIS) في هذا العمل لتقييم كيفية تأثير الجفاف على الغطاء النباتي ودرجة حرارة سطح الأرض في حوض الزاب الكبير على مدار ٣٢ عامًا، من ١٩٩٠ إلى ٢٠٢٢. لهذه الأطروحة، تم تنزيل واستخدام ٦٤ صورة عبر القمر الصناعي لاندسات. تم استخدام أربع صور تغطي منطقة الدراسة بأكملها في كل سنة من فترة الدراسة. تم إنشاء خرائط الجفاف المصنفة متعددة الزمان باستخدام مؤشر درجة حرارة سطح الأرض(LST) ، ومؤشر الاختلاف الطبيعي للغطاء النباتي(NDVI) ، ومؤشر حالة الغطاء النباتي(VCI) ، ومؤشر الغطاء النباتي المعدل للتربة .(MSVI) وأظهرت النتائج زيادة في وتيرة وشدة الجفاف خلال فترة الدراسة، وخاصة في عامي ٢٠٠٠ و٢٠٠٨، والتي تميزت بارتفاع درجات حرارة سطح الأرض، وفقدان الغطاء النباتي، ونقص متوسط هطول الأمطار. وتراوح متوسط LST من ٣٧,٢٨ درجة مئوية في عام ٢٠٠٨ إلى ٣٧,٥٦ درجة مئوية في عام ٢٠١٤. وكما هو موضح في مؤشر الغطاء النباتي للغطاء النباتي للحوض، فإن أحد آثار ارتفاع LST هو انخفاض الغطاء النباتي في الأجزاء الجنوبية الشرقية والجنوبية الغربية من منطقة الزاب الكبير وكانت السنوات ذات أدنى قراءات NDVIهي ٢٠٠٠ و٢٠٠٢ و٢٠٠٨ على التوالي، بقيم (٠,١٩٦، ٠,١٣١، و٠,٢٠٢) كيلومتر مربع. كانت السنوات الأربع في هذا التحليل هي الأكثر عرضة لخطر الجفاف، وفقًا لمؤشرVCI ، وهي الأعوام ١٩٩٢ و٢٠٠٠ و٢٠٠٢ و٢٠٠٨. وفي منطقة واسعة من المنطقة، سادت ظروف الجفاف الشديد بين عامي ٢٠٠٠ و٢٠٠٨. كما سادت بياناتنا أيضًا وكشف أن ١٣٦٦٧,٥ كم٢، أو ٦٦,٥٪ من المساحة الإجمالية، كانت مغطاة بمنطقة الجفاف الشديد في الحوض مع قيم MSAVI أقل من ٠,٢. تظهر الأجزاء الشمالية من منطقة الدراسة بالمقاطعة انخفاضًا في الغطاء النباتي. وهناك تفسير آخر لهذا الانخفاض وهو عدم التوافق بين هطول الأمطار الطبيعي واحتياجات النباتات خلال موسم النمو الحاسم.

أيضاً، في الأطروحة الحالية، تمت محاكاة البيانات المناخية اليومية من الماضي والمستقبل المتوقع باستخدام .LARS-WG 6.0 كما تم استخدام النموذج لتقدير هطول الأمطار اليومي ودرجة الحرارة اليومية. استخدام سيناريوهات الانبعاثات الرئيسية RCP4.5 و RCP8.5لتقدير المناخ المستقبلي طوال القرن الحالي باستخدام نماذج الدوران العام (GCMs)MIROC5 و CanESM2و HadGEM2-ESو ESM1-Mو .CSIRO-Mk3.6.0 وقد تم ذلك في ظل

حالة عدم اليقين الكبيرة المتعلقة بتقدير المناخ المســـتقبلي. تم التحقق من صـــحة النموذج، الذي تم إنشــاؤه باســتخدام بيانات تاريخية تعود إلى ثلاثين عامًا، باســتخدام بيانات المناخ من حوض الزاب الكبير في شمال العراق (١٩٩٠-٢٠٢١). وفقًا للبيانات، تنخفض درجة الحرارة القصوى الشهرية بمقدار ٦,٢٠-٥,٧٨ درجة مئوية تحت RCP4.5 و٦,١٠-٥,٥٨ درجة مئوية تحتRCP8.5 ، بحلول نهاية العصر الحادي والعشرين، للأجزاء الشمالية والجنوبية للحوض. تظهر توقعات هطول الأمطار من جميع نماذج الدوران العالمية أنماطًا مختلفة. وبالنظر إلى أن بعض النماذج، مثل CanESM2، تتوقع ارتفاعًا في هطول الأمطار، بينما تتوقع نماذج أخرى، مثلMIROC5 ، مستقبلًا دون تغيير في هطول الأمطار أو اتجاه هبوطي. علاوة على ذلك، عانى الجزء الجنوبي من الحوض أكثر من غيره خلال فترات الجفاف في الفترة ١٩٩٩-٢٠٠٠ و٢٠٠٧-٢٠٠٨، حيث بلغ متوســـط قيمRDIst -١,٩٧و-١,٦٤ على التوالي. ومع ذلك، فقد تعرض الجزء الشـــمالي من الحوض لموجات جفاف معتدلة إلى شـــديدة في الفترتين ١٩٩٩-٢٠٠٠ و٢٠٠٧-٢٠٠٨، حيث بلغ متوسط قيمRDIst -٠,٨١ و-١,٨٤، على التوالي. وهذا يوضح المستوى الكبير من عدم اليقين في التنبؤ بهطول الأمطار عند اســـتخدام نموذج واحد فقط .ســـوف تتأثر كمية المياه المتوفرة في موقع منطقة الدراسة بشكل كبير بالتغيرات في هطول الأمطار ودرجة الحرارة.

جمهورية العراق
وزارة التعليم العالي والبحث العلمي
جامعة بابل/ كلية الهندسة
قسم الهندسة المدنية

التحري المعتمد على البيانات المكانية لتأثير الجفاف الجوي على الغطاء النباتي ودرجة حرارة سطح الارض في حوض نهر الزاب الكبير

رسالة مقدمة إلى قسم الهندسة المدنية، كلية الهندسة، جامعةِ بابل وهي جزء مِنْ متطلبات الحصول على درجة الماجستير علوم في الهندسة/ الهندسة المدنية / هندسة الموارد المائية

من قبل:

دعاء رياض محمد علي محمد حسين

بأشراف:

م. د : رقية كاظم محمد

١٤٤٥ ٢٠٢٣